LA-UR-13-27015
Approved for public release; distribution is unlimited.

Title:	EBS Report - LANL Experimental update of buffer/backfill at elevated P,T
Author(s):	Caporuscio, Florie A
Intended for:	UFD campaign EBS deliverable
Issued:	2013-09-09

EBS Report - LANL Experimental update of buffer/backfill at elevated P,T

Fuel Cycle Research & Development

Authors

Florie A. Caporuscio, Michael C. Cheshire, Michael S. Rearick, Mary Kate McCarney[1]
Los Alamos National Laboratory

[1] presently at University of Wyoming, Department of Geology and Geophysics, Laramie, WY, 82071

Carlos Jove-Colon
Sandia National Laboratory

Document Report number : FCRD-UFD-2013-000207

Milestone number : FT-13LA080602

SUMMARY

The Used Fuel Disposition campaign is presently investigating various generic repository options for disposal of used fuel. Of interest are the disposal of high heat load canisters (up to 300 °C), which may allow for a reduced repository footprint. The focus of this experimental work is to increase our understanding on the stability of bentonite barriers under different geochemical and mineralogical conditions other than what has been previously investigated. Experiments were performed at 150 – 160 bars at temperatures up to 300 °C for five to six weeks. Unprocessed Wyoming bentonite was saturated with a K-Ca-Na-Cl-rich water at a 9:1 water:rock ratio. Experiments contained various steel plates or Cu-foil and were buffered to low Eh conditions using magnetite and metallic iron. Other experiments for international EBS research included mixed buffers and a heated bentonite with 20 wt. % free moisture for LBNL. The mixed buffer experiments (bentonite-graphite, bentonite-quartz sand) were conducted to investigate potential mineralogic/petrologic changes to mixed buffer systems proposed by the German nuclear repository program. Reaction products associated with the international EBS research were characterized by LANL with thermal-mechanical properties to be characterized by LBNL. The pH, K^+, and Ca^{2+} concentrations dropped, while $SiO_{2(aq)}$, Na^+, and SO_4^{2-} concentrations increased throughout the experiments. The alkali and alkaline earth metals aqueous concentrations appear to be buffered via the montmorillonite and clinoptilolite exchange reactions. Illite or illite/smectite mixed-layer formation is significantly retarded in the closed system due to Na^+ and $SiO_{2(aq)}$ accumulation and limited K^+ supply. Precursor clinoptilolite underwent extensive dissolution during the six week, 300 °C experiments subsequently producing a high-silicon analcime in addition to authigenic silica phases. Analcime and feldspar formation partially sequesters aqueous Al^{3+}, thereby potentially inhibiting illitization. Associated with the zeolite alteration is a ~ 17 % volume decrease (assuming quartz formation) that translates into ~ 2% volume loss in the bulk bentonite. Pyrite decomposition is first observed at ~210 °C, generating available $H_2S_{(aq,g)}$ that reacts with metal plates or evolves as a gas. The copper rapidly degrades in the presence of $H_2S_{(aq,g)}$, resulting in the formation of a chalcocite crust on the copper. A layer of Fe-saponite (or rarely, chlorite) forms at the steel bentonite interface, potentially acting as a passivating agent to retard further metal corrosion. Zeolite mineralogy alteration, metal-bentonite interface reactions, and illitization retardation under these experimental repository conditions are important considerations for the long-term stability evaluation of a used fuel repository.

CONTENTS

FIGURES

TABLES

USED FUEL DISPOSAL CAMPAIGN/ ENGINEERED BARRIERS SYSTEM

LANL EXPERIMENTAL UPDATE OF BUFFER/BACKFILL AT ELEVATED P,T

Introduction

The United States has initiated the Used Fuel Disposition campaign to evaluate various generic geological repositories for the permanent disposal of used nuclear fuel. The development and evaluation of engineered barrier system (EBS) design concepts and their potential interactions with the natural barrier or with other EBS interfaces are inherently important to the long-term (i.e., tens of thousands of years) safety and performance of geological repositories (Jove-Colon et al. 2011; Nutt et al. 2011). One of the more commonly proposed ideas for high-level nuclear waste repository is to surround waste canisters with bentonite in an underground repository (Pusch 1979; Meunier et al. 1998). There have been numerous investigations on the stability of bentonites under various repository conditions and in contact with various metals replicating possible canister compositions (Pusch 1979; Madsen 1998; Meunier et al. 1998; Guillaume et al. 2003; Wersin et al. 2007; Mosser-Ruck et al. 2010; Ferrage et al. 2011). However, there remain uncertainties regarding the long-term stability of bentonite EBS and corrosion products under potential repository conditions. The focus of this experimental work is to expand our understanding of the stability of bentonite barriers under different geochemical, mineralogical, and engineering conditions than what has been previously investigated. Alteration of smectite to other minerals (i.e., illite, illite/smectite, chlorite), steam-induced swelling loss, and interaction of smectite with metal waste canisters are some of the more prevalent concerns (Couture 1985; Wersin et al. 2007; Mosser-Ruck et al. 2010). Most previous investigations focused on cleaned, cation exchanged smectites. Jobmann and Buntebarth (2009) examined the effect of adding graphite or quartz sand to bentonite to enhance the thermo-physical properties of buffer materials. This report addresses the various authigenic minerals occurring within

unprocessed Wyoming bentonite and clay/metal interface reactions during hydrothermal investigations replicating a high temperature repository-like environment.

Methods

Experimental setup

The bentonite used in this experimental work is mined from a reducing horizon in Colony, Wyoming. The bentonite was pulverized and sieved to < 3 mm and used with a free moisture of ~15.5 wt. %. The synthetic groundwater solution was chosen to replicate a deep groundwater composition (Table 1, Stripa sample V2 (69-4), Frape et al. 2003). The groundwater solution was prepared using reagent grade materials dissolved in double deionised water. KOH and HCl were added to adjust the initial solution pH. This solution was then filtered through a 0.45 μm filter and sparged with He before each experiment. The salt solution was added at a 9:1 water: bentonite ratio. Initial components for all experiments have been summarized in Table 2.

Species	mg/L
Ca^{2+}	89
Cl^{-}	1045
K^{+}	583
Na^{+}	167
Si	1
SO_4^{2-}	47
Sr^{2+}	0.05
TDS	1934
pH	8.59

Table 1. Synthetic groundwater chemistry used in each experiment.

The redox conditions for each system were buffered using a 1:1 mixture (by mass) of Fe_3O_4 and Fe° added at 0.07 wt. % of the bentonite mass. Approximately 7 wt. % (of total mass) 304 stainless steel (NIST SRM 101g), 316 stainless steel (NIST SRM 160b), Cu-foil, and low-

carbon steel (provided by Sandia National Laboratory) were added to the experiments to mimic the presence of a waste canister.

Reactants were loaded into either a flexible gold or titanium bag and fixed into a 500 mL Gasket Confined Closure reactor (Seyfried et al. 1987). Experiments were pressurized to 150 - 160 bar and were heated following two different temperature profiles: 1) 120 °C for 2 weeks, 210 °C for 2 weeks, and then 300 °C for 1 week and 2) isothermal at 300 °C for 6 weeks. Reaction liquids were extracted during the experiments and analyzed to investigate the aqueous geochemical evolution in relationship to mineralogical alterations. The sampled reaction liquids were split three-ways producing aliquots for unfiltered anion, unfiltered cation, and filtered (0.45 μm syringe filter) cation determination. All aliquots were stored in a 1 °C refrigerator until analysis.

	Clay, g	Brine, g	pH	Fe°, g	Fe_3O_4, g	Accessory, g	EBS Component	Run temp, °C	Run time
EBS-1	7.4	79.0	8.59	0.257	0.252	na	na	25/100/200/300/25	4 weeks
EBS-2	7.2	62.0	8.59	0.251	0.253	4.980	304SS	25/100/200/300/25	4 weeks
EBS-3	6.790	59.4	7.56	0.255	0.261	4.245	316SS	25/100/200/300/25	5 weeks
EBS-4	16.207	145.0	7.56	0.574	0.579	9.753	Cu	25/100/200/300/25	5 weeks
EBS-5	15.770	135.9	6.73	0.505	0.505	11.189	304SS	300	6 weeks
EBS-6	12.109	104.2	9.48	0.424	0.424	8.375	Low-C Steel	25/100/200/300/25	5 weeks
EBS-7	14.627	157.9	6.69	0.589	0.586	3.656	Graphite	25/100/200/300/25	5 weeks
EBS-8	15.284	131.9	7.72	0.489	0.489	10.816	Cu	300	6 weeks
EBS-9	15.516	167.6	7.16	0.625	0.625	3.878	Quartz sand	25/100/200/300/25	5 weeks
EBS-10	21.105	182.3	6.36	0.675	0.675	14.937	316SS	300	6 weeks
EBS-11	15.039	129.8	6.74	0.481	0.481	10.643	Cu	300	6 weeks
EBS-12	208.5	41.7	6.74	na	Na	na	none	300	7 weeks

Table 2. Initial components and reaction conditions for EBS experiments. EBS-8 developed a leak during experiment. This experiment was discarded and was repeated as EBS-11.

Mineral analyses

X-ray diffraction (XRD) analyses of experimental materials determined mineral compositions. Each sample was ground with 20 wt. % corundum (Al_2O_3) for quantitative XRD analysis of the bulk rock (Chung 1974). XRD measurements were conducted with a Siemens D500 diffractometer using Cu-Kα radiation. Data were collected from 2 to 70 °2θ with a 0.02 º2θ step-size and count times of 8 to 12 seconds per step. To better analyze the non-clay and clay fractions, the < 2 μm particles were separated via sedimentation in DI H_2O. An aliquot of the < 2 μm suspension was dropped on a zero-background quartz plate and dried. This oriented mount was X-rayed from 2 to 40 °2θ at 8 to 12 s per step. The oriented mount was then saturated with ethylene glycol in a 60 °C oven for 24 hours and XRD analysis was repeated. A portion of the > 2 μm particles was ground with a mortar/pestle, deposited on a zero-background quartz plate, and X-rayed under the same parameters as the bulk powder material. The remaining > 2 μm portion was used for electron microscopy. Mineral identification and unit-cell parameters analysis was performed using Jade© 7.5 X-ray data evaluation program with ICDD PDF-4 database. Quantitative phase analysis was performed using FULLPAT (Chipera and Bish 2002).

X-ray florescence (XRF) analysis of the experimental materials was performed using a Rigaku ZSX Primus II. Samples were mixed with Li-metaborate at 7:1 or 36:1 and fluxed at 1100° C for 45 minutes. All reported values exceed three times the reported detection limits. A portion of the < 2 μm fraction from the reaction products and starting bentonite was analyzed to determine the structural formulas. All other starting materials were analyzed without separation. Loss on ignition (LOI) was determined by heating the sample to 1000 °C for 30 minutes.

Electron microscopic analyses were performed using a FEI™ Inspect F scanning electron microscope (SEM). All samples were Au-coated prior to SEM analysis. Imaging with the SEM was performed using a 5.0 kV accelerating voltage and 1.5 spot size. Energy dispersive X-ray spectroscopy (EDX) was performed at 30 kV and a 3.0 spot size.

Electron microprobe analyses were performed at the University of Oklahoma using a Cameca SX50 electron microprobe equipped with five wavelength-dispersive spectrometers and PGT PRISM 2000 energy-dispersive X-ray detector. Petrographic characterization was

performed by backscattered electron imaging coupled with energy-dispersive X-ray analysis, using beam conditions of 20 kV acceleration and 20 nA sample current. Quantitative analysis was performed by wavelength-dispersive spectrometry using 20 kV accelerating voltage, 20 nA beam current, and 2 µm spot size. Matrix corrections employed the PAP algorithm (Pouchou and Pichoir 1985), with oxygen content calculated by stoichiometry. Counting times were 30 seconds on peak for all elements, yielding minimum levels of detection (calculated at 3-σ above mean background) in the range of 0.01 to 0.03 wt% of the oxides for all components except F (0.16 wt%). All standards for elements in the silicates were analyzed using 30 second count times on peak, using K-alpha emissions. The standards and oxide detection limits are presented in Appendix A. Sodium analyses for clinoptilolite are problematic due to sodium migration under an electron beam, whereas analcime shows no sodium migration (Broxton *et al.*, 1987). Zeolite structural formulae were calculated from data that have Al + Fe/(Na + K + 2*(Ca + Mg)) ratios within a range of 1.20 to 0.80. Microprobe results of select silicates are presented in Appendix B.

Aqueous geochemical analyses

Major cations and trace metals were analyzed via inductively coupled plasma-optical emission spectrometry (Perkin Elmer Optima 2100 DV) and inductively coupled plasma-mass spectrometry (Elan 6100) utilizing EPA methods 200.7 and 200.8. Ultra-high purity nitric acid was used in sample and calibration preparation prior to sample analysis. Internal standards (Sc, Ge, Bi, and In) were added to samples and standards to correct for matrix effects. Standard Reference Material (SRM) 1643e Trace Elements in Water was used to check the accuracy of the multi-element calibrations. Inorganic anion samples were analyzed by ion chromatography (IC) following EPA method 300 on a Dionex DX-600 system. Aqueous geochemical results are presented in Appendix C.

Reaction modeling and phase diagrams were calculated via The Geochemist's Workbench v.8.0.8 using a modified *thermo.dat* database. These thermodynamic databases were modified to incorporate various mineral compositions that are more consistent to what is found in these experiments (Neuhoff et al. 2004; Wilkin and Barnes 1998; Blanc and Vieillard 2010). Solution chemistry data (analyzed at room temperature) was adjusted to reflect the activities present at reaction temperatures. Temperature corrected data were plotted on phase diagrams to

show the geochemical progression. Pressures for the GWB modeling were held at water saturation pressures.

Results

Bentonite Pre- and Post-Reaction Characteristics

The starting bentonite used in this experiment is a Na-montmorillonite with minor amounts of clinoptilolite, feldspars, biotite, cristobalite, quartz, and pyrite (Table 3). This material differs from the more commonly evaluated MX-80 bentonite by lacking calcite and gypsum, but contains significant amounts of clinoptilolite (Guillaume et al. 2004; Karnland 2010). The montmorillonite displays the typical foily or 'cornflake' morphology associate with smectite (Figure 1a). The bulk and < 2 μm bentonite compositions are listed in Table 4. Montmorillonite associated with this bentonite has a structural formula of $(Na_{.31},Ca_{.04},K_{.01})(Al_{1.53},Fe_{.21},Mg_{.18},Ti_{.01})(Si_{3.98},Al_{.02})O_{10}(OH)_2$. Clinoptilolite in the bentonite appears to maintain the precursor volcanic shard morphology (Figure 1b) with a structural composition of $(Na_{4.30},Ca_{0.39},K_{0.14},Mg_{0.20})(Si_{29.82},Al_{6.28},Fe_{0.03})O_{72}{\cdot}nH_2O$ (n ~ 21, based on stoichiometric clinoptilolite). Feldspars are primarily albitic plagioclases ($Na_{0.71}Ca_{0.19}K_{0.07}(Si_{2.80}Al_{1.21})O_8$) and K-feldspars ($K_{0.66}Na_{0.29}Ca_{0.01}(Si_{2.97}Al_{1.05})O_8$). The bentonite contains no more than 0.4 wt. % pyrite. There are two forms of pyrite in the starting bentonite: 1) framboidal pyrite from microbial activity (Figure 1c) and 2) cubic pyrite principally from abiotic processes (Figure 1d).

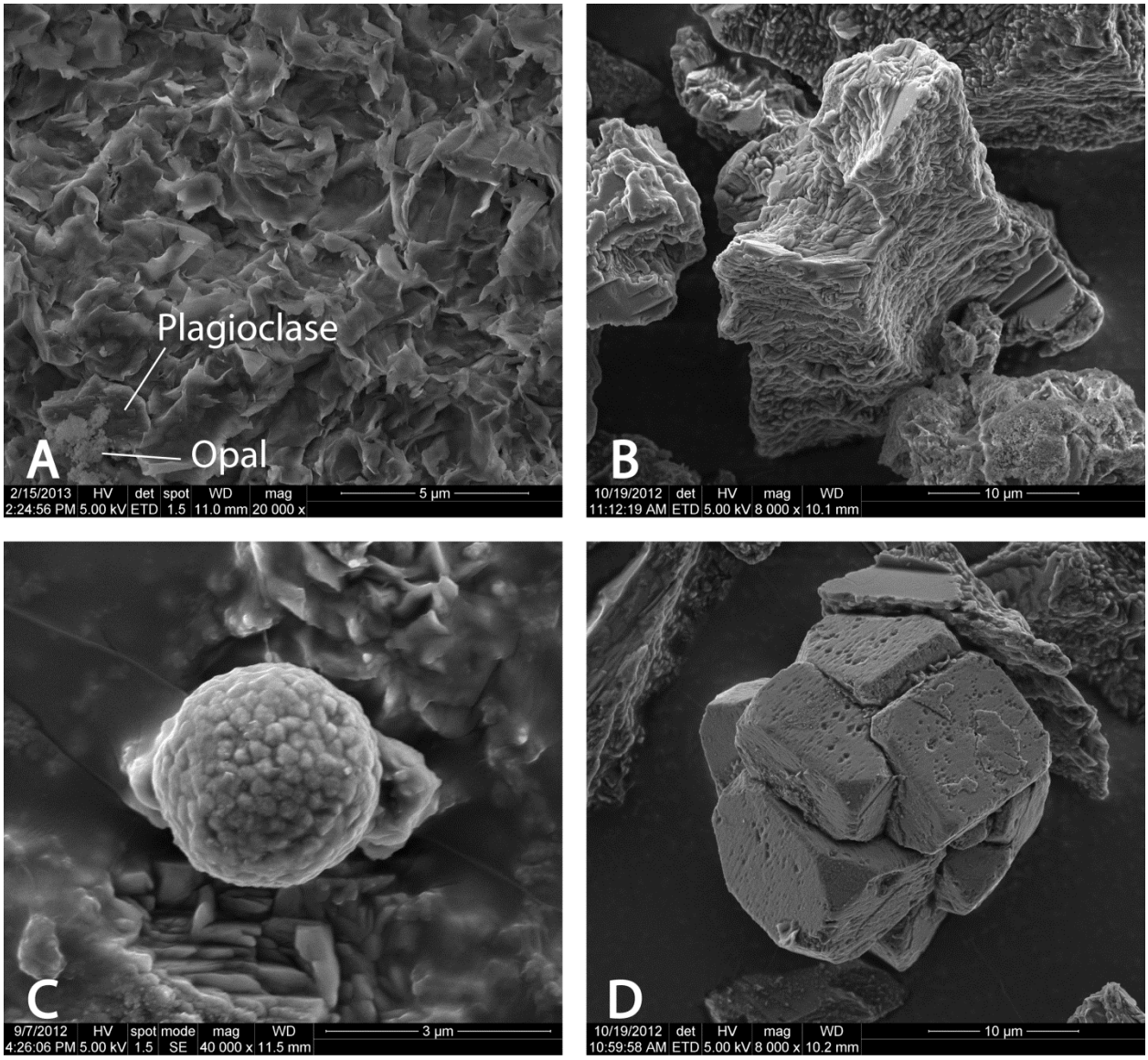

Figure 1. Minerals associated with the Colony, WY bentonite A) typical montmorillonite foily morphology with discrete plagioclase and possibly cristobalite/opal-C phases, B) tabular clinoptilolite replacing precursor volcanic shards, C) framboidal pyrite, and D) cubic pyrite.

		Ramped heating 120 to 300C							Isothermal 300C			
	Initial Bentonite	EBS-1 --	EBS-2 304SS	EBS-3 316SS	EBS-4 Cu	EBS-6 LC Steel	EBS-7 graphite	EBS-9 quartz	EBS-5 304SS	EBS-10 316SS	EBS-11 Cu	EBS-12 20% H_2O
Montmorillonite	72	81	75	79	79	81	75	73	79	79	80	71
Quartz	1	2	1	2	1	2	3	16	2	3	2	3
Crist/Opal-C	2	2	3	2	1	4	1	2	4	2	2	10
Clinoptilolite	13	8	9	6	6	7	5	6	2	6	8	4
Analcime	b.d.l.	b.d.l.	b.d.l.	b.d.l.	b.d.l.	b.d.l.	b.d.l.	b.d.l.	3	1	1	1
Feldspar	9	6	9	8	9	4	3	3	7	8	7	10
Biotite	3	2	4	1	2	1	+	+	2	1	+	+
Pyrite	0.4	b.d.l.	b.d.l.	b.d.l.	b.d.l.	b.d.l.	b.d.l.	b.d.l.	b.d.l.	b.d.l.	b.d.l.	+
Magnetite	b.d.l.	b.d.l.	b.d.l.	2	1	+	+	1	1	b.d.l.	b.d.l.	b.d.l.
Graphite	b.d.l.	b.d.l.	b.d.l.	b.d.l.	b.d.l.	b.d.l.	12	b.d.l.	b.d.l.	b.d.l.	b.d.l.	b.d.l.
Halite	b.d.l.	b.d.l.	b.d.l.	b.d.l.	+	b.d.l.	b.d.l.	b.d.l.	+	b.d.l.	b.d.l.	b.d.l.

Table 3. Bulk mineralogical composition (wt. %) of the starting bentonite and post-reaction samples. b.d.l. indicates below detection limits. “+” indicates present but is < 0.5 wt. %.

				Ramped heating 120 to 300 °C							Isothermal 300 °C				
	Bentonite bulk		Bentonite < 2 μm	EBS-1 < 2 μm	EBS-2 < 2 μm	EBS-3 < 2 μm	EBS-4 < 2 μm	EBS-6 < 2 μm	EBS-7 < 2 μm	EBS-9 < 2 μm	EBS-5 < 2 μm	EBS-10 < 2 μm	EBS-11 < 2 μm	EBS-12 < 2 μm	Detection
Metal	n = 4	1 s		none	304SS	316SS	Cu	LC St.	gr	qtz	304SS	316SS	Cu	H2O	Limits
fuse ratio	7:1	7:1	36:1	36:1	36:1	36:1	36:1	36:1	36:1	36:1	36:1	36:1	36:1	36:1	36:1
Na_2O	2.85	0.025	2.57	2.35	2.10	2.22	2.40	2.23	2.30	2.54	2.39	2.16	2.60	2.58	0.163
MgO	1.64	0.023	1.96	2.04	2.00	1.91	1.87	1.84	1.85	1.89	1.92	1.75	1.81	1.98	0.0891
Al_2O_3	19.5	0.038	20.9	20.6	20.5	20.6	20.1	19.8	19.6	20.0	20.9	19.7	19.5	20.9	0.0778
SiO_2	61.9	0.116	63.3	62.3	63.2	62.5	62.2	63.6	61.0	61.2	62.8	59.9	63.0	61.1	0.293
P_2O_5	0.044	0.002	**b.d.l.**	**b.d.l**	**b.d.l**	**b.d.l.**	**b.d.l.**	**b.d.l.**	0.012	0.010	**b.d.l.**	**b.d.l.**	**b.d.l.**	**b.d.l.**	0.0174
K_2O	0.572	0.005	0.174	0.700	0.660	0.684	0.702	0.982	0.160	0.182	0.193	0.399	0.345	0.147	0.0224
CaO	0.860	0.019	0.636	0.736	0.547	0.710	0.746	0.792	0.755	0.733	0.764	0.721	0.663	0.682	0.0298
TiO_2	0.142	0.001	0.137	0.121	0.121	0.124	0.132	0.132	0.125	0.128	0.120	0.122	0.127	0.118	0.0344
MnO	0.013	0.001	**b.d.l.**	**b.d.l.**	0.015	0.021	0.024	0.018	0.022	0.030	0.021	0.020	0.017	0.013	0.0128
Fe_2O_3	4.12	0.039	4.49	4.55	4.55	5.24	5.87	4.83	6.22	7.59	5.12	5.45	4.82	4.67	0.074
V	7	0.96	**b.d.l.**	**b.d.l.**	**b.d.l.**	**b.d.l.**	**b.d.l.**	**b.d.l.**	**b.d.l.**	**b.d.l.**	**b.d.l.**	**b.d.l.**	**b.d.l.**	**b.d.l.**	44
Cr	6	1.7	**b.d.l.**	**b.d.l.**	**b.d.l.**	**b.d.l.**	**b.d.l.**	**b.d.l.**	**b.d.l.**	**b.d.l.**	**b.d.l.**	**b.d.l.**	**b.d.l.**	**b.d.l.**	73
Co			**b.d.l.**	**b.d.l.**	**b.d.l.**	**b.d.l.**	**b.d.l.**	**b.d.l.**	**b.d.l.**	**b.d.l.**	**b.d.l.**	**b.d.l.**	**b.d.l.**	**b.d.l.**	69
Ni	5	0.82	41	46	56	48	33	47	53	42	35	35	41	53	26
Cu	7	2.5	54	61	252	94	119	45	63	73	55	66	193	62	27
Zn	96	16	**b.d.l.**	**b.d.l.**	**b.d.l.**	**b.d.l.**	58	**b.d.l.**	**b.d.l.**	**b.d.l.**	**b.d.l.**	34	75	40	26
Ge			**b.d.l.**	**b.d.l.**	**b.d.l.**	**b.d.l.**	**b.d.l.**	**b.d.l.**	**b.d.l.**	**b.d.l.**	**b.d.l.**	**b.d.l.**	**b.d.l.**	**b.d.l.**	47
As			**b.d.l.**	**b.d.l.**	**b.d.l.**	**b.d.l.**	**b.d.l.**	**b.d.l.**	**b.d.l.**	**b.d.l.**	**b.d.l.**	**b.d.l.**	**b.d.l.**	**b.d.l.**	71
Rb	18	0.82	**b.d.l.**	**b.d.l.**	**b.d.l.**	**b.d.l.**	**b.d.l.**	**b.d.l.**	**b.d.l.**	**b.d.l.**	**b.d.l.**	171	**b.d.l.**	**b.d.l.**	23
Sr	297	3.9	133	139	164	126	125	215	101	130	110	164	134	177	27
Zr	196	1.5	144	137	143	150	144	139	140	145	149	61	144	141	30
Ba	664	15.3	**177**	149	**b.d.l.**	**b.d.l.**	**b.d.l.**	230	**b.d.l.**	**b.d.l.**	**b.d.l.**	**b.d.l.**	**b.d.l.**	**126**	105

W		**b.d.l.**	**b.d.l.**	**b.d.l.**	**b.d.l.**	**b.d.l.**	**b.d.l.**	**b.d.l.**	**b.d.l.**	**b.d.l.**	**b.d.l.**	**b.d.l.**	**b.d.l.**	209
U		**b.d.l.**	**b.d.l.**	**b.d.l.**	**b.d.l.**	**b.d.l.**	**b.d.l.**	**b.d.l.**	**b.d.l.**	**b.d.l.**	**b.d.l.**	**b.d.l.**	**b.d.l.**	33
LOI	8.21	5.76	6.46	6.13	5.85	5.88	5.61	7.82	5.66	5.69	9.71	6.95	7.63	
total	99.99	99.98	99.91	99.88	99.90	99.97	99.90	99.90	100.00	99.95	99.98	99.89	99.88	

Table 4. Chemical composition (XRF) of the starting bentonite and < 2 μm size fractions from post-reaction samples from each EBS experiment. Oxides and loss on ignition (LOI) data are presented as wt.% and trace element data are presented as ppm. *Total iron is represented as Fe_2O_3. b.d.l. indicates below detection limits.

Ramped Thermal Profile. There were no significant alterations to the montmorillonite away from the metal plates (> 1 mm from metal surface) during the ramped heating cycle. However, there were significant changes to the phyllosilicates due to metal interaction at the bentonite-metal interface producing Fe-rich phyllosilicates (i.e., Fe-saponite and chlorite) on steel surfaces and chalcocite on copper surfaces. The various reactions away from the bentonite-metal interface all showed similar mineralogical reactions indicating various metallic plates do not significantly influence the bulk bentonite (Table 3). The glycol saturated samples yielded d_{001} of 17 Å with higher order $d_{00\ell}$ consistent with integer values of the d_{001} values (Figure 2). The XRD data suggests that neither illite nor illite-smectite was produced during the reactions. Additionally, there appears to be no major morphological changes to the montmorillonite (Figure 3a). The structural formulae (calculated from XRF analyses of < 2 μm size separates (Table 4)) of the post-reaction montmorillonites has been summarized in Table 5. All structural iron has been assumed to be in the ferric-state. However, the true nature of the montmorillonite's structural iron is unknown and most likely contains both ferric to ferrous iron. Clinoptilolite maintains a similar composition to the starting clinoptilolite, but has a slight K^+ and Ca^{2+} enrichment, $(Na_{3.17},K_{0.65},Ca_{0.73},Mg_{0.09})(Si_{29.84},Al_{6.36},Fe_{0.03})O_{72}{\cdot}nH_2O$ (Appendix B).

Run Conditions	Run #	Metal Plate	Montmorillonite Structural Formulae
Initial Bentonite	Na	Na	$(Na_{.31},Ca_{.04},K_{.01})(Al_{1.53},Fe_{.21},Mg_{.18},Ti_{.01})(Si_{3.98},Al_{.02})O_{10}(OH)_2$
Ramped, 120 to 300 °C 150 – 160 bar 5 weeks	EBS-1	None	$(Na_{.29},K_{.06},Ca_{.05})(Al_{1.51},Fe^{3+}_{.22},Mg_{.19},Ti_{.01})(Si_{3.96},Al_{.04})O_{10}(OH)_2$
	EBS-2	304SS	$(Na_{.26},K_{.04},Ca_{.05})(Al_{1.53},Fe^{3+}_{.22},Mg_{.19},Ti_{.01})(Si_{4.00})O_{10}(OH)_2$
	EBS-3	316SS	$(Na_{.27},K_{.06},Ca_{.05})(Al_{1.50},Fe^{3+}_{.25},Mg_{.18},Ti_{.01})(Si_{3.96},Al_{.04})O_{10}(OH)_2$
	EBS-4	Copper	$(Na_{.30},K_{.06},Ca_{.05})(Al_{1.46},Fe^{3+}_{.28},Mg_{.18},Ti_{.01})(Si_{3.95},Al_{.05})O_{10}(OH)_2$
	EBS-6	low C Steel	$(Na_{.27},K_{.08},Ca_{.05})(Al_{1.47},Fe^{3+}_{.23},Mg_{.17},Ti_{.01})(Si_{4.02})O_{10}(OH)_2$
	EBS-7	Graphite	$(Na_{.28},K_{.01},Ca_{.05})(Al_{1.31},Fe^{3+}_{.30},Mg_{.17},Ti_{.01})(Si_{3.85},Al_{.15})O_{10}(OH)_2$
	EBS-9	Quartz	$(Na_{.31},K_{.02},Ca_{.05})(Al_{1.35},Fe^{3+}_{.36},Mg_{.18},Ti_{.01})(Si_{3.86},Al_{.14})O_{10}(OH)_2$
Isothermal, 300 °C 150 – 160 bar	EBS-5	304SS	$(Na_{.31},K_{.02},Ca_{.05})(Al_{1.46},Fe^{3+}_{.26},Mg_{.19},Ti_{.01})(Si_{3.83},Al_{.17})O_{10}(OH)_2$
	EBS-10	316SS	$(Na_{.28},K_{.03},Ca_{.05})(Al_{1.18},Fe^{3+}_{.27},Mg_{.17},Ti_{.01})(Si_{3.64},Al_{.36})O_{10}(OH)_2$
	EBS-11	Copper	$(Na_{.33},K_{.03},Ca_{.05})(Al_{1.37},Fe^{3+}_{.24},Mg_{.18},Ti_{.01})(Si_{3.85},Al_{.15})O_{10}(OH)_2$

Table 5. Structural formula for post-reaction montmorillonites. Calculated from XRF analyses of the < 2 μm size fractions.

Odor of the aqueous samples and loss of pyrite in post-experiment samples suggests pyrite decomposition occurred during the experiments yielding $H_2S_{(aq,g)}$. Experiments containing stainless steel evolved $H_2S_{(g)}$ more readily due to limited interactions with steel surfaces. Experiments with copper plates did not evolve substantial $H_2S_{(g)}$ due to the formation of chalcocite (Cu_2S) on the copper surfaces.

SEM evidence suggests that minor authigenic plagioclase and K-feldspars are formed during these reactions (Figure 3c). Plagioclases are albitic with a structural composition of $(Na_{0.68}Ca_{0.26}K_{0.05})(Al_{1.25}Si_{2.75}Fe_{0.01})O_8$. K-feldspar has a structural composition of $(K_{.68}Na_{0.29}Ca_{0.01})(Al_{1.01}Si_{3.00})O_8$.

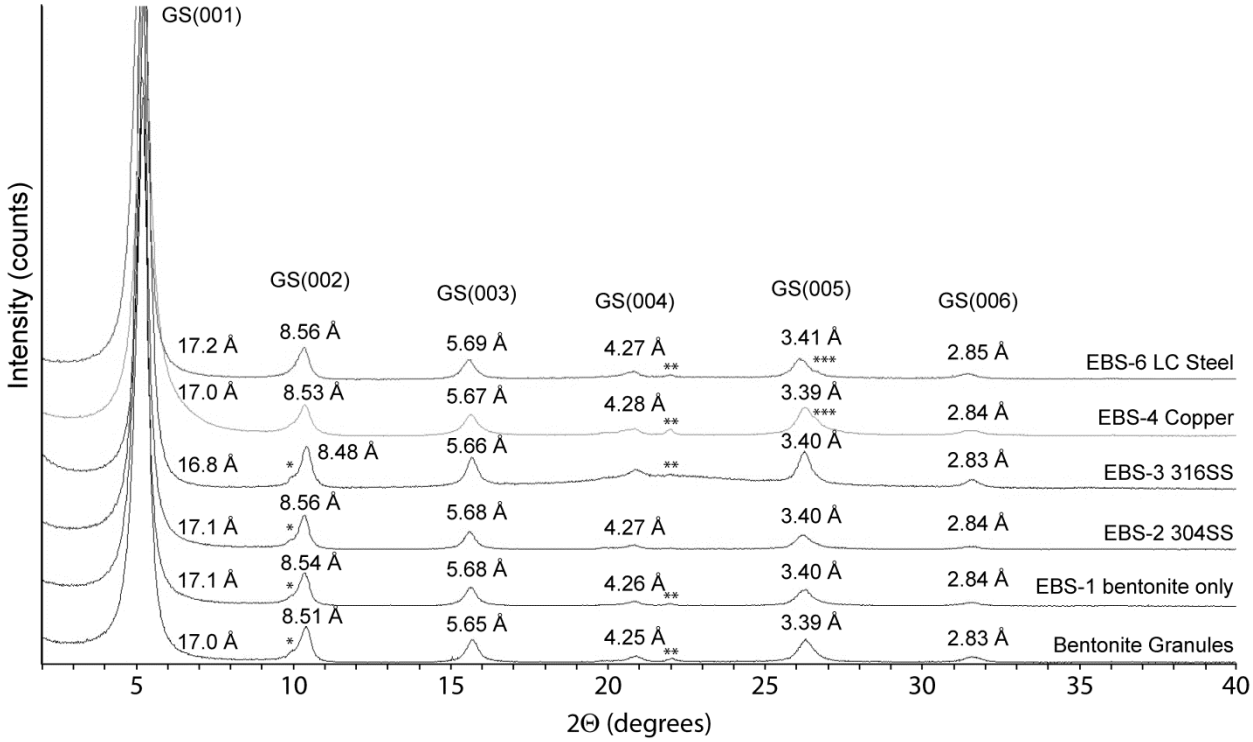

Figure 2. Oriented XRD patterns for the glycolated, < 2 μm fraction from the ramped thermal profile experiments with d-spacings labeled above each peak. XRD results show no alteration of the montmorillonite to illite/smectite. Minor amounts of clinoptilolite (*), cristobalite/opal-C (**), and quartz (***) are also present in the < 2 μm fraction.

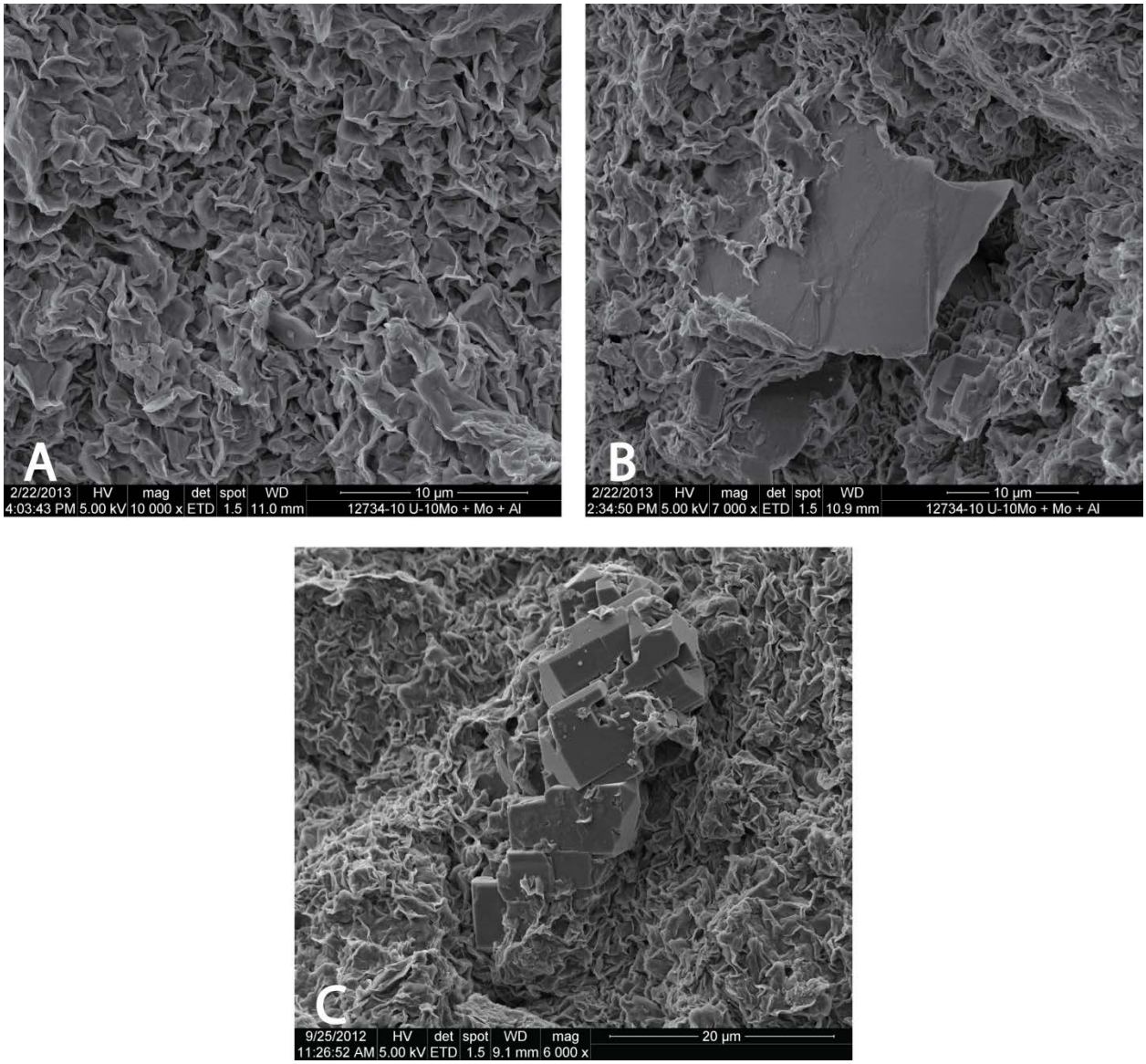

Figure 3. Post-reaction mineralogical characteristics from ramp heating experiments A) typical montmorillonite foily morphology from EBS-2, B) montmorillonite foily morphology with biotite and feldspars from EBS-2, and C) authigenic albitic plagioclase embedded in montmorillonite from EBS-1.

Isothermal, 300 ºC Profile. Partial dissolution of the montmorillonite developed rough edges during the long-term, isothermal 300 °C experiments (Figure 5a). Structural formulas presented in Table 5 have been adjusted for SiO_2 contribution from 5 wt. % cristobalite/opal-C (indicated by XRD).

The glycol saturated samples yielded d_{001} of 17 Å with higher order $d_{00\ell}$ consistent with integer values of the d_{001} values (Figure 4), suggesting illite-smectite is not present. However, there does appear to be a minor 10 Å peak present in the < 2 μm fraction (Figure 4). Additionally, there possibly is a broadened peak superimposed over the 10 Å biotite peak associated with the > 2 μm samples. These broadened 10 Å peaks do not shift upon glycolation, suggesting an occurrence of an illitic phase. SEM examination of the bulk material and > 2 μm fraction indicates an abundance of a newly formed fibrous mineral. These fibers occur as bundles or isolated fibers (Figure 5b). Lengths of the fibers range from 1.5 μm to 17.4 μm with widths ranging from 0.10 μm to 0.51 μm, producing aspect ratios (l/w) ranging from 15.5 to 55.5. Chemical analyses of the fiber were not collected due to mixing with montmorillonite. The SEM and XRD data would indicate authigenic fibrous illite formed during the long-term, 300 °C experiments. Considering the absence of illite-smectite mixed-layers in all experiments, the illite appears to be from direct crystallization.

Minor amounts of authigenic plagioclase and K-feldspars are formed during these reactions. Possible plagioclase overgrowths (Figure 6c) have an average structural formula of $(Na_{0.84},Ca_{0.16},K_{0.05})Al_{1.16}Si_{2.84}O_8$. K-feldspars have a structural composition of $(K_{0.67}Na_{0.27}Ca_{0.01})(Al_{1.02}Si_{3.00})O_8$.

Isothermal 300^o C experiments yielded analcime and cristobalite as a result of an apparent dissolution of clinoptilolite and silica saturation (Cheshire et al. 2013). Analcime formed with an average Si/Al ratio of 2.93 (n = 18; σ = 0.08) with a calculated structural composition of $(Na_{0.64},Ca_{0.05})(Si_{2.23},Al_{0.76})O_6{\cdot}nH_2O$.

$$(Na_{4.30},Ca_{0.39},K_{0.14},Mg_{0.20})(Si_{29.82},Al_{6.28},Fe_{0.03})O_{72}{\cdot}21H_2O + 0.92\ Na^+ + 0.02\ Ca^{2+} \rightarrow$$

clinoptilolite

$$8.16\ (Na_{0.64},Ca_{0.05})(Si_{2.23},Al_{0.77})O_6{\cdot}1H_2O + 0.14\ K^+ + 0.20\ Mg^{2+} + 11.62\ SiO_{2(aq)} + 12.64\ H_2O +$$

analcime

$$0.03\ Fe^{2+} + 0.40\ H^+$$

Analcime occurs as 5 to 10 μm anhedral to subhedral trapezohedrons (Figure 5d). Anhedral analcime formed initially as an agglomeration of nano-sized, spherical crystals followed by coarsening of analcime nuclei to subhedral, trapezohedral analcime (Figure 6). The growth of analcime appears to have been stopped due to the quenching of the reaction preserving the various stages of analcime ripening. There appears to be a systematic variation in Si/Al ratios related to the various analcime growth stages (Figure 6). The Si/Al ratio tends to be low during early analcime formation compared to the 2.97 Si/Al ratios found in the subhedral analcime. Authigenic analcime from these experiments have higher Si/Al ratio than most naturally occurring analcime, which typically range from 1.50 to 2.85 (Neuhoff et al. 2004). But, analcime found in felsic tuffs have shown Si/Al ratios as high as 2.89. Upon microscopic examination, there are no independent silica phases or silicate minerals mixed within the analcime agglomerates that would cause an anomalously high silica concentration. Analcime can be seen both growing as isolated crystals in the smectite groundmass and replacing the precursor clinoptilolite (Figure 5e).

The analcime Si/Al ratio is confirmed by X-ray diffraction analyses. The a-parameter for the synthesized analcime is 13.66 Å which corresponds to about 2.2 – 2.3 Si per 6 framework oxygen (Coombs and Whetten 1967; Neuhoff et al. 2004) with a unit-cell volume of 2,548.9 $Å^3$.

Plagioclase overgrowths have an average structural formula of $(Na_{0.84},Ca_{0.16},K_{0.05})Al_{1.16}Si_{2.84}O_8$ (Figure 5d). K-feldspars have a structural composition of $(K_{0.67}Na_{0.27}Ca_{0.01})(Al_{1.02}Si_{3.00})O_8$.

Odor of the aqueous samples and loss of pyrite in post-experiment samples suggests pyrite decomposition occurred during the experiments yielding $H_2S_{(aq,g)}$. Experiments containing stainless steel evolved $H_2S_{(g)}$ more readily, limiting interaction with steel surfaces. There is evidence of a 0.4 – 0.8 μm sulfur-rich layer (Figures 13 and 17) developed on outer surfaces of the steel plates. Experiments with Cu° plates did not evolve substantial $H_2S_{(g)}$ due to the formation of chalcocite (Cu_2S) on the Cu surfaces.

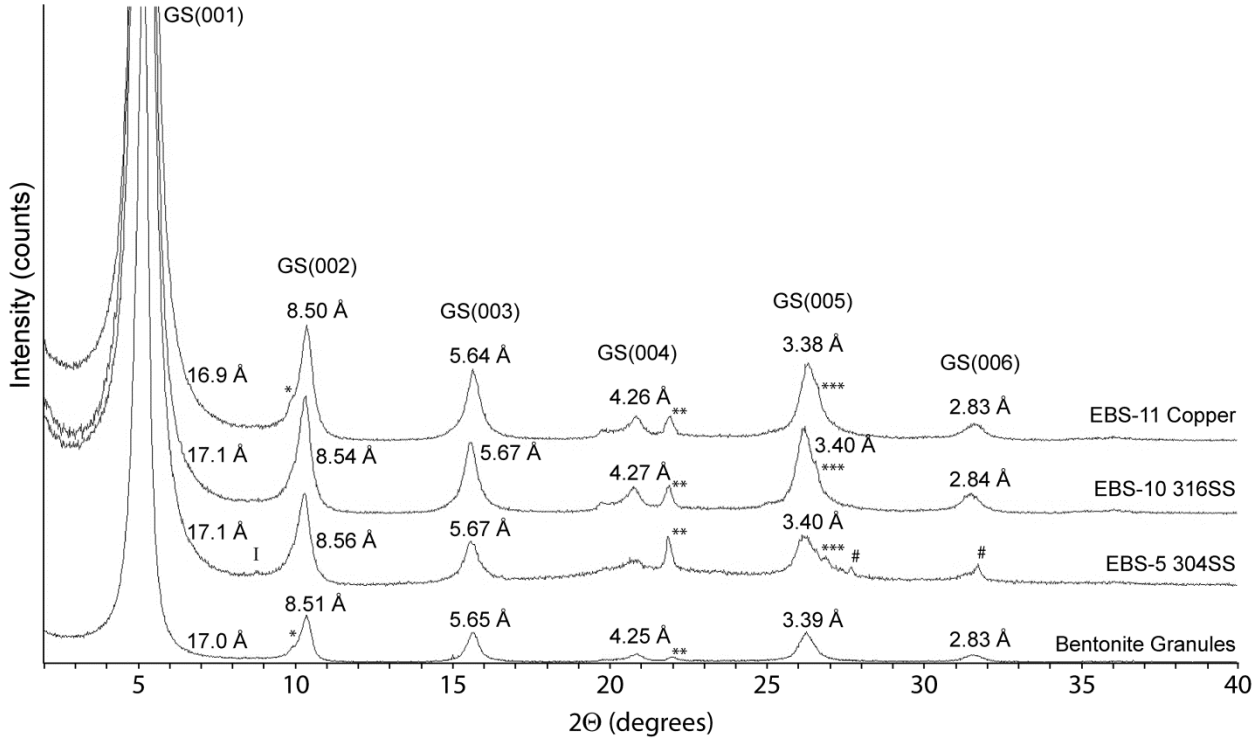

Figure 4. Oriented XRD patterns for the glycolated, < 2 μm fraction from the isothermal, 300 °C thermal profile experiments. XRD results show no alteration of the montmorillonite to illite/smectite. A small, 10 Å peak (possibly illite (I)) appears to be present in EBS-5 material. Minor amounts of clinoptilolite (*), cristobalite/opal-C (**), quartz (***), and halite (#) are also present in the < 2 μm fraction.

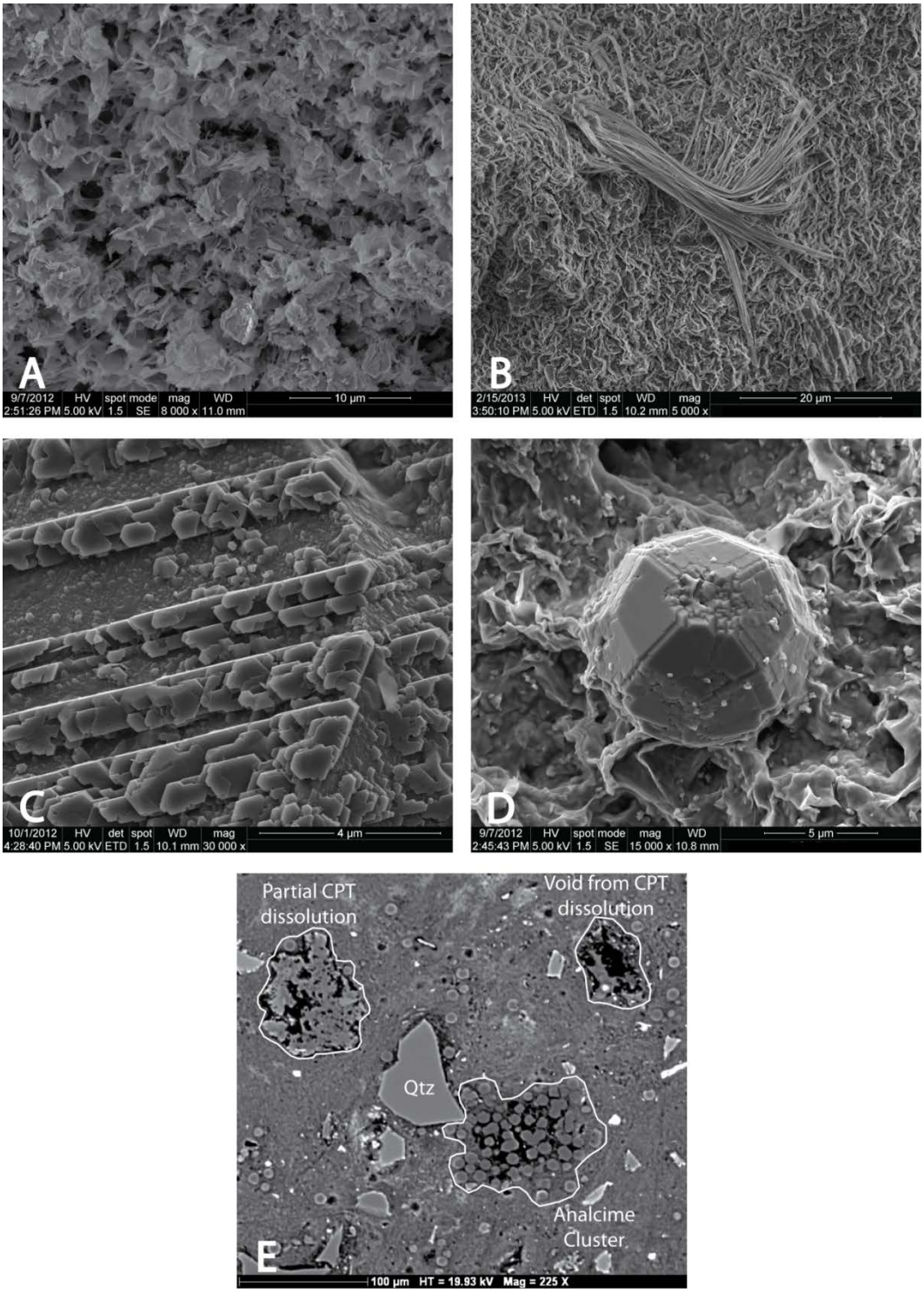

Figure 5. Post-reaction SEM images showing mineralogical characteristics from the isothermal 300 °C experiments including A) montmorillonite foils displaying partially deteriorated edges, B) bundle of authigenic fibrous illite, C) authigenic albitic plagioclase overgrowths showing possible polysynthetic twinning, D) subhedral analcime formed from the dissolution of clinoptilolite, and E) backscatter electron image showing discrete analcime crystals, various stages of clinoptilolite dissolution, and clinoptilolite replacement by analcime.

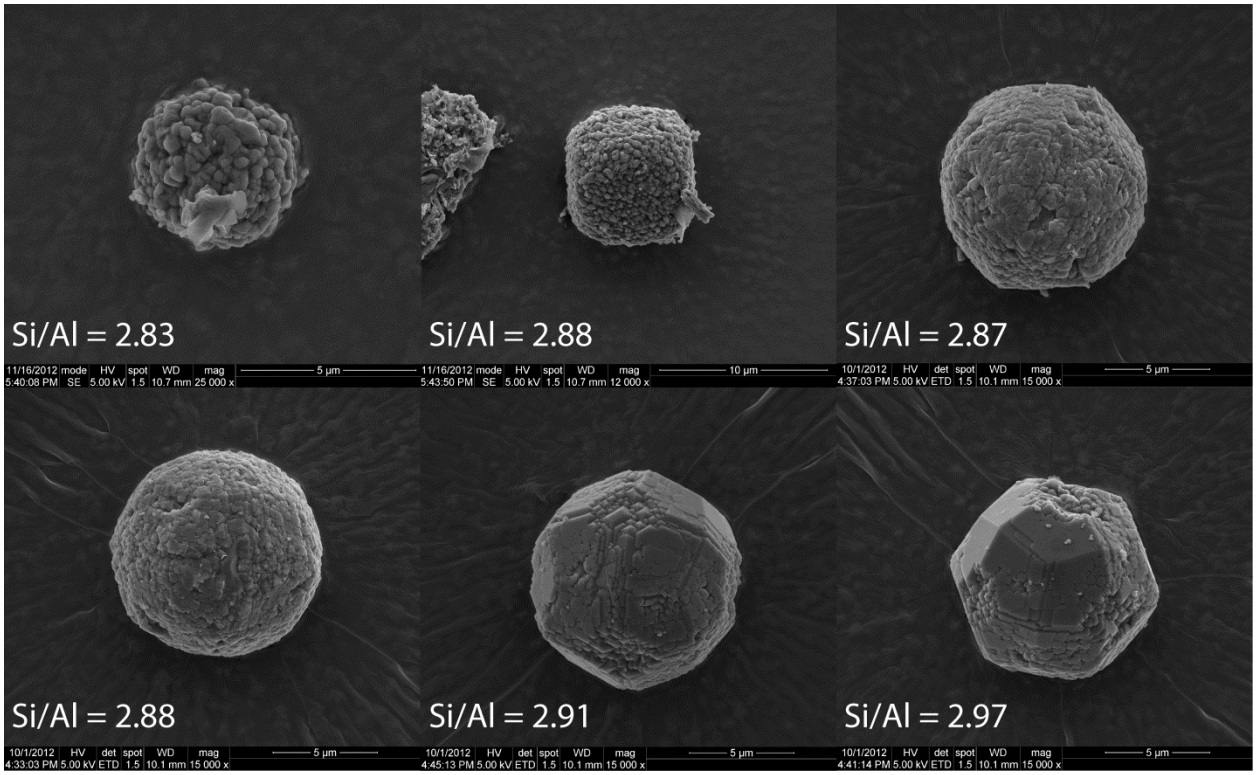

Figure 6. Analcime growth stages associated with a systematic Si/Al changes. Anhedral analcime formed initially as an agglomeration of nano-sized, spherical crystals followed by ripening of analcime nuclei to subhedral, trapezohedral analcime.

Aqueous geochemistry

Changes to the solution chemistry are fairly consistent between the different EBS experiments. There is an exchange of Na^+ for K^+ in the solution most likely controlled by the cation exchange capacity of both the Na-smectites and clinoptilolite (Figure 7a and 8a). This cation exchange yielded ~ 451 mg/L Na^+ enrichment and ~ 542 mg/L K^+ depletion in solution producing a K+ enriched montmorillonite. There is also a decline in the Ca^{2+} aqueous concentrations (~76 mg/L) during experiments mostly due to montmorillonite exchange.

Silica activity stays saturated with respect to cristobalite as the temperature increases (Figures 7b and 8b). Silica concentrations increase in increments closely following the temperature profile of the ramped heating cycle, indicating that silicate mineral dissolution is closely tied to the reaction temperature (Figure 7b). During the 300 °C experiments, silica (Si) concentrations rapidly increase to ~500 mg/L and remained fairly steady for the experiment

duration. Partial smectite dissolution and clinoptilolite alteration are the most likely controls on the silica activity.

Sulfur evolution is complicated by the occurrence of multiple redox states and interaction with metal plates. Sulfur concentrations during the ramped experiments increased from ~47 mg/L to ~125 mg/L until reactions temperatures reached 300 °C, when sulfur values dropped to ~46 mg/L (Figure 9a). During the 300 °C experiments, sulfur concentrations steadily climbed to a ~191 mg/L. Aluminum concentrations tend to increase in increments closely following the temperature profile during the ramped heating cycle (Figure 9b). The changes in aluminum concentration are similar to the observed changes in the silica concentration. During the 300 °C experiments, aluminum concentrations rapidly increase to ~1.5 to 3.5 mg/L. After the initial increase the aluminum concentrations slowly decreased. The decrease is likely related to the crystallization of analcime, fibrous illite, and feldspars.

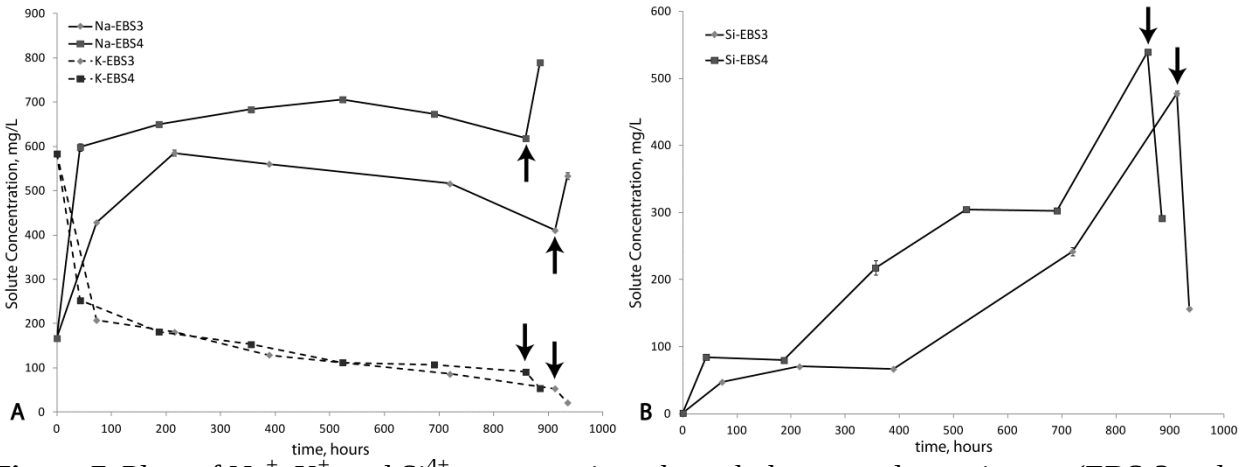

Figure 7. Plots of Na^{+}, K^{+}, and Si^{4+} concentrations through the ramped experiments (EBS-3 and EBS-4) showing evolution of solutes in contact with bentonite. Quenching experiment to room temperature (black arrows) significantly changes the solution chemistry. Note silica precipitation upon quenching.

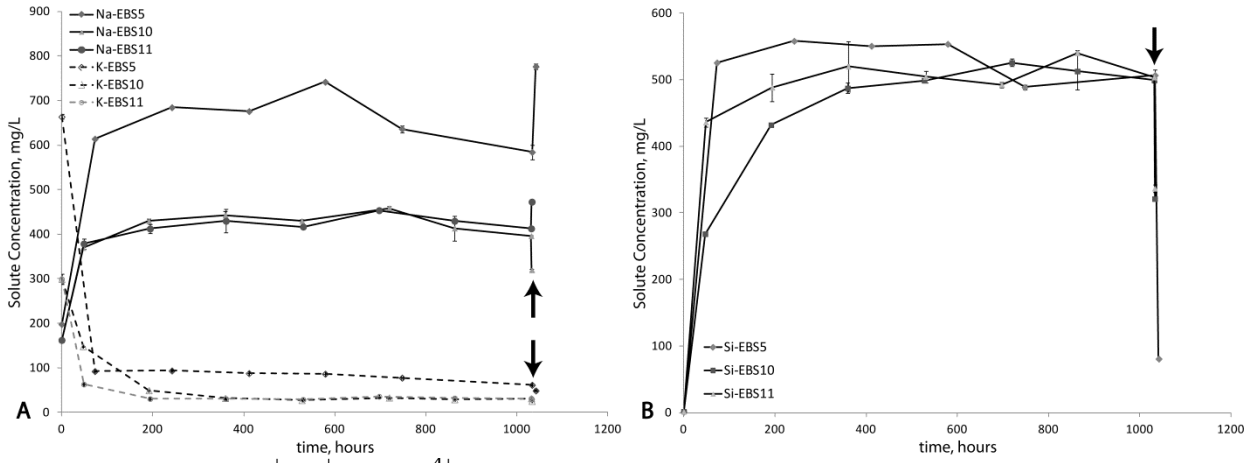

Figure 8. Plots of Na^{+}, K^{+}, and Si^{4+} concentrations through the isothermal 300 °C long-term experiments (EBS-5, EBS-10, and EBS-11) showing evolution of solutes in contact with bentonite. Quenching experiment to room temperature (black arrows) significantly changes the solution chemistry. Note silica precipitation upon quenching.

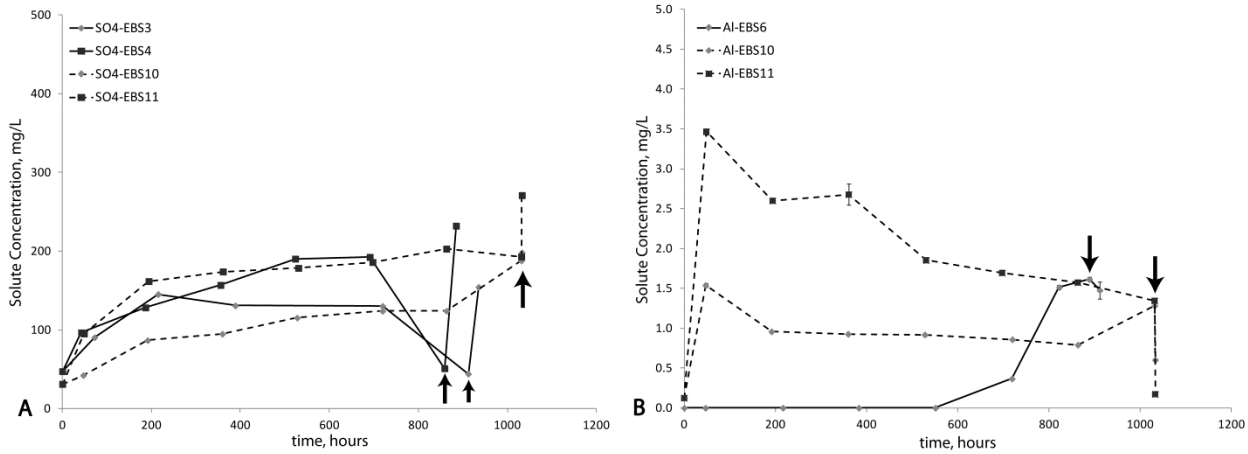

Figure 9. Sulfate (left) and aluminum (right) solution chemistry evolution during the ramped and isothermal experiments. Quenching experiment to room temperature (black arrows) significantly changes the solution chemistry.

Metal-Bentonite Interface

Steel reaction with bentonite

304 SS. The initial 304 SS (NIST SRM 101g) is an iron alloy primarily with 18.46 wt.% Cr, 10.00 wt. % Ni, 1.08 wt. % Si, and 0.029 wt.% Cu. 304SS underwent uniform interface reaction during the ramped and isothermal, 300 °C experiments. Post-reaction 304 SS formed a layer of smectite and chlorite covering the surface of the steel plate (Figure 10). However, smectite was the only phyllosilicates associated with the reaction site products in the six week,

300 °C reaction (Figure 11). The primary type smectite associated with the steel surface appears to be an Fe-saponite. Smectite expands upon ethylene glycol saturation to 16.8 Å (with 002 at 8.35 Å) suggesting no significant amount of mixed-layering is present. Pentlandite ((Cu, Ni, Fe)-sulfide) appears to have formed sparingly in both 304 SS experiments along with an unknown fibrous material (Figure 12A and B). The smectite and chlorite morphologies tend to be fairly consistent producing a bladed to micaceous habit with a rose-like texture (Figure 12). The initial montmorillonite has a distinctly different foily morphology (Figure 12C) suggesting smectite associated with the 304SS is newly formed. The interface reaction products have thicknesses ranging from 9 to 44 μm with crystallites occurring perpendicular to 304SS substrate (Figures 12D and 13). There was no significant change in the interface layer thicknesses with increased reaction time at 300 °C. Chemical analyses of post-reaction 304SS and the smectite mantle indicates there was a slight Fe leaching from the 304SS forming a Cr-enriched steel outer layer and a Fe-rich smectite and chlorite coating (Figure 13). The reaction products do include varying degrees of Cr and Ni substitutions. Accurate chemical formula for the interface reaction products are not possible due to the intimate mixing of multiple phases. The average bulk chemistry of the corrosion layer is provided in Table 6. Fe-rich phyllosilicates that formed on steel plates in the ramped experiments have two 06ℓ diffraction bands 1.536 and 1.523 Å (9.138 and 9.216 Å b-parameters), corresponding to trioctahedral chlorite and smectite (Figure 21). It is uncertain which minerals species correspond to the b-parameters as there is overlap in the unit-cell parameters between the Mg, Fe-saponites (9.120 (Mg^{2+}) to 9.30 (Fe^{2+}) Å) and chlorite (9.228 to 9.294 Å) species (Kohyama et al. 1973; Moore and Reynolds 1997). The Fe-smectite produced in the six week, 300 °C experiment has a 1.547 Å (9.282 Å b-parameters) 06ℓ diffraction band, consistent with Fe-saponite (Kohyama et al. 1973).

	SiO_2	Al_2O_3	Cr_2O_3	FeO*	MnO	MgO	NiO	CaO	Na_2O	K_2O	Total
EBS-2	33.47	13.14	1.25	31.03	0.38	1.98	1.26	1.31	1.60	0.62	86.04

Table 6. Bulk chemical composition from the 304 SS corrosion layer developed from the ramped heating cycle (EBS-2)

316SS. The initial 316 SS (NIST SRM 160b) is an iron alloy primarily with 18.37 wt. % Cr, 12.35 wt. % Ni, 2.26 wt. % Mo, 1.619 wt. % Mn, 0.5093 wt. % Si, and 0.175 wt. % Cu. 316 SS underwent exfoliation corrosion during the ramped and isothermal, 300 °C experiments. Post-

reaction 316 SS formed smectite dominated interface reaction products with some chlorite covering the surface of the steel plate (Figure 14). However, smectite was the only phyllosilicates associated with interface reaction products in the six week, 300 °C reaction (Figure 15). The primary type smectite associated with the steel surface appears to be an Fe-saponite. Smectite expands to 16.8 Å (with 002 at 8.44 Å) upon ethylene glycol saturation suggesting no significant amount of mixed-layering is present. However, the six weeks, 300 °C smectite product expands to 16.3 Å (002 at 8.25 Å) upon ethylene glycol saturation indicating a possible decrease in swelling capacity. A pentlandite-like ((Cu, Ni, Fe)-sulfide) material appears to have also been formed in both 316 SS experiments along with what appears to be fibrous sulfides (Figure 16 A, B, and D). The smectite and chlorite morphologies tend to be fairly consistent producing a bladed to micaceous habit with a rose-like texture (Figure 16). The interface reaction products have thicknesses ranging from 20 to 40 μm with crystallites occurring perpendicular to 316 SS substrate (Figures 16 and 17). There was no significant change in the interface reaction layer thicknesses with increased reaction time at 300 °C. Chemical analyses of post-reaction 316 SS and mantling products indicates there was significant Fe leaching from the 316 SS forming a Cr-enriched steel outer layer up to 4 μm thick. The Cr-enriched layer also underwent oxidation and sulfidation producing a noticeable alteration zone (Figure 17). Smectite and chlorite coatings were enriched in iron most likely from the iron leached from the 316 SS (Figure 17). Fe-rich phyllosilicates that formed on steel plates in the ramped experiments have 06ℓ diffraction bands 1.535 (9.210 Å b-parameters), corresponding to a trioctahedral phyllosilicate (Figure 21; Kohyama et al. 1973; Moore and Reynolds 1997). It is uncertain which minerals species correspond to the b-parameters, however the b-parameter is probably related to an Fe-saponite due to a smectite dominance in the corrosion products. The Fe-smectite produced in the six week, 300 °C experiment has a fairly broad 1.54 Å (9.24 Å b-parameters) 06ℓ diffraction band, consistent with Fe-saponite (Kohyama et al. 1973).

Low-carbon steel. The initial low-carbon steel contains 0.19 wt. % Cr, 0.16 wt. % Ni, 1.07 wt. % Mn, 0.24 wt. % Si, and 0.30 wt. % Cu. Low-carbon steel underwent pitting corrosion during the ramped and isothermal, 300 °C experiments. Post-reaction low-carbon steel developed a smectite coating the steel plate surfaces (Figures 18 and 19A). Unlike the 304SS and 316SS, there was no evidence of any chlorite phases present in the interface reaction product of the low-carbon steel. The primary type smectite associated with the steel surface appears to be an Fe-

saponite. Smectite expands to 16.6 Å (with 002 at 8.32 Å) upon ethylene glycol saturation suggesting no significant amount of mixed-layering is present (Figure 18). Also, pyrrhotite ($Fe_{1-x}S$) platelets formed concurrently with the smectite phases as determined their spatial distribution (Figure 19C). Smectite morphology is varied between a honeycombed texture and rose-like texture with a bladed to micaceous habit (Figure 19B and D). In addition to the small scaled textures, there is an overlying botryoidal texture with the interface reaction products (Figure 19C). These interface reaction products have thicknesses ranging from 13 to 56 μm with additional ~ 7 μm corrosion pits. The bladed to micaceous crystallites tend to occur with the longer dimensions perpendicular to the steel substrate (Figures 19 and 20). Chemical analyses of post-reaction low-carbon steel and interface reaction products indicate no chemical fractionation associated with the phase transformation process. Accurate chemical formula for the interface reaction products are not possible due to the intimate mixing of multiple phases. The average bulk chemistry of the interface reaction layer is provided in Table 7. There does appear to be oxidation and sulfidation associated with the surface (Figure 20). Smectite is enriched in iron most likely due to the iron dissolved from the steel (Figure 20). The Fe-rich smectite has 06ℓ diffraction bands of 1.547 Å (9.264 Å b-parameters), corresponding to a trioctahedral smectite (Figure 21; Kohyama et al. 1973; Moore and Reynolds 1997).

	SiO_2	Al_2O_3	Cr_2O_3	FeO*	MnO	MgO	NiO	CaO	Na_2O	K_2O	Total
EBS-6	36.00	12.80	0.02	33.75	0.22	0.83	0.01	0.64	1.02	0.35	85.63

Table 7. Bulk chemical composition (EMPA) from the low-carbon corrosion layer developed from the ramped heating cycle (EBS-6)

Copper reaction with bentonite

The initial copper foil appears to be 100% Cu (based on EDX analyses). The primary corrosion product for both types of experiments is chalcocite (Cu_2S) (Figures 22 and 23). Corrosion seems to take place with an initial dissolution of the copper developing dissolution features on the surface of the copper (Figure 24A). Chalcocite forms a hexagonal morphology ranging from discrete plates to completely coalesce patches on the copper surface (Figure 24A and C). Also, there are minor amounts of an unknown fibrous material associated with the copper surface (Figure 24B).

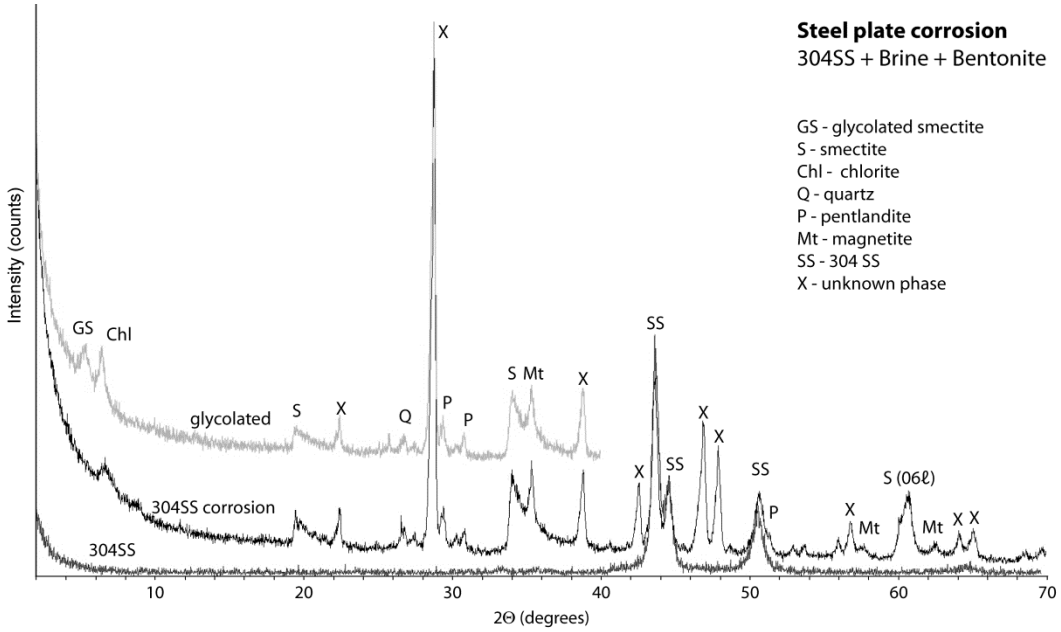

Figure 10. XRD patterns of the air-dried and ethylene glycol saturated corrosion products on the 304 SS plate used in the EBS-2 experiment. Smectite, chlorite, and a pentlandite-like material are the dominant interface reaction phases. Starting 304 SS XRD plot is also shown for comparison.

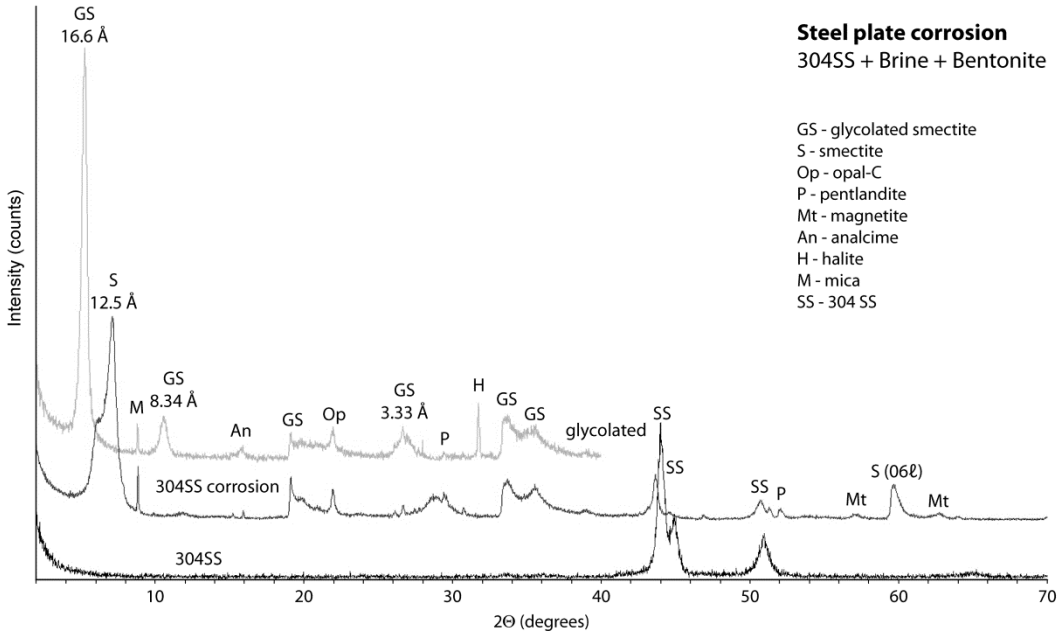

Figure 11. XRD patterns of the air-dried and ethylene glycol saturated corrosion products on the 304 SS plate used in the EBS-5 experiment. Smectite and a pentlandite-like material are the dominant interface reaction phases. Starting 304 SS XRD plot is also shown for comparison.

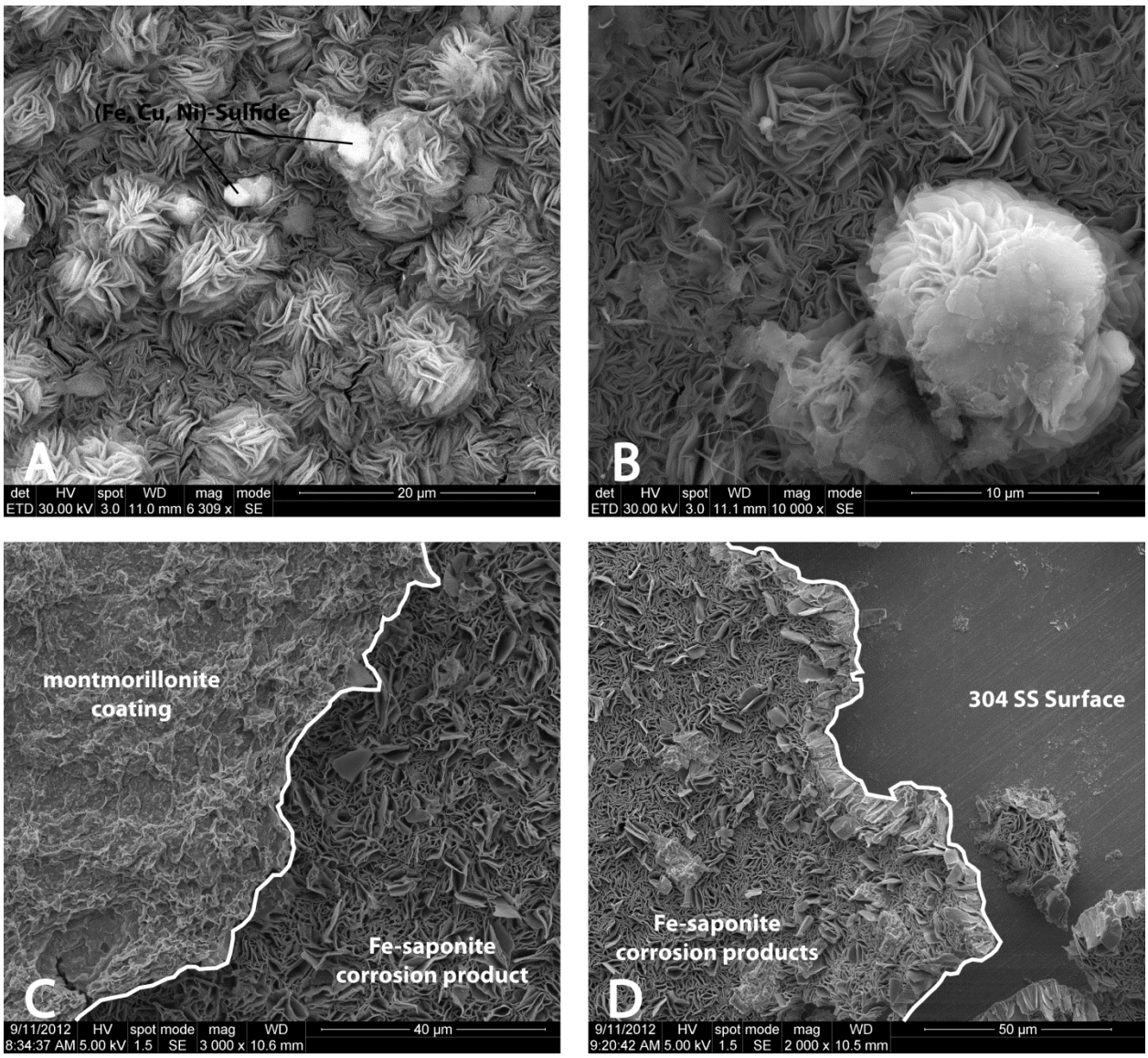

Figure 12. SEM image (plan view) of Fe-phyllosilicates (saponite and chlorite) using 304 SS as a growth substrate from both ramped (EBS-2) and isothermal, 300 °C (EBS-5) heating profiles. A) Fe-saponite and chlorite growths with later-stage pentlandite-like ((Fe, Cu, Ni)-sulfide) material from EBS-2. B) Unknown fibers overlaying rose-like Fe-saponite and chlorite interface reaction products from EBS-2. C) Montmorillonite coating on Fe-saponite showing the distinct morphology between the two smectites from EBS-5. D) Boundary between the Fe-saponite interface reaction product and 304 SS surface from EBS-5.

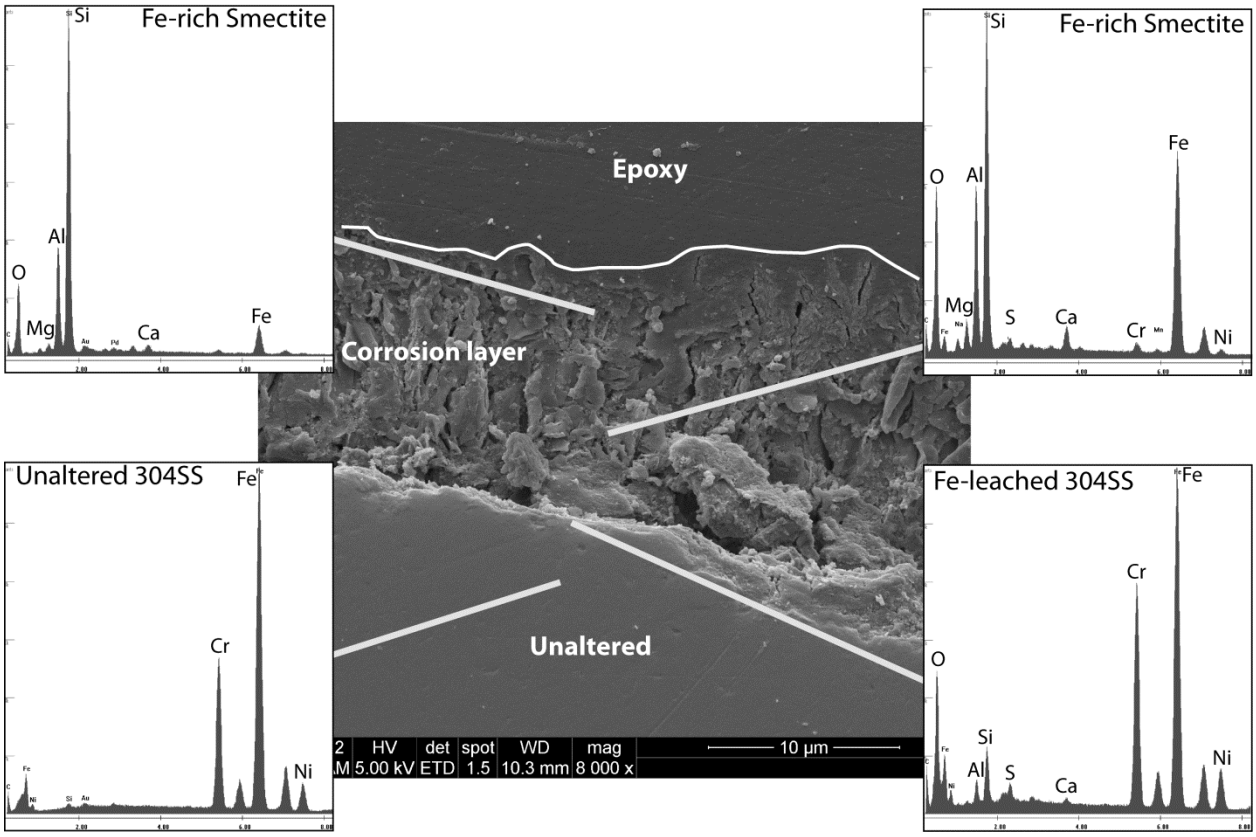

Figure 13. SEM image of 304 SS cross-section showing Fe-saponite interface reaction products using steel surface as a growth substrate. EDX analyses of post-reaction 304SS and interface reaction products indicates Fe is leached from the 304 SS forming a slightly Cr-enriched steel outer layer and an Fe-rich aluminosilicate (Fe-saponite/chlorite) coating. Uniform corrosion of the 304 SS does not appear to develop significant incongruent dissolution.

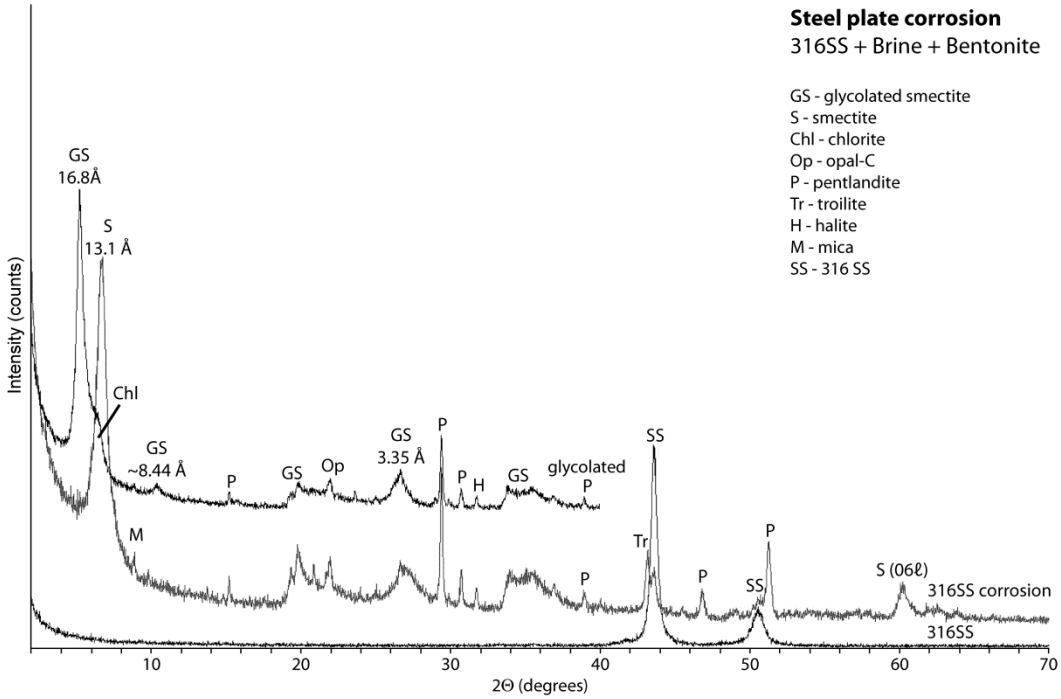

Figure 14. XRD patterns of the air-dried and ethylene glycol saturated interface reaction products on the 316 SS plate used in the EBS-3 experiment. Smectite, chlorite, and a pentlandite-like material are the dominant corrosion phases. Starting 316 SS XRD plot is also shown for comparison.

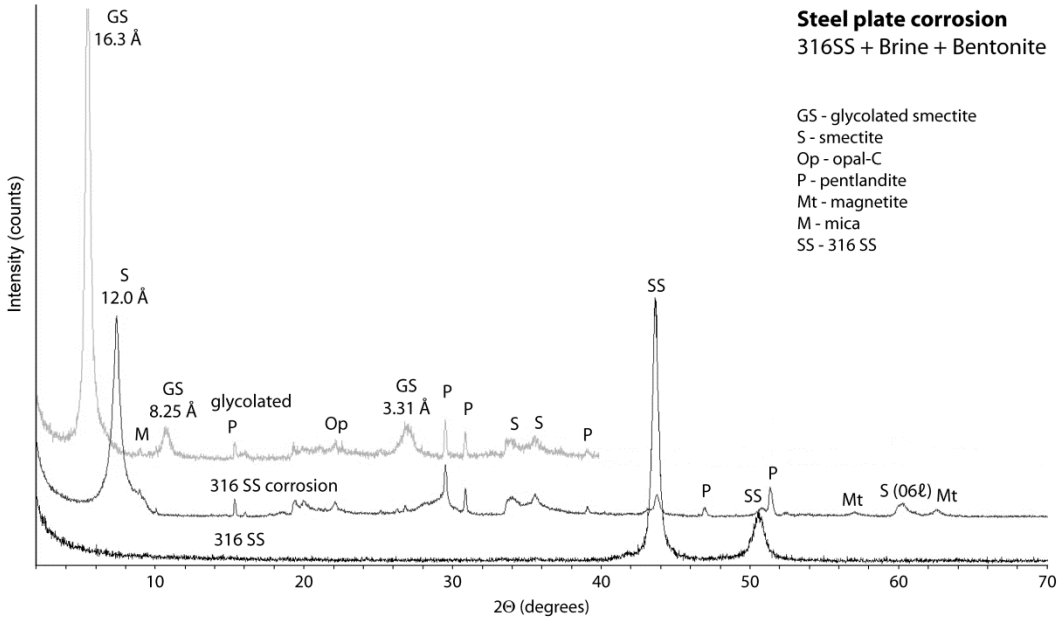

Figure 15. XRD patterns of the air-dried and ethylene glycol saturated interface reaction products on the 316 SS plate used in the EBS-10 experiment. Smectite and a pentlandite-like material are the dominant corrosion phases. Starting 316 SS XRD plot is also shown for comparison.

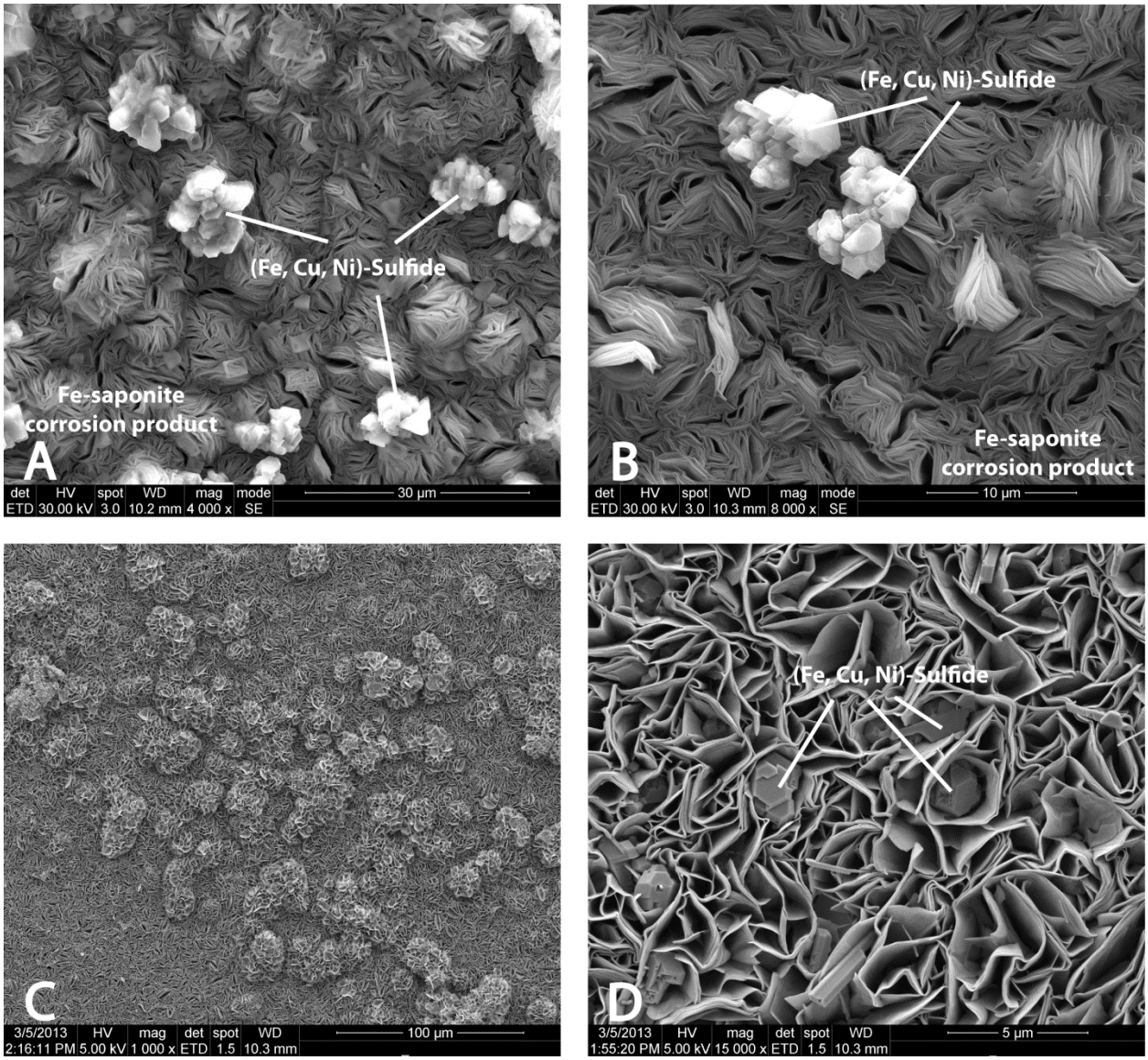

Figure 16. SEM image (plan view) of Fe-saponite using 316 SS as a growth substrate from both ramped (EBS-3) and isothermal, 300 °C (EBS-10) heating profiles. A) Dense growth of Fe-saponite and chlorite with late-stage pentlandite-like ((Fe, Cu, Ni)-sulfide) material from EBS-3. B) Close-up of pentlandite-like ((Fe, Cu, Ni)-sulfide) material on Fe-phyllosilicates from EBS-3. C) Honeycomb and rose-like textures associated with Fe-saponite interface reaction products from EBS-10. D) Fe-saponite rose-like texture with pentlandite-like materials occurring between Fe-saponite foils from EBS-10.

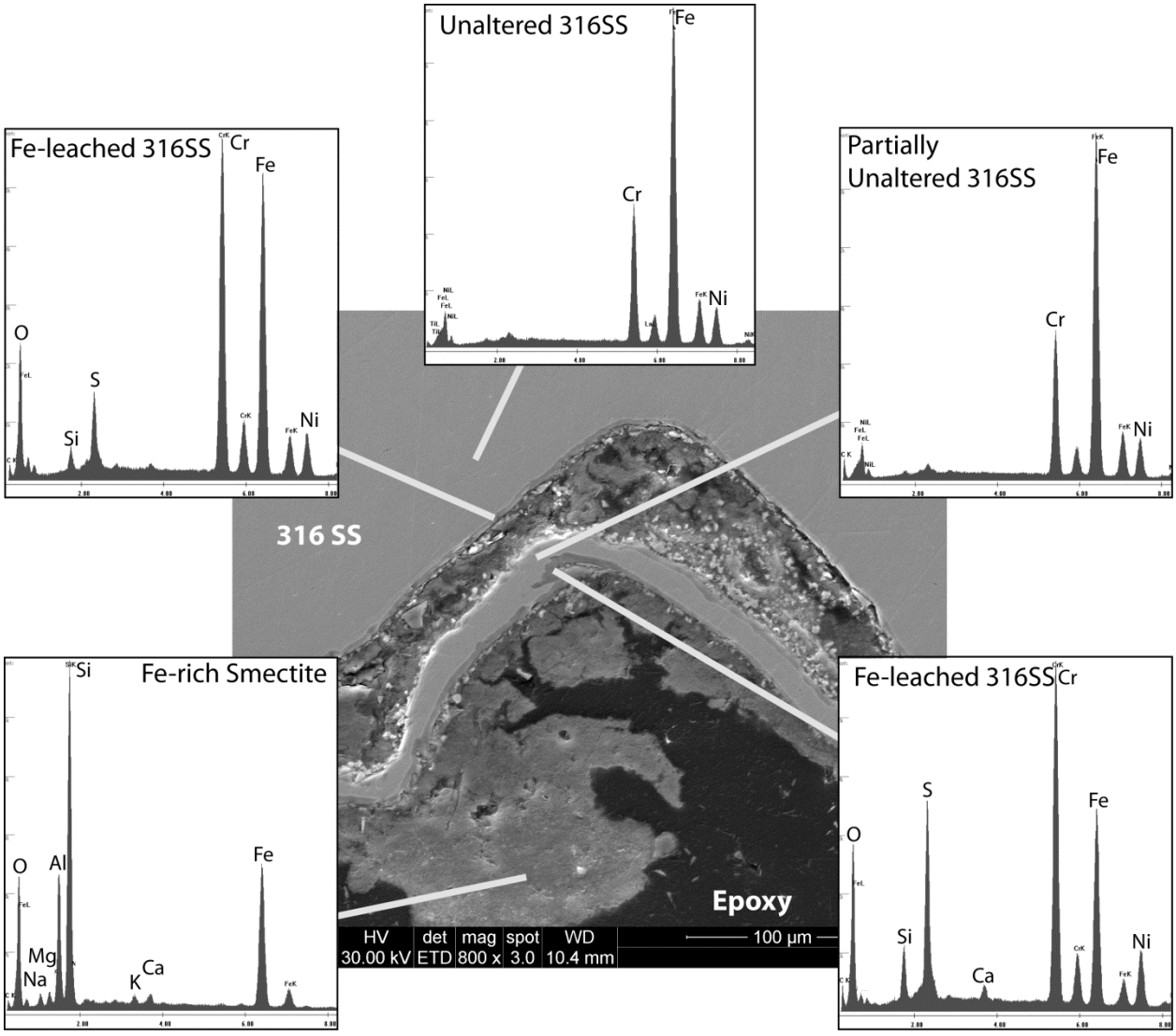

Figure 17. SEM image of 316 SS cross-section showing Fe-saponite/chlorite growth due to exfoliation corrosion from EBS-3. Chemical analyses of post-reaction 316 SS and interface reaction products indicates there was significant Fe leaching from the 316 SS forming a Cr-enriched steel outer layer up to 4 µm thick.

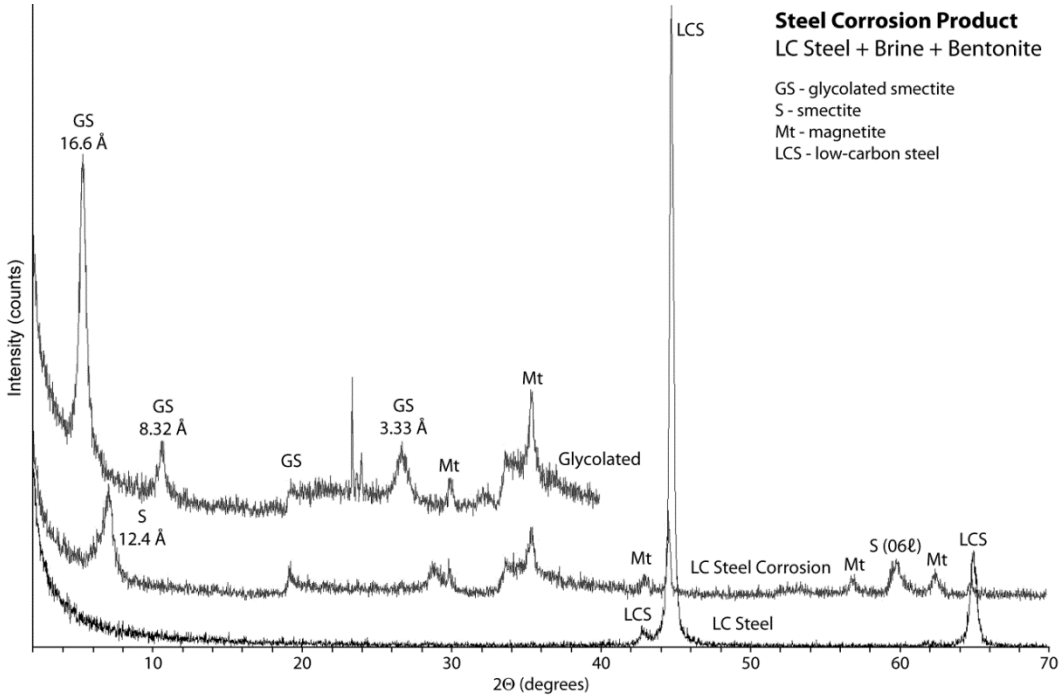

Figure 18. XRD patterns of the air-dried and ethylene glycol saturated interface reaction products on the low-carbon steel plate used in the EBS-6 experiment. Smectite is the dominant interface reaction phase. Magnetite is most likely from the starting magnetite materials used to control redox conditions. Initial low-carbon steel XRD plot is also shown for comparison.

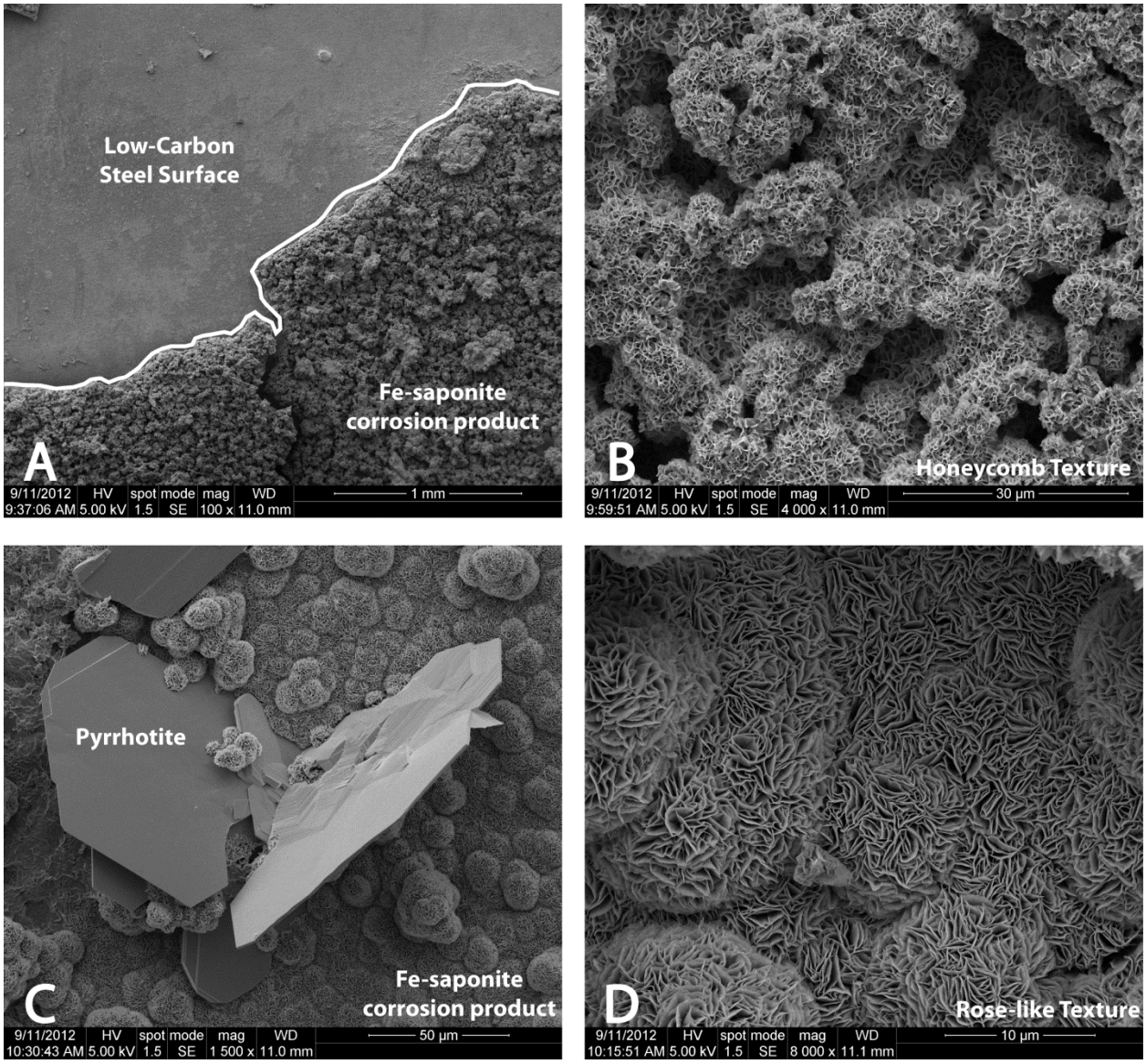

Figure 19. SEM image (plan view) of Fe-saponite growth on low-carbon steel from the ramped (EBS-6) heating experiment. A) Boundary between the Fe-saponite interface reaction product and low-carbon steel surface. B) Honeycombed Fe-saponite. C) Botryoidal Fe-saponite interface reaction product with pyrrhotite platelets from EBS-6. D) Rose-like texture of Fe-saponite.

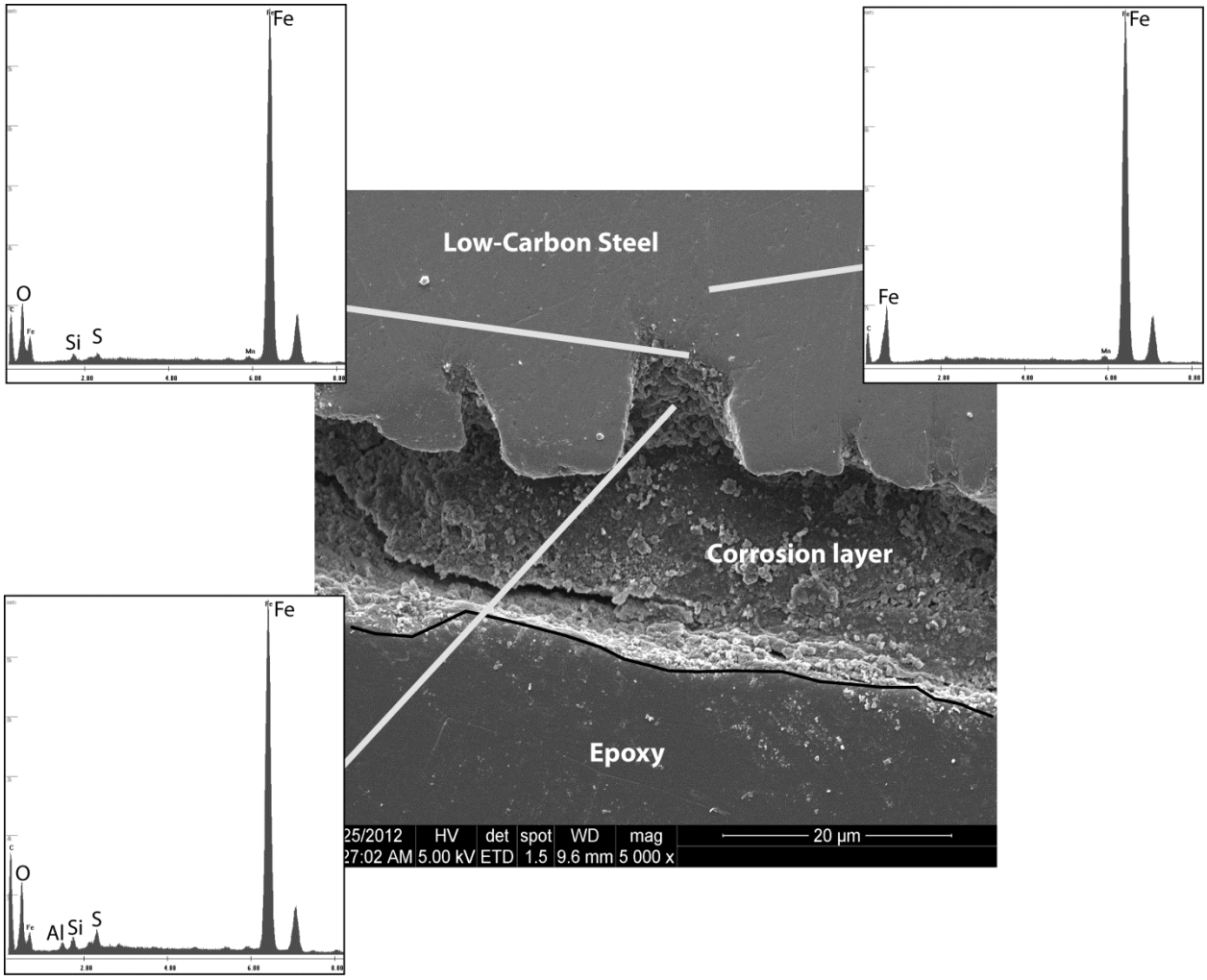

Figure 20. SEM image of low-carbon steel cross-section showing Fe-saponite reaction products using steel surface as a growth substrate. EDX analyses of post-reaction low-carbon steel and interface reaction n surfaces show a slight oxidation and sulfidation of the surface (probably due to oxide and sulfide precipitates). EDX composition of the reaction product was not collected due to erosion of Fe-saponite during sample preparation. Extensive pitting corrosion of the low-carbon steel occurs during the ramped experiments (EBS-6).

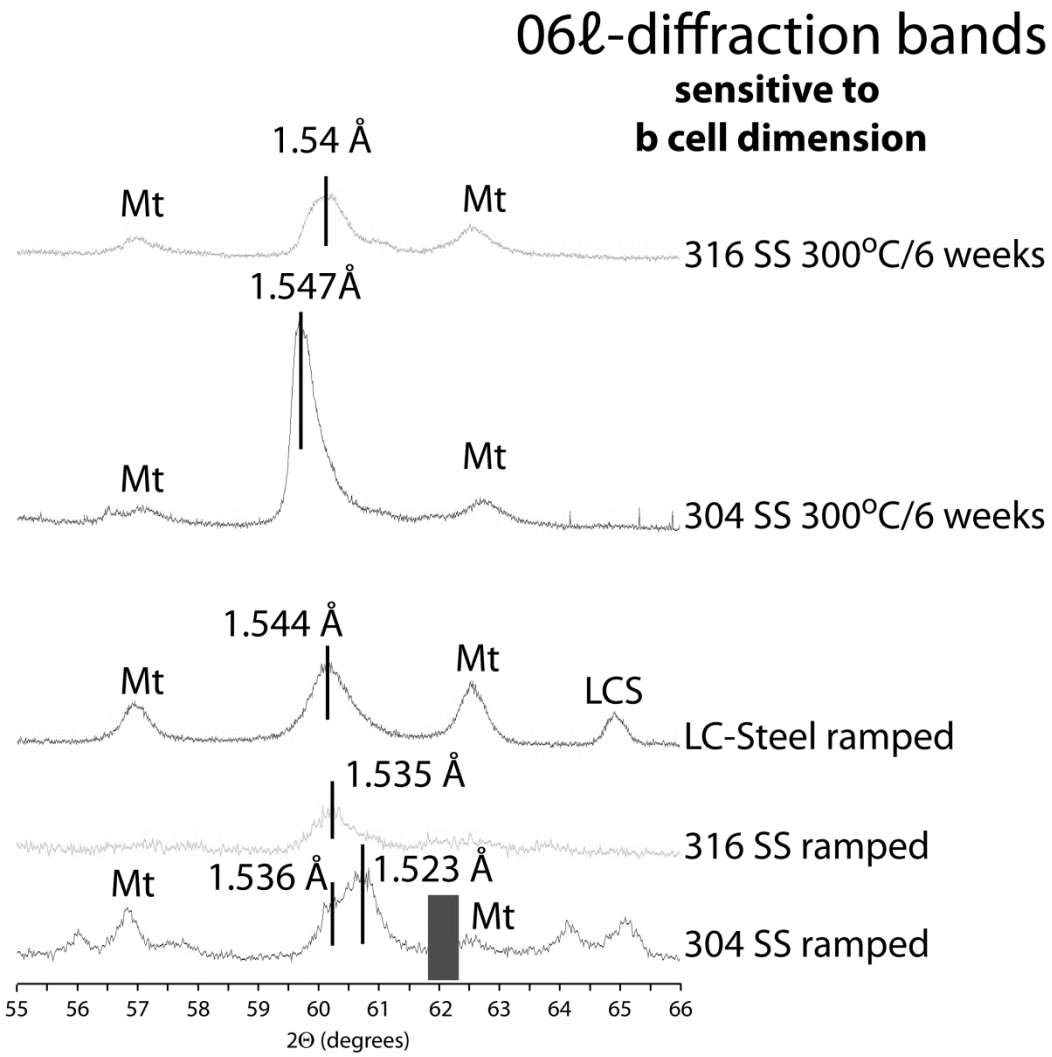

Figure 21. XRD plots of the 06l diffraction bands showing Fe-rich smectite and chlorite formed as a interface reaction product are trioctahedral. Montmorillonite (dioctahedral) typically has a 1.492 – 1.504 Å 06l band (black box). The smectite principally is a Fe-saponite with varying amounts of Ni and Cr substitutions. Contributions from magnetite (Mt) are probably from magnetite used in the initial experimental setup.

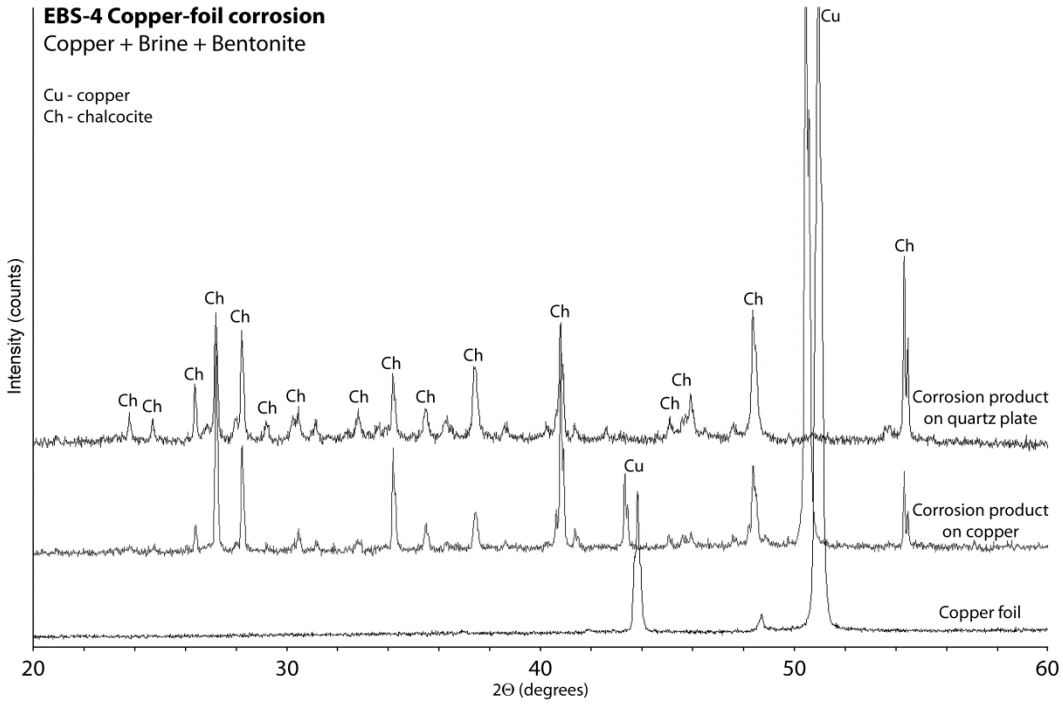

Figure 22. XRD plots for corrosion products on the copper foils used in the ramped heating experiment (EBS-4). Chalcocite (Cu_2S) is the principal corrosion phase.

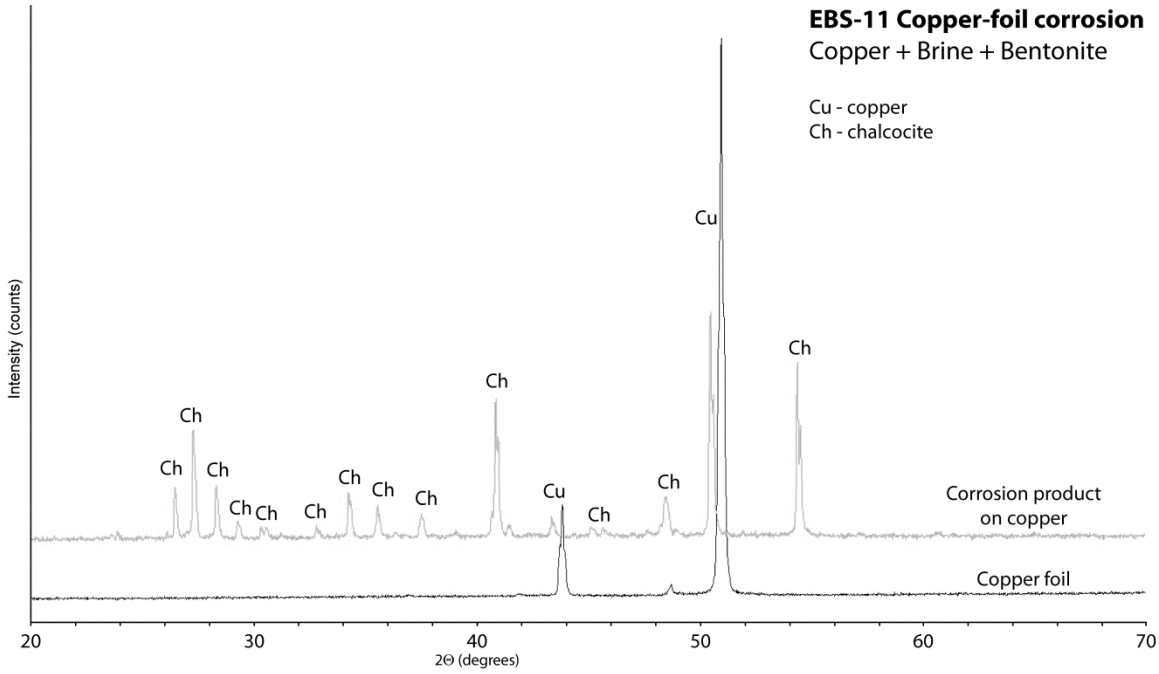

Figure 23. XRD plots for corrosion products on the copper foils used in the six week, 300 °C heating experiment (EBS-11). Chalcocite (Cu_2S) is the principal corrosion phase.

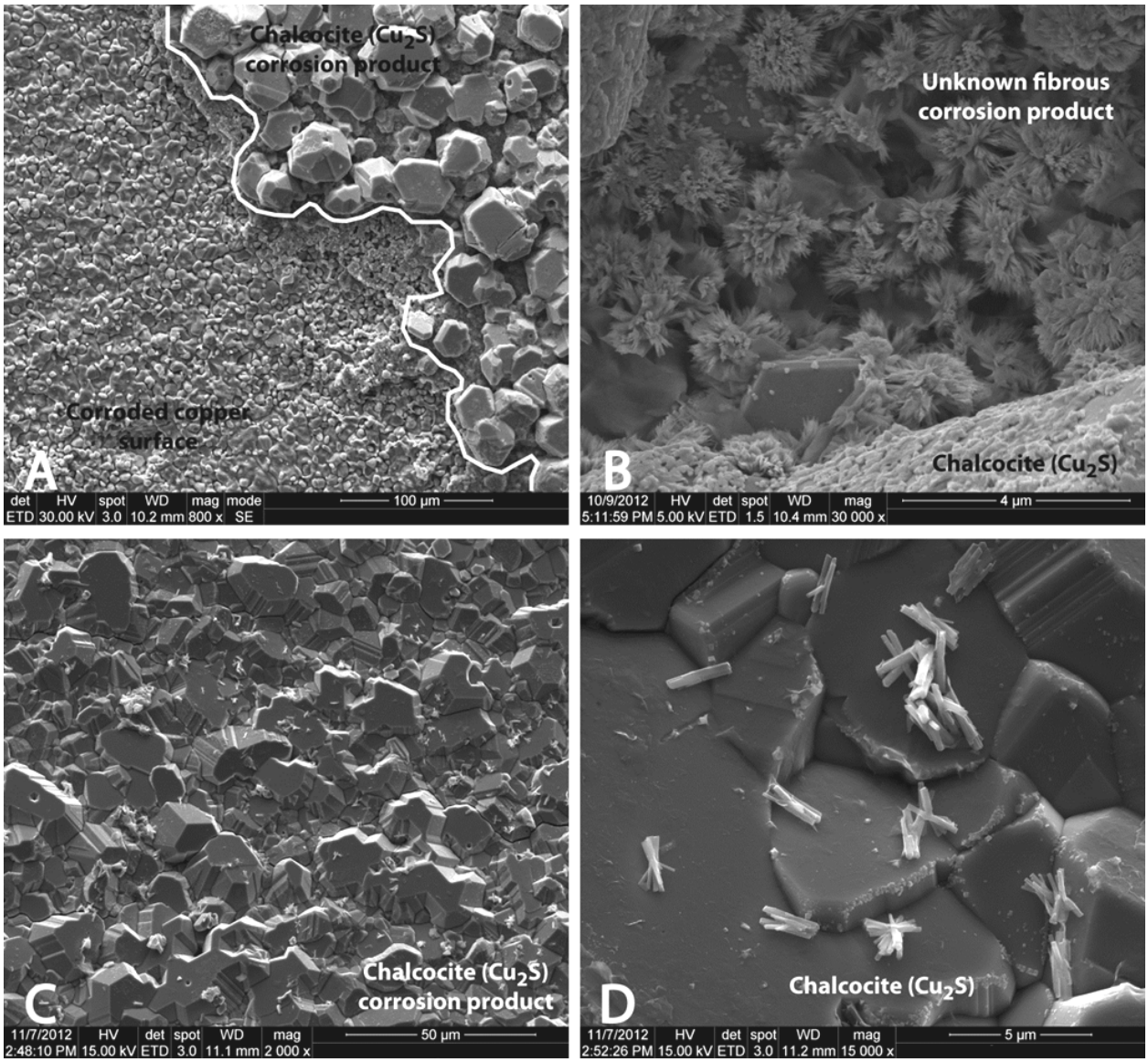

Figure 24. SEM image (plan view) of copper surface showing corroded copper surfaces and various interface reaction products from both ramped (EBS-4) and isothermal, 300 C (EBS-8) heating profiles. A) Boundary between the corroded copper surface and chalcocite (Cu_2S) from EBS-4. B) Unknown fibers occurring on the copper surface in between chalcocite growths from EBS-4. These fibers might be a late-stage oxide or chloride corrosion product upon depletion of sulfide. C) Intergrown chalcocite from EBS-8. D) Close-up of the chalcocite surface in Figure XXC showing unknown short rods with a radiating texture.

Discussion

Geochemical modeling

The collection of aqueous samples composition during the experiments allows examination of the effects aqueous composition evolution has on the mineralogical alteration. Both, aNa^+/aH^+ and aK^+/aH^+ values at 120 °C tend to be scattered, but converge to a single solution composition as the reaction progresses to 300 °C (Figures 25 and 26). The $SiO_{2(aq)}$ composition becomes saturated with respect to cristobalite beginning around 210 °C, but it appears montmorillonite and zeolite dissolution/alteration is controlling the silica activity.

The aNa^+/aH^+ and silica activities appear to be suitable for the clinoptilolite alteration and high-silicon analcime crystallization during the early reaction stages (Figure 25). However, this analcime formation was not observed until the long-term, 300 °C experiments, suggesting the delayed analcime formation appears to be a kinetic issue. Experimental work (Wilkin and Barnes 1998; Wilkin and Barnes 2000) indicates that analcime formation is significantly retarded at circum-neutral pH's and increased pressures.

The aK^+/aH^+ and silica activities early in the reaction plot within the K-clinoptilolite stability field, but the solution evolution shift the aqueous data into the illite ($K_{.85}Al_2(Si_{3.15}Al_{.85})O_{10}(OH)_2$) stability field (Figure 25). Much like the analcime formation, the solution chemistry imparts controls on the illitization rates. High sodium and silica activities along with limited aluminum availability probably retarded illite formation via a illite-smectite transition state. However, direct precipitation of fibrous illite appears to have occurred which is further supported by Figure 26.

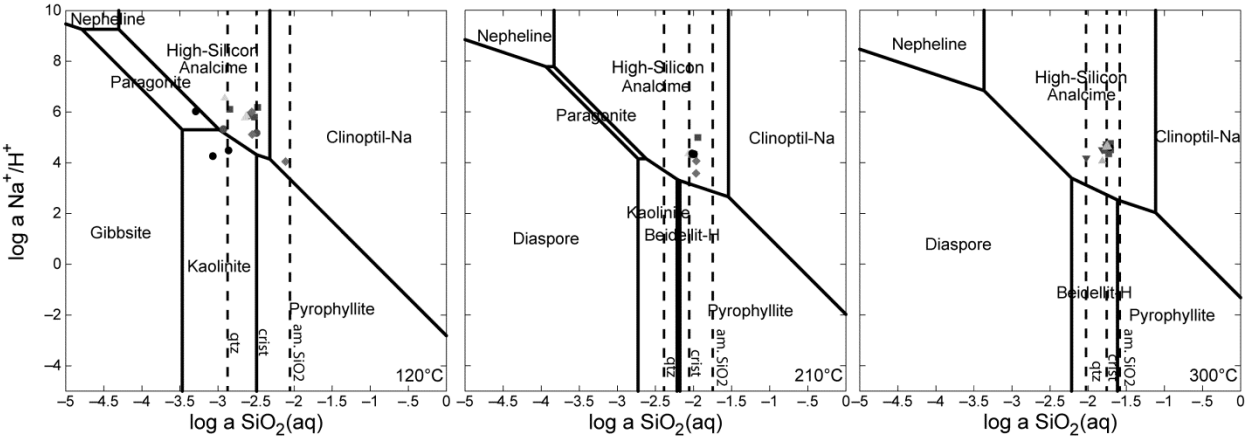

Figure 25. Log aNa^+/aH^+ and Log $aSiO_{2(aq)}$ data from the a) 120 °C solution chemistries, b) 210 °C solution chemistries, and c) 300 °C solution chemistries plotted on a Na-H_2O-SiO_2 phase diagram. Analcime thermodynamic data has been adjusted to a high-silicon analcime ($Na_{0.75}Al_{0.75}Si_{2.25}O_6 \cdot 1.13H_2O$) after Neuoff et al. (2004).

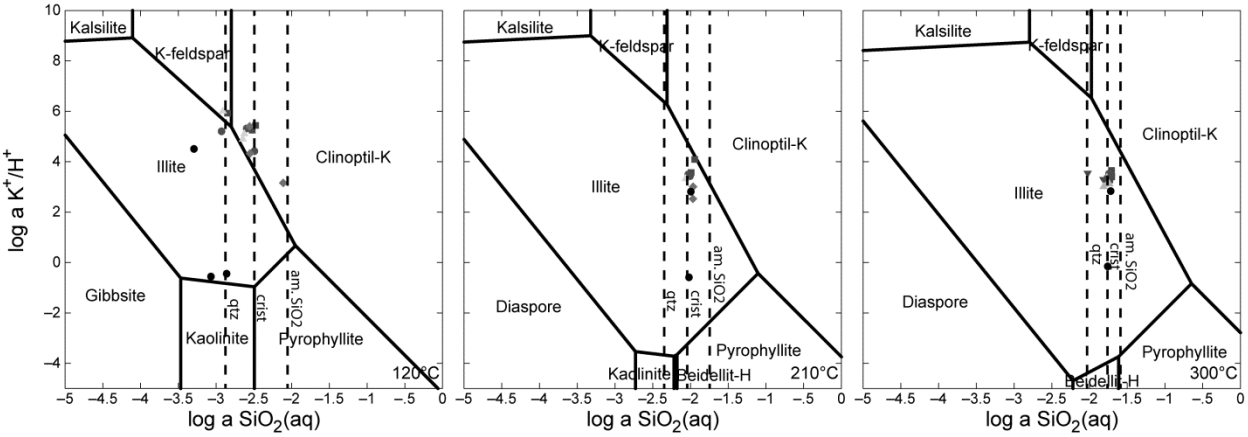

Figure 26. Log aK^+/aH^+ and Log $aSiO_{2(aq)}$ data from the a) 120 °C solution chemistries, b) 210 °C solution chemistries, and c) 300 °C solution chemistries plotted on a K-H_2O-SiO_2 phase diagram.

Absence of Smectite Illitization

There was no evidence of illite-smectite mixed-layering from any of the experiments conducted in this investigation. Many reports (Perry and Hower 1970; Reynolds and Hower 1970; Hower et al. 1976; Altaner 1989; Mosser-Ruck et al. 2001) indicate that smectite illitization occurs during diagenesis under elevated temperatures with a reactive K^+ source via the following reaction scheme (assuming aluminum conservation)

$$1.617\ Na_{0.33}(Al_{1.67}Mg_{0.33})Si_4O_{10}(OH)_2 + 0.90\ K^+ + 0.502\ H^+ \rightarrow$$

Na-montmorillonite

$$K_{0.90}(Al_{1.90}Mg_{0.10)}(Si_{3.20}Al_{0.80})O_{10}(OH)_2 + 3.268\ SiO_2 + 0.534\ Na^+ + 0.434\ Mg^{2+} + 0.868\ H_2O.$$

illite

This general reaction is believed to go through a sequence starting with a K-montmorillonite phase followed by various stages of illite-smectite mixed-layering leading into a discrete illite phase (Moore and Reynold 1997). It is evident that early in the experiments K^+ is exchanged into the montmorillonite interlayer generating a Na-rich solution. Changes in solution chemistry and mineralogical data indicate that 11 to 20 % of the exchangeable cations in the initial montmorillonite were replaced with K^+. Montmorillonite and clinoptilolite at this stage in the reaction appear to be buffering synthetic groundwater to high Na^+ and low K^+ activities. Maintaining relatively high Na^+ activity with a limited supply of K^+ has been shown in experimental data (Eberl and Hower 1977; Eberl et al. 1978; Roberson and Lahann 1981; Mosser-Ruck et al. 1999) to significantly retard smectite illitization rates. The cation exchange reactions associated with montmorillonite and clinoptilolite appear to be facilitating illitization retardation.

However, experimental results from Whitney and Velde (1993) and Mosser-Ruck et al. (1999) show K-saturated Wyoming montmorillonite in a Na-rich solution can still produce an I/S with about 29 to 40 % non-expandable (illitic) component under the same time and temperature parameter of the current investigation. These results indicate that even in a Na-rich system, illitization still can occur provided there is a sufficient K^+ supply available in the system (i.e., K-bearing minerals). An example of this process has been argued that the observed smectite illitization in the Gulf Coast sediment is tied directly to the availability of K^+ from the dissolution of K-feldspars (Hower et al. 1976). Bulk K_2O content in Gulf Coast sediments tend to range from 2.27 to 3.68 wt. % with K_2O concentrations increasing (1.98 to 5.65 wt. %) in the < 0.1 μm size fraction (Hower et al. 1976). However, there is much less K_2O associated with the bentonite (0.572 wt.%) used in this investigation with even less K_2O (0.174 wt.%) in the < 2 μm

fraction. It is uncertain if this is enough K_2O to overcome the Na-rich system. If there is an external source of K^+ (e.g., host rock or groundwater) then illitization possibly could proceed.

There have been no satisfactory explanations as to why K^+ is necessary for illitization reactions to proceed, considering illitic materials are defined by the layer charge, in which the interlayer cations have no direct control over the layer charge (Moore and Reynolds 1997). Illitic materials have an increased layer charge (z ~ 0.6 - 0.9) compared to montmorillonite (z ~ 0.2 – 0.6) due to higher amounts of Al-substitution into the tetrahedral sheet (Moore and Reynolds 1997). In fact, there have been numerous reported occurrences (Bannister 1943; Frey 1969; Środoń 1999) of Na-illite (i.e., brammalite) and ordered Na-I/S (~0.80 illite) in nature. This leads to the question as to why the presence of Na^+, Ca^{2+}, Mg^{2+} significantly retards the illitization rates, whereas K^+ facilitates illitization. However, experimental data does indicate Na-illite and Na-I/S start reacting at much higher temperatures than those at which K^+ equivalents react (Eberl and Hower 1977; Eberl 1978). In light of this evidence, illitization is probably not directly related to K^+, Na^+, Ca^{2+}, or Mg^{2+} concentrations, but these elements likely have an indirect influence by changing the minerals' phase equilibria.

Solutions saturated with respect to cristobalite probably contributed to the illitization retardation. The silica activity in these experiments is controlled by silicate mineral dissolution and alteration. Systems with high silica activity should have a significant influence on illitization rates because illite formation is sensitive to Al^{3+} and Si^{4+} concentrations. But, it is important to consider the difference between closed systems such as these experiments versus repositories environments that are open to the surrounding environment. Many processes that are described above might be mitigated in an open system where solutes can move in and out of the environment.

Authigenic Illite

Even though there is an absence of illite-smectite mixed layering there is direct evidence that fibrous illite directly crystallized from solution. The formation controls of fibrous illite are not well understood, but has been suggested that high silica activities, slightly alkaline to mildly acidic solution, and rapid crystallization facilitates the formation of a fibrous morphology (Small

et al. 1992). Additionally, it has been suggested that fibrous illite is partially due to organic sorption on the (010) faces poisoning growth along [010] direction and forcing crystallization in the [100], [$\bar{1}$10], and [$\bar{1}\bar{1}$0] directions (Small et al. 1992; Small 1993; Güven 2001). However, these fibrous illites are metastable in the illite growth phase and will eventually ripen into a more stable platy morphology (Small et al. 1992).

Clinoptilolite-to-analcime transformation

We have shown that at higher silica activities (i.e., cristobalite saturation) clinoptilolite is altered to a high-silica analcime (Si/Al ~2.89) under experimental repository conditions. This zeolite alteration reaction has not been observed within a bentonite under repository-type experiments. Previous studies (Smyth 1982; Kerrisk 1983; Duffy 1984; Bish and Aronson 1993; Chipera and Bish 1997; Wilkin and Barnes 1998; 2000; Bish et al. 2003; Cheshire et al. 2013) have linked changes in Na^+, Al^{3+}, and Si^{4+} activities with the replacement of clinoptilolite with analcime. Increased Na^+ activity under elevated temperatures (T > 84 °C) has been suggested to promote alteration of clinoptilolite to analcime (Smyth 1982). Alternatively, it has been argued (Kerrisk 1983; Duffy 1984; Bish and Aronson 1993) that when silica activity is saturated with respect to quartz, clinoptilolite is destabilized compared to analcime. They (Kerrisk 1983; Duffy 1984; Bish and Aronson 1993) also suggested that when silica activity is cristobalite or opal saturated, clinoptilolite is the more stable phase and analcime will not crystallize. However, experimental work from Wilkin and Barnes (1998) indicate silica activity influences clinoptilolite alteration by affecting the reaction affinity rather than controlling the reaction equilibrium. Wilkin and Barnes (1998) show that analcime can form in an environment saturated with respect to cristobalite provided there is a sufficient change in the Na^+ and/or Al^{3+} activities. Natural paragenetic sequences suggest that clinoptilolite to analcime may progress at temperatures as low as 75 - 90° C (Smyth 1982; Masuda et al. 1996), the current study produced analcime formation only during the long-term, 300° C experiments. Reaction kinetics in nuclear repository conditions is an important variable that needs to be further considered. Analcime might form in the low-temperature experiments with longer reaction times. Evolution of zeolites associated with bentonite has been suggested (Masuda et al. 1996) to be a major factor in the stability of smectite through the control of pore-water chemistry. Solubility and kinetic studies

on clinoptilolite and analcime show that at higher pH's (9 - 10) solutions saturated with respect to analcime rapidly precipitate analcime with rates varying from 0.067 μm/h (138 bar) to 0.016 μm/h (345 bar) at 175^{o} C. (Wilkin and Barnes 2000) However, analcime growth rates were significantly retarded at circum-neutral pH's, to the point no analcime was observed during experiments lasting up to 26 days with temperatures > 100° C. (Wilkin and Barnes 1998) Analcime retardation at circum-neutral pH's could explain the lack of analcime formation in the ramped experiments, which were only at 300° C for 1 week and consistently obtained pH values of 6 – 7.

Silica is released during clinoptilolite alteration, thereby contributing to authigenic silica mineral formation (e.g., cristobalite, opal-C, quartz). There is a ~ 17 % volume (assuming quartz formation) decrease associated with analcime crystallization. Given that there is a ~ 13 wt. % clinoptilolite in the bentonite, a clinoptilolite-to-analcime volume loss will translate into ~ 2% volume loss in the bulk bentonite. It is uncertain how much volume loss will be recovered in response to the montmorillonite swelling due to the water loss in the zeolite alteration reaction. Additionally, analcime and feldspar formation sequesters aqueous Al^{3+}, thereby potentially limiting illitization. Aluminum availability, in addition to silica, alkali, and alkaline earth activities, probably is a crucial step for the long-term stability of bentonite-based engineered barriers.

Sulfide destabilization

Production of $H_2S_{(aq,g)}$ is most likely related to pyrite solubility in a chloride-bearing solution (Crerar et al. 1978; Ohmoto et al. 1994).

$$FeS_{2(s)} + 2H^{+} + nCl^{-} + H_2O_{(aq)} \rightarrow FeCl_n^{2-n} + 2H_2S_{(aq,g)} + ½O_2$$

The highly reducing nature of the experimental system easily preserves the $H_2S_{(aq,g)}$ species. Sulfide-induced corrosion of the waste canisters is the primary concern in repository systems (Börjesson et al. 2010). The Swedish Nuclear Fuel and Waste Management Company (SKB) have emplaced fairly strict sulfur specifications (sulfide content < 0.5 wt.%; total sulfur < 1 wt.%) for the bentonite buffer used in their repositories (Börjesson et al. 2010).

Metal-bentonite reaction interface

Results from these experiments have shown the more dynamic environment associated with this system is at the bentonite-metal interface. Fe-rich phyllosilicates (i.e., trioctahedral, Fe-rich saponite and chlorite) are crystallized on steel surfaces forming a reactive substrate with a high surface area compared to the original steel surfaces. Alternatively, chalcocite (Cu_2S) crystallized on the copper surfaces due to available H_2S from the decomposition of pyrite in the hydrothermal environment. It is evident that the formation of these surface bound minerals is from the direct crystallization from solution in the localized environments surrounding the metal plates. However, it is not yet well documented to what extent these authigenic minerals will have an effect on the repository system.

Synthetic Fe-saponites have been crystallized in dilute solutions and gels of silica, Fe-, Al-chlorides at temperatures up to 850 °C and pHs of 8.5 – 9.5 (Kloprogge et al. 1999). This is consistent with a partial dissolution of the steel plates contributing ferrous iron into a fluid phase with silica and aluminum, thereby facilitating Fe-saponite (smectite) crystallization with the steel surfaces acting as a growth substrate. Further, Fe-saponite alteration into chlorite has been suggested (Mosser-Ruck et al., 2010) in the presence of ferrous iron at temperatures approaching 300 °C and near-neutral pHs. The lack of chlorite consistency in our experiments is unexplained, but could be related to the ferrous iron availability.

Copper corrosion in a sulfide-bearing, compacted bentonite environment has been suggested to be a function of both sulfate reducing bacteria growth conditions (e.g., available carbon, sulfate concentrations, and electron donors) and geochemical parameters effecting sulfide diffusion (e.g., bentonite density, fluid content, and ferrous iron concentrations) to the copper surfaces (Pederson 2010). The overall reaction associated with sulfide-induced copper corrosion is

$$Cu° + H_2S \rightarrow Cu_2S_{(s)} + 2e^- + 2H^+.$$

Under the anoxic and high temperature repository conditions, chloride and sulfide corrosion will be the primary (non-radiolytic) mechanism affecting waste canisters. Biotic sulfate reduction probably will be minimal at high-temperature conditions therefore, the dominant sulfide source is likely from sulfide minerals associated with the original bentonite. Mitigating sulfide-induced

corrosion might be achieved by maintaining a high bentonite density thereby restricting sulfide diffusion (Pederson 2010).

One of the big unknowns regarding the steel and copper surface alteration is whether surface passivation is occurring. This could be an important factor to consider in the long-term modeling of the repository system. There was no substantial change in the mineral thicknesses or surface coverage on both steel and copper between the ramped and isothermal, 300 °C experiments. This lack of mineral growth can be a clue in the possible steel or copper passivation, but can also be explained by depletion in the corrosive elements. In the case of copper, as sulfide is depleted from the system, chloride (in an anoxic environment) is the primary corrosive agent, subsequently altering the corrosion rate (King et al. 1992; Carlsson 2008). The fact that the reactant surface thicknesse do not change with temperature or run durations is critical. This has promising implications and needs to be investigated with further experiments. A long term experiment (ramp up – hold at 300 °C - ramp down) would be critical to understanding both passivation potential and general post heat pulse reactions.

Fe-phyllosilicates tend to have strong sorption properties towards actinides and other radioactive materials, therefore, they have the potential to provide added barrier properties for actinide containment. The dynamics and reactivity of actinide adsorption need to be incorporated into the long term repository performance evaluation models. However, this work has never been addressed in repository studies. Inclusion of a reactive, high surface-area canister into used-fuel repositories performance assessments should help provide a viable repository evaluation.

International EBS research

Experiments for international EBS research included two mixed buffer reactions and a heated bentonite sample at 20 wt. % free moisture intended for cooperative research with LBNL. The mixed buffer experiments (bentonite-graphite, bentonite-quartz sand) using the same water chemistry and ratios as the experiments detailed above were conducted to investigate potential mineralogic/petrologic changes to mixed buffer systems (Jobmann and Buntebarth, 2009) of interest to the German nuclear repository program. The cooperative study with LBNL involved heating Colony, Wyoming bentonite to 300 °C with 20 wt. % free moisture. The reaction

products would be geologically characterized by LANL while thermal mechanical properties would be conducted by LBNL.

Mixed buffer experiments. Jobmann and Buntebarth (2009) conducted studies of bentonite – graphite and bentonite – quartz sand to determine if the clay buffer heat conduction could be enhanced to values similar to the host rock. The authors used bentonite, quartz sand, and a variety of graphites in their experimental runs. Temperatures spanned from 35 to 150 °C and a uniaxial 2MPa pressure was applied. Jobmann and Buntebarth (2009) determined that the necessary conductivity could not be obtained with quartz, but that the addition of 15 wt% graphite was able to achieve heat conductivity values (2.5 W $m^{-1}K^{-1}$) in the mixed buffer similar to that of Opalinus Clay. Our ramped heating experiments (Table 2) for bentonite – graphite (EBS-7, 20 wt. % pre experiment, 12 wt. % post experiment graphite) and bentonite – quartz (EBS-9, 20 wt.% pre experiment 15 wt. % post experiment quartz) were developed to examine mineralogic/petrologic parameters coincident to the experiments of Jobmann and Buntebarth (2009). The only significant change in our post experiment reaction products, other than a reduction in carbon and quartz sand, was a decrease in the amount of clinoptilolite. However, as with the other ramped experiments, there was no attendant development of analcime. Further petrographic examinations will be performed on these product run materials.

High-temperature, 20 wt. % free moisture bentonite. A cooperative research activity initiated between LBNL and one of our authors (FAC) resulted in a plan to investigate Colony bentonite under “dry” peak heat repository conditions. As noted above, the bentonite with 20 wt. % free moisture (Stripa brine composition), was subjected to 300 °C for 7 weeks. The experiment (EBS-12) was concluded on May 30, 2013. Our laboratory will conduct mineralogic/petrologic characterization of the run products, while LBNL will perform thermo-mechanical studies on the same materials. The combined results will be utilized by the DECALOVEX modeling team. As seen in Table 2 the bentonite in EBS-12 reacts in a similar manner to all the other experiments conducted for 6 weeks at 300 °C. That is, clinoptilolite reacts to analcime, and no illitization was observed. The only mineralogic change from the other long term 300 °C experiments is an increase in cristobalite/ opal-C (10 wt. %). Further

characterization and thermodynamic modeling should help explain this change in reactant products.

Potential EBS mineralogic/petrologic effects on geological repository - Conclusions

There have been a large number of investigations on bentonite stability under various repository conditions (Madsen 1998; Meunier et al. 1998; Pusch and Kasbohm 2002; Guillaume et al. 2003; Guillaume et al. 2004; Wilson et al. 2006; Marty et al. 2010; Mosser-Ruck et al. 2010; Ferrage et al. 2011). Yet, there remain questions regarding bentonite's overall stability and more importantly whether montmorillonite will remain relatively unaltered through the repository life-time. After initial used-fuel emplacement there will be a pulse of heat flowing into the bentonite buffer producing an environment in which montmorillonite do not typically occur. However, many believe that the initial heat pulse will start to decay after about 100 to 1,000 years (Wersin et al. 2007). The repository is expected to remain dry during the initial 100 to 1,000 years and therefore illitization should be kept to a minimum as there is a limited supply of Al^{3+} and K^{+} available for interaction (Wersin et al. 2007). The buffering capacity of montmorillonite should maintain a Na-rich system even if a wet environment should occur, thereby inhibiting illitization. Additionally, the very low hydraulic conductivity (~3×10^{-13} m/s) of the bentonite should help inhibit the redistribution or influx of Al^{3+} and K^{+} further retarding illitization (Pusch and Kasbohm 2002; Wersin et al. 2007).

Most often repository investigations focus on the MX-80 bentonite from Wyoming. The slightly different bentonite used in this investigation contains ~12 wt. % clinoptilolite, while MX-80 has ~2 wt. % calcite and no clinoptilolite. It is expected mineralogical variation will play a key role in the bentonite stability. For example, the presence of clinoptilolite develops reactions that have not been documented in bentonite buffer systems (Cheshire et al. 2013). Natural paragenetic sequences indicate that clinoptilolite to analcime may progress at temperatures as low as 90 – 100 °C (Smyth 1982). However, analcime formation does not occur until the long-term, 300 °C conditions indicating reaction kinetics are essential in the repository validation.

The Swedish Nuclear Fuel and Waste Management Company (SKB) have emplaced fairly strict sulfur specifications (sulfide content < 0.5 wt. %; total sulfur < 1 wt. %) for the bentonite buffer used in their repositories (Börjesson et al. 2010). Results from these experiments have shown that sulfide release from pyrite deposition will interact with waste canisters in various manners depending on the canister composition.

There have been a number of similar investigations on bentonite stability under various repository conditions and in contact with various metals replicating possible canister compositions (Guillaume et al. 2003; Guillaume et al. 2004; Wilson et al. 2006; Mosser-Ruck et al. 2010; Ferrage et al. 2011). These investigations tend to focus on the Fe-bearing phases (i.e., Fe-saponite, vermiculite, chlorite, and 7Å phases (odinite, berthierine, cronstedtite)) forming during their experiments. Newly formed Fe-rich phyllosilicates in the current investigation are primarily associated with the steel plate-bentonite interface and magnetite particles. Away from these Fe-rich zones there was little to no clay alteration. These observations agree well with the model results from Marty et al. (2010), in which the Fe-rich phases are associated with bentonite/steel interface. Bentonite not in contact with the steel waste container does not show the formation of these Fe-rich phyllosilicates. The occurrence of Fe-rich phyllosilicates most likely will not form in the bentonite away from the waste container because there is a low abundance of iron in the system.

Thermodynamic modeling (Marty et al., 2010) of MX-80 under repository conditions indicates the bentonite barrier system will develop three discrete alteration zones post-closure: 1) zone of mass transport of groundwater through bentonite, 2) middle zone where bentonite stays fairly unreacted, and 3) and inner zone where waste container has a strong influence on the bentonite alteration. Results from this experimental series would suggest that our experimental design corresponds to the outer zone in contact with groundwater and the inner zone influenced by the waste canister. The initial mineralogical composition and closed system of our reaction setup however changes the environment compared to modeled systems by Marty et al. (2010).

These experimental results demonstrate that understanding the mineralogical composition of bentonite barrier materials and the possible alteration pathways is essential in designing a high-level radioactive waste repository. The combination of a Na-rich environment, limited K^+ supply, and precipitation of Al-bearing minerals (analcime and feldspars) appear to have

inhibited the formation of illite-smectite mixed-layers. This is important considering many researchers have argued that illite formation is detrimental to the long-term stability of a used fuel repository. Even though mineral reactions do take place, there are added properties that potentially will compensate for the alteration of clinoptilolite to analcime (e.g., swelling of smectite due to water absorption and a potential of sealing cracks via silica precipitation). Further work needs to be done to better understand the kinetics of analcime formation in a bentonite barrier system and what impact these reactions have on the barrier's mechanical and physical properties.

FY'13 – FY'14 Experimental program

Research objectives for the upcoming year will be a natural progression of experimental results obtained in FY'12-FY'13. For the remainder of FY'13, an emphasis will be put on characterizing the results of the 10 major experiments accomplished and producing peer-reviewed journal manuscripts (zeolites transformations and metal interface mineral growth).

Going forward, there will be three major experimental campaigns. The first would be to incorporate the repository wall rock (granite) into our present components. We would run a series of high pressure, temperature experiments containing brine – bentonite – metal – granite. These experiments would provide the first insights into how minerals (and cation exchange) from the enclosing repository rocks would affect EBS components.

The second major experiment theme would be to run long term (i.e., 6 month) experiments that replicate the complete thermal pulse event (ramp up to temperature – hold at 300 °C – ramp down to ambient temperature) of a repository. One run would consist of brine – bentonite – steel, while the second would include the additional component of granite. Critical information would be gleaned from petrographic information, which would allow us to trace mineral transitions through P, T, T (pressure, temperature, time) space. These experiments would be the first to duplicate the events occurring during a thermal pulse and will provide date on irreversible mineral transformations.

The third research theme would be further investigation of the formation of illite or lack there of. Experiments this year indicated that illite does not form in the chemical compositional

space of our studies. Later experiments allowed the growth of fibrous illite in a K^+ dominated system. Although we now have narrowed down the potential growth mechanisms and chemical parameters needed, further investigation is still needed. These critical experiments are required since many repository systems consider illitization of bentonite as a constraint on EBS designs.

Other research that will be ongoing include: (1) further investigation of Fe-saponite and chalcocite reaction surfaces on steel and copper, respectively, as potential passivating agents, and (2) cation transfer and exchange between the aqueous geochemistry and aluminosilcate matrix. The transition from clinoptilolite to analcime in bentonite matrix is important due to the loss of water from the zeolite's structure, the volume contraction, the release of SiO_2, and the change in retardation factors of the zeolites. If time and resources permit, EBS component system (brine – bentonite) reactions with Opalineous clay will be conducted at elevated pressure and temperature.

Characterization techniques we would like to include in FY14 are: sulfur isotopic analyses of chalcocite growths, transmission electron microscopy, Raman spectroscopy, neutron tomography, focused ion beam microscopy, acoustic measurements to capture elastic moduli of the metals, electrochemical impedance spectroscopy to determine whether reacted metal have become passive, and various synchrotron techniques.

The proposed lines of study are presented in bullet form below for easy reference.

- Finish 300º C experiment characterizations.
- Repeat EBS reactions at 300º C for 6 weeks incorporating wall rock material (granite).
- Provide information on complete repository thermal pulse event, using long term (6 month) experiments.
- Investigate the chlorite formation kinetics.
- Further detailed studies on Fe-saponite, chalcocite growth at metal interface with bentonite.
- Further investigation of SiO_2 precipitation and aluminosilicate formation.
- Investigate further methods for the characterization of the solid phase reaction products, e.g., S isotopes, TEM, Raman spectroscopy, neutron tomography, FIBS, PDF, acoustic measurements of metals, and various synchrotron techniques.

Acknowledgements

We would like to thank Emily Kluk for XRF analyses and Liz Miller for assistance in the lab. Scanning electron microscopy facilities were provided by Materials Science and Technology group at Los Alamos National Laboratory. Dr. George Mason at the University of Oklahoma was instrumental in the obtaining of EMP analyses. Funding was through the Department of Energy's Used Fuel Disposition campaign.

References

Altaner, S.P. (1989) Calculation of K diffusional rates in bentonite beds. Geochimica et Cosmochimica Alta, 53, 923-931.

Bannister, R.A. (1943) Brammalite (sodium-illite) a new mineral from Llandebie, South Wales. Mineralogical Magazine, 26, 304-307.

Bish, D.L. and Aronson, J.L. (1993) Paleogeothermal and paleohydrologic conditions in silicic tuff from Yucca Mountain, Nevada. Clays and Clay Minerals, 41, 148-161.

Bish, D.L., Vaniman, D.T., Chipera, S.J., and Carey, J.W. (2003) The distribution of zeolites and their effects on the performance of a nuclear waste repository at Yucca Mountain, Nevada, U.S.A. American Mineralogist, 88, 1889-1902.

Blanc, P. and Vieillard, P. (2010) Thermochimie: Estimation of the thermodynamic properties of dehydrated phyllosilicates. Bureau de Recherches Géologiques et Miniéres Technical Report, RP-57798-FR, pp. 64.

Börjesson, L., Gunnarsson, D., Johannesson, L-E., and Jonsson, E. (2010) Design, production and initial state of the buffer. Svensk Kärnbränslehantering Technical Report, TR-10-15, pp. 89.

Broxton, D.E., Bish, D.L., and Warren, R.G. (1987) Distribution and chemistry of diagenetic minerals at Yucca Mountain, Nye County, Nevada. Clays and Clay Minerals, 35, 89-110.

Carlsson, T. (2008) Interactions between copper corrosion products and MX-80 bentonite. Svensk Kärnbränslehantering Working Report, TR-08-46, pp. 24.

Cheshire, M.C., Caporuscio, F.A., Jové-Colón, C., and McCarney, M.K. (2013) Alteration of clinoptilolite into high-silica analcime within a bentonite barrier system under used nuclear fuel repository conditions. Proceeding from the 14th International High-Level Radioactive Waste Management Conference, 410-415.

Chipera, S.J. and Bish, D.L. (1997) Equilibrium modeling of clinoptilolite-analcime equilibria at Yucca Mountain, Nevada, USA. Clays and Clay Minerals, 42, 226-239.

Chipera, S.J. and Bish, D.L. (2002) FULLPAT: a full-pattern quantitative analysis program for X-ray powder diffraction using measured and calculated patterns. Journal of Applied Crystallography, 35, 744–749.

Chung, F.H. (1974a) Quantitative interpretations of X-ray diffraction patterns of mixtures. I. Matrix flushing method for quantitative multicomponent analysis. Journal of Applied Crystallography, 7, 519-525.

Coombs, D.S. and Whetten, T. (1967) Composition of analcime from sedimentary and burial metamorphic rocks. *Geological Society of America Bulletin*, **78**, 269-282.

Couture, R.A. (1985) Steam rapidly reduces the swelling capacity of bentonite. Nature, 318, 50-52.

Crerar, D.A., Susak, N.J., Borcsik, M., and Schwartz, S. (1978) Solubility of the buffer assemblage pyrite + pyrrhotite + magnetite in NaCl solution from 200 to 350 °C. Geochimica et Cosmochimica Acta, 42, 1427-1437.

Duffy, C.J. (1984) Hydrothermal geochemistry. Research and Development Related to the Nevada Nuclear Waste Storage Investigation July 1 – September 30, 1982. Eds., Wolfsberg, K. and Vaniman, D.T. Los Alamos National Lab Report, LA-10032-PR, pp. 76.

Eberl, D. (1978) Reaction series for dioctahedral smectites. Clays and Clay Minerals, 26, 327-340.

Eberl, D. and Hower, J. (1977) The hydrothermal transformation of sodium and potassium smectite into mixed-layer clay. Clays and Clay Minerals, 25, 215-227.

Eberl, D., Whitney, G., and Khourym, H. (1978) Hydrothermal reactivity of smectite. American Mineralogist, 63, 401-409.

Ferrage, E., Vidal, O., Mosser-Ruck, R., Cathelineau, M., and Cuadros, J. (2011) A reinvestigation of smectite illitization in experimental hydrothermal conditions: Results from X-ray diffraction and transmission electron microscopy. American Mineralogist, 96, 207-223.

Frape, S.K., Blyth, A., Blomqvist, R., McNutt, R.H., and Gascoyne, M. (2003) Deep Fluids in the Continents: II. Crystalline Rocks, Treatise on Geochemistry, 5, J. I. Drever, ed., 541-580.

Frey, M. (1969) A mixed-layer paragonite/phengite of low-grade metamorphic origin. Contribution to Mineralogy and Petrology, 24, 63-65.

Guillaume, D., Neaman, A., Cathelineau, M., Mosser-Ruck, R., Peiffert, C., Abdelmoula, M., Dubessy, J., Villieras, F., Baronnet, A., and Michau, N., (2003) Experimental synthesis of chlorite from smectite at 300 °C in the presence of metallic Fe. Clay Minerals, 38, 281-302.

Guillaume, D., Neaman, A., Cathelineau, M., Mosser-Ruck, R., Peiffert, C., Abdelmoula, M., Dubessy, J., Villieras, F., and Michau, N., (2004) Experimental study of the transformation of smectite at 80 to 300 ^{o}C in the presence of Fe oxides. Clay Minerals, 39, 17-34.

Güven, N. (2001) Mica structure and fibrous growth of illite. Clays and Clay Minerals, 49, 189-196.

Hower, J., Eslinger, E.V., Hower, M.E., and Perry, E.A. (1976) Mechanism of burial metamorphism of argillaceous sediments. Geological Society of America Bulletin, 87, 725-737.

Jobmann, M. and Buntebarth, G. (2009) Influence of graphite and quartz addition on the thermo-physical properties of bentonite for sealing heat-generating radioactive waste. Applied Clay Science, 44, 206-210.

Jové-Colón, C.F., et al. (2011) Disposal systems evaluations and tool development – engineered barrier system (EBS) evaluation (Fuel cycle research and development). Sandia National Laboratory, FCRD-USED-2011-000132, 16-48.

Karnland, O. (2010) Chemical and mineralogical characterization of the bentonite buffer for the acceptance control procedure in a KBS-3 repository. Svensk Kärnbränslehantering Technical Report, TR-10-60, pp. 29.

Kerrisk, J.F. (1983) Reaction-path calculations of groundwater chemistry and mineral formation at Rainier Mesa, Nevada. Los Alamos National Lab Report, LA-9912-MS, pp. 41

King, F., Litke, C.D., and Ryan, S.R. (1992) A mechanistic study on the uniform corrosion of copper in compacted Na-montmorillonite/sand mixtures. Corrosion Science, 33, 1979-1995.

Kloprogge, J.T., Komarneni, S., and Amonette, J.E. (1999) Synthesis of smectite clay minerals: A critical review. Clays and Clay Minerals, 47, 529-554.

Kohyama, N., Shimoda, S., and Sudo, T. (1973) Iron-rich saponite (ferrous and ferric forms). Clays and Clay Minerals, 21, 229-237.

Madsen, F.T. (1998) Clay mineralogical investigations related to nuclear waste disposal. Clay Minerals, 33, 109-129.

Marty, N.C.M., Fritz, B., Clément, A., and Michau, N. (2010) Modelling the long term alteration of the engineered bentonite barrier in an underground radioactive waste repository. Applied Clay Science, 47, 82-90.

Masuda, H., O'Neil, J.R., Jiang, W-T, and Peacor, D.R. (1996) Relation between interlayer composition of authigenic smectite, mineral assemblages, I/S reaction rate and fluid composition in silicic ash of the Nankai Trough. *Clays and Clay Minerals*, **44**, 443-459.

Meunier, A., Velde, B., and Griffault, L. (1998) The Reactivity of Bentonites: a Review. An Application to Clay Barrier Stability for Nuclear Waste Storage. Clay Minerals, 33, 187-196

Moore, D. M. and Reynolds, R.C. (1997) X-ray Diffraction and the Identification and Analysis of Clay Minerals. Oxford University Press, pg. 377.

Mosser-Ruck, R., Cathelineau, M., Baronnet, A., and Trouiller, A. (1999) Hydrothermal reactivity of K-smectite at 300 °C and 100 bar: dissolution-crystallization process and non-expandable dehydrated smectite formation. Clay Minerals, 34, 275-290.

Mosser-Ruck, R., Cathelineau, M., Guillaume, D., Charpentier, D., Rousset, D., Barres, O., and Michau, N. (2010) Effects of Temperature, pH, and Iron/Clay and Liquid/Clay Ratios on Experimental Conversion of Dioctahedral Smectite to Berthierine, Chlorite, Vermiculite, or Saponite. Clays and Clay Minerals, 58, 280-291

Mosser-Ruck, R., Pironon, J., Cathelineau, M., and Trouiller, A. (2001) Experimental illitization of smectite in a K-rich solution. European Journal of Mineralogy, 13, 829-840.

Neuhoff, P.S., Hovis, G.L., Balassone, G., and Stebbins, J.F. (2004) Thermodynamic properties of analcime solid solutions. American Journal of Science, 304, 21-66.

Nutt, M. Voegele, M., Jove Colon, C.F., Wang, Y., Howard, R., Blink, J., Liu, H.H., Hardin, E., and Jenni, K. (2011) Used fuel disposition campaign disposal research and development road map (Fuel cycle research and development). Sandia National Laboratory.

Ohmoto, H., Hayashi, K-I, and Kajisa, Y. (1994) Experimental study of the solubilities of pyrite in NaCl-bearing aqueous solutions at 250-350 °C. Geochimica et Cosmochimica Acta, 58, 2169-2185.

Pederson, K. (2010) Analysis of copper corrosion in compacted bentonite clay as a function of clay density and growth conditions for sulfate-reducing bacteria. Journal of Applied Microbiology, 108, 1094-1104.

Perry, E.A. and Hower, J. (1970) Burial diagenesis of Gulf Coast politic sediments. Clays and Clay Minerals, 18, 165-177.

Pouchou J.L. and Pichoir F. (1985) “PAP” $\phi(\rho z)$ correction procedure for improved quantitative microanalysis. Microbeam Analysis. Ed. Armstrong, J.T. San Francisco Press, pp. 104-106.

Pusch, R. (1979) Highly compacted sodium bentonite for isolating rock-deposited radioactive waste products. Nuclear Technology, 45, 153-157.

Pusch, R. and Kasbohm, J. (2002) Alteration of MX-80 by hydrothermal treatment under high salt content conditions. Svensk Kärnbränslehantering Technical Report, TR-02-06, pp. 44.

Reynolds, R.C. and Hower, J. (1970) The nature of interlayering in mixed-layer illite-montmorillonite. Clays and Clay Minerals, 18, 25-36.

Roberson, H.E. and Lahann, R.W (1981) Smectite to illite conversion rates: Effects of solution chemistry. Clays and Clay Minerals, 29, 129-135.

Seyfried, J.R., Janecky, D.R., and Berndt, M.E. (1987) Rocking autoclaves for hydrothermal experiments II. The flexible reaction-cell system. Hydrothermal Experimental Techniques. Eds. Ulmer, G.C. and Barnes, H.L. John Wiley and Sons, pp. 216 - 239

Small, J.S. (1993) Experimental determination of the rates of precipitation of authigenic illite and kaolinite in the presence of aqueous oxalate and comparison to the K/Ar ages of authigenic illite in reservoir sandstones. Clays and Clay Minerals, 41, 191-208.

Small, J.S., Hamilton, D.L., and Habesch, S. (1992) Experimental simulation of clay precipitation within reservoir sandstones 2: Mechanism of illite formation and controls on morphology. Journal of Sedimentary Petrology, 62, 520-529.

Smyth, J.R. (1982) Zeolite stability constraints on radioactive waste isolation in zeolite-bearing volcanic rocks. Journal of Geology, 90, 195-201.

Środoń, J. (1999) Nature of mixed-layer clays and mechanisms of their formation and alteration. Annual Review of Earth and Planetary Sciences, 27, 19-53.

Wersin, P., Johnson, L.H., and McKinley, I.G. (2007) Performance of the bentonite barrier at temperatures beyond 100^{o} C: A critical review. Physics and Chemistry of the Earth, 32, 780-788.

Whitney, G. and Velde, B. (1993) Changes in particle morphology during illitization: An experimental study. Clays and Clay Minerals, 41, 209-218.

Wilkin, R.T. and Barnes, H.L. (1998) Solubility and stability of zeolites in aqueous solution: I. Analcime, Na-, and K-clinoptilolite. American Mineralogist, 83, 746-761.

Wilkin, R.T. and Barnes, H.L. (2000) Nucleation and growth kinetics of analcime from precursor Na-clinoptilolite. American Mineralogist, 85, 1329-1341.

Wilson, J., Cressey, G., Cressey, B., Cuadros, J., Ragnarsdottir, K.V., Savage, D., and Shibata,

M. (2006) The effect of iron on montmorillonite stability (II) Experimental investigation.

Geochimica et Cosmochimica Acta, 70, 323-336.

Appendix A:
EMP standards and oxide detection limits for silicate analyses

Phlogopite (Synthetic): MgO = 0.02 wt.% , F = 0.11 wt.%

Albite (Amelia, NC, U.S.A, Rutherford mine): Na_2O = 0.02 wt.%

Labrodorite (Chihuahua, Mexico): Al_2O_3 = 0.02 wt.%, SiO_2 = 0.02 wt.%, CaO = 0.01 wt.%

Tugtupite (Greenland): Cl = 0.01 wt.%

Adularia (St. Gotthard, Switzerland): K_2O = 0.01 wt.%

Titanite glass (Penn State): TiO_2 = 0.02 wt.%

MagnesioChromite (Synthetic): Cr_2O_3 = 0.04 wt.%

Rhodonite (unknown locality): MnO = 0.02 wt.%

Augite (unknown locality): FeO = 0.02 wt.%

Liebenbergite (synthetic): NiO = 0.06 wt.%

Gahnite: ZnO = 0.05 wt.%

Appendix B:
Electron Microprobe Mineral Data

Fe-SAPONITE/CHLORITE

Oxide Abundance wt. %	SiO_2	TiO_2	Al_2O_3	Cr_2O_3	FeO*	MnO	MgO	NiO	ZnO	CaO	Na_2O	K_2O	F	Cl	Total
(6) Ave. EBS-2	33.96	0.02	12.83	1.35	30.94	0.38	1.95	1.34	0.03	1.32	1.62	0.61	0.13	0.41	86.66
1σ	*3.48*	*0.03*	*0.97*	*1.39*	*3.53*	*0.15*	*0.34*	*0.93*	*0.02*	*0.67*	*0.27*	*0.29*	*0.09*	*0.29*	*0.60*
Atoms per formula unit	Si	Ti	Al	Cr	Fe	Mn	Mg	Ni	Zn	Ca	Na	K	F	Cl	Sum
18 oxygen	4.87	0.00	2.17	0.16	3.74	0.05	0.42	0.16	0.00	0.20	0.45	0.11	0.06	0.10	12.32
1σ	0.49	0.01	0.20	0.26	0.88	0.03	0.11	0.17	0.00	0.16	0.09	0.08	0.07	0.11	0.40
12 oxygen	3.25	0.00	1.45	0.11	2.49	0.02	0.28	0.07	0.00	0.13	0.30	0.07	0.04	0.07	8.22

Table B1. EMPA of Fe-phyllosilicates grown on 304 SS plate during EBS-2. The Fe-phyllosilicates are a mixture of Fe-saponite and chlorite, therefore 18 oxygen (chlorite) and 12 oxygen (saponite) formula units were calculated.

SAPONITE

Oxide Abundance wt. %	SiO_2	TiO_2	Al_2O_3	Cr_2O_3	FeO*	MnO	MgO	NiO	ZnO	CaO	Na_2O	K_2O	F	Cl	Total
(8) Ave. EBS-6	36.20	0.01	12.95	0.02	33.99	0.22	0.83	0.01	0.01	0.67	0.98	0.32	0.03	0.04	86.24
1σ	*0.81*	*0.01*	*0.95*	*0.01*	*0.89*	*0.10*	*0.04*	*0.01*	*0.01*	*0.18*	*0.39*	*0.17*	*0.03*	*0.03*	*1.71*

Atoms per formula unit	Si	Ti	Al	Cr	Fe	Mn	Mg	Ni	Zn	Ca	Na	K	F	Cl	Sum
12 oxygen	3.42	0.00	1.44	0.00	2.69	0.02	0.12	0.00	0.00	0.07	0.18	0.04	0.01	0.01	7.974
1σ	*0.15*	*0.00*	*0.20*	*0.00*	*0.10*	*0.00*	*0.20*	*0.00*	*0.00*	*0.04*	*0.17*	*0.05*	*0.02*	*0.01*	*0.110*

Table B2. EMPA of Fe-saponite grown on low-carbon steel plates during EBS-6. There are other sulfides and oxides mixed within the saponite, therefore the atoms per formula unit should be considered as a guide and not the absolute saponite composition.

Pre-experiment clinoptilolite data

Oxide Abundance wt. %	SiO_2	TiO_2	Al_2O_3	Cr_2O_3	FeO*	MnO	MgO	NiO	ZnO	CaO	Na_2O	K_2O	F	Cl	Total
(9) Ave. mine run	71.28	0.01	12.6	0.01	0.09	0	0.3	0.01	0.01	0.95	4.57	0.2	0.02	0.00	90.03
1σ	*2.19*	*0.01*	*0.33*	*0.01*	*0.02*	*0.01*	*0.34*	*0.01*	*0.01*	*0.63*	*1.31*	*0.13*	*0.04*	*0.00*	*2.21*
Atoms per formula unit	Si	Ti	Al	Cr	Fe	Mn	Mg	Ni	Zn	Ca	Na	K	F	Cl	Sum
72 oxygen	30.02	0.00	6.26	0.00	0.03	0.03	0.19	0.00	0.00	0.43	3.73	0.11	0.03	0.00	40.78
1σ	*0.06*	*0.00*	*0.04*	*0.00*	*0.00*	*0.00*	*0.07*	*0.00*	*0.00*	*0.10*	*0.35*	*0.02*	*0.02*	*0.00*	*0.2*

Table B3. EMPA of clinoptilolite in the initial, unprocessed bentonite.

Post-experiment clinoptilolite data

Oxide Abundance wt. %	SiO_2	TiO_2	Al_2O_3	Cr_2O_3	FeO*	MnO	MgO	NiO	ZnO	CaO	Na_2O	K_2O	F	Cl	Total
(10) Ave. EBS-1	71.13	0.01	12.87	0.00	0.09	0.00	0.14	0.01	0.00	1.63	3.90	1.26	0.02	0.00	91.05
1σ	*0.98*	*0.01*	*0.32*	*0.00*	*0.05*	*0.00*	*0.03*	*0.01*	*0.00*	*0.30*	*0.38*	*0.31*	*0.03*	*0.00*	*1.01*
Atoms per formula unit	Si	Ti	Al	Cr	Fe	Mn	Mg	Ni	Zn	Ca	Na	K	F	Cl	Sum
72 oxygen	29.84	0.00	6.36	0.00	0.03	0.00	0.09	0.00	0.00	0.73	3.17	0.65	0.02	0.00	40.89
1σ	*0.05*	*0.00*	*0.06*	*0.00*	*0.01*	*0.00*	*0.01*	*0.00*	*0.00*	*0.04*	*0.10*	*0.05*	*0.01*	*0.00*	*0.05*

Table B4. EMPA of residual clinoptilolite in EBS-1 bentonite.

Analcime data

Oxide Abundance wt. %	SiO_2	TiO_2	Al_2O_3	Cr_2O_3	FeO*	MnO	MgO	NiO	ZnO	CaO	Na_2O	K_2O	F	Cl	Total
(10) Ave. EBS-5	69.96	0.00	19.29	0.01	0.17	0.01	0.01	0.00	0.00	1.89	4.47	0.07	0.07	0.02	95.95
1σ	*0.76*	*0.01*	*0.25*	*0.01*	*0.04*	*0.01*	*0.02*	*0.01*	*0.01*	*0.18*	*0.23*	*0.02*	*0.04*	*0.02*	*0.57*
Atoms per formula unit	Si	Ti	Al	Cr	Fe	Mn	Mg	Ni	Zn	Ca	Na	K	F	Cl	Sum
6 oxygen	2.33	0.00	0.76	0.00	0.01	0.00	0.00	0.00	0.00	0.07	0.29	0.00	0.01	0.00	3.45
1σ	*0.04*	*0.00*	*0.05*	*0.00*	*0.00*	*0.00*	*0.00*	*0.00*	*0.00*	*0.03*	*0.06*	*0.00*	*0.01*	*0.00*	*0.04*

Table B5. EMPA of authigenic analcime from EBS-5.

Appendix C:
Solution Chemistry

Unfilter (UF) samples

Sample ID	1/0 UF	1/1 UF	1/2 UF	1/3 UF	1/4 UF	1/5 UF	1/6 UF	1/7 UF
Date analyzed	na	na	na	na	na	na	na	na
Date sampled		7/27/2011	8/1/2011	8/8/2011	8/11/2011	8/15/2011	8/22/2011	8/23/2011
Hours	0.00	23.55	144.00	308.90	381.80	479.30	645.00	670.00
Temp, C	25	118	121	120	212	212	300	22
pH	8.59	8.96	8.31	8.78	6.59	7.69	6.03	5.83
Al	<0.05	0.09(0)	<0.05	<0.05	0.38(1)	0.16(1)	1.10(0)	<0.05
B								
Ba	<0.05	0.09(0)	0.10(0)	0.12(0)	0.09(0)	0.14(0)	0.08(0)	0.02(0)
Br								
Ca	89(0)	35(0)	20(0)	19(0)	13(1)	11(0)	4(0)	10(0)
Cl	1045	1077	1131	1125	1225	1185	1128	1458
F	<0.2	<0.2	0.37	0.65	0.97	1.09	1.46	1.39
Fe	<0.5	<0.5	<0.5	<0.5	<0.5	1.1(0)	0.7(0)	<0.5
K	583(3)	457(0)	282(2)	203(1)	167(1)	152(1)	95(0)	37(0)
Li								
Mg								
Mn								
Na	167(2)	405(6)	590(15)	649(9)	640(10)	673(13)	590(10)	584(2)
NO2								
NO2-N								
NO3	<0.2	2.81	2.50	8.17	2.72	1.91	0.20	<0.2
NO3-N	<0.05	0.63	0.57	1.84	0.61	0.43	0.05	<0.05

PO4								
Si	1(0)	45(0)	88(1)	104(2)	286(1)	322(3)	550(1)	137(1)
SiO2	2(0)	97(0)	189(1)	223(4)	611(2)	689(7)	1176(3)	293(2)
SO4	47	64	109	352	154	155	59	201
Sr	0.05(0)	0.26(0)	0.25(0)	0.23(0)	0.13(0)	0.09(0)	<0.05	0.06(0)
Ti	<0.05	<0.05	<0.05	<0.05	0.09(1)	0.08(0)	0.11(0)	0.02(0)
Zn	<0.05	<0.05	<0.05	0.70	0.46(0)	0.41(0)	0.54(1)	0.04(0)
TDS	1934	2139	2326	2580	2816	2870	3056	2585
Cation	27	31	34	34	33	34	28	27
Anion	30	32	34	39	38	37	33	45
Balance	-0.07	-0.01	0.00	-0.07	-0.07	-0.04	-0.08	-0.26
Na/K	0.286	0.886	2.09	3.20	3.84	4.44	6.24	15.7

Sample ID	2/0 UF	2/1 UF	2/2 UF	2/3 UF	2/4 UF	2/5 UF	2/6 UF	2/7 UF
Date analyzed	na	na	na	na	na	na	na	na
Date sampled		7/27/2011	8/1/2011	8/8/2011	8/11/2011	8/15/2011	8/22/2011	8/22/2011
Hours	0.00	25	146	311	383	477	646	672
Temp, C	25	121	121	121	212	213	301	22
pH	8.59	7.91	8.54	7.70	6.77	6.44	6.16	6.21
Al	<0.05	0.05(1)	<0.05	<0.05	0.20(0)	0.14(2)	0.45(0)	3.50(5)
B								
Ba	<0.05	0.09(0)	0.08(0)	0.09(0)	0.09(0)	0.09(0)	0.09(0)	0.02(0)
Br								
Ca	89(0)	41(0)	20(0)	19(0)	19(0)	17(0)	4(0)	11(0)
Cl	1045	1067	1014	974	968	915	801	772
F	<0.2	<0.2	0.25	0.48	0.86	1.06	1.93	1.62
Fe	<0.5	<0.5	<0.5	<0.5	<0.5	<0.5	<0.5	<0.5
K	583(3)	468(0)	257(1)	167(0)	146(1)	117(1)	78(0)	44(1)
Li								
Mg								
Mn								
Na	167(2)	362(4)	536(3)	559(9)	563(14)	511(1)	428(7)	407(7)
NO2								
NO2-N								
NO3	<0.2	1.36	1.72	4.49	1.26	1.20	0.10	<0.2
NO3-N	<0.05	0.31	0.39	1.01	0.29	0.27	0.02	<0.05
PO4								
Si	1(0)	34(0)	76(0)	92(0)	262(1)	278(4)	510(2)	129(1)
SiO2	2(0)	73(0)	162(1)	196(0)	561(3)	596(9)	1092(4)	276(3)
SO4	47	64	105	115	115	197	40	114
Sr	0.05(0)	0.21(0)	0.16(0)	0.12(0)	0.09(0)	0.08(0)	<0.05	0.08(0)
Ti	<0.05	<0.05	<0.05	<0.05	0.09(0)	0.07(1)	0.10(0)	0.03(0)
Zn	<0.05	<0.05	0.63(1)	0.52(0)	0.67(0)	0.45(0)	0.64(1)	0.01(0)

TDS	1934	2077	2096	2036	2376	2356	2446	1629
Cation	27	30	31	29	29	26	21	20
Anion	30	31	31	30	30	30	23	24
Balance	-0.07	-0.03	0.00	-0.01	-0.01	-0.07	-0.06	-0.10
Na/K	0.286	0.774	2.09	3.36	3.84	4.37	5.48	9.16

Sample ID	3/0 UF	3/1 UF	3/2 UF	3/3 UF	3/4 UF	3/5 UF	3/6 UF
Date analyzed	na	05/10/12	05/10/12	05/10/12	05/10/12	05/15/12	05/10/12
Date sampled	na	3/22/2012	3/28/2012	4/4/2012	4/18/2012	4/25/2012	4/27/2012
Hours	0.00	72.3	215.2	388.6	719.6	912.1	935.2
Temp, C	25	120	121	120	212	303	22
pH	8.59	9.55	8.49	8.43	6.83	6.36	7.51
Al	<0.05	0.07(1)	<0.05	<0.05	0.45(1)	1.1(0)	12(0)
B		0.62(1)	1.55(1)	1.89(2)	8.68(1)	8(0)	7(0)
Ba	<0.05	<0.05	<0.05	0.06(1)	<0.05	<0.05	0.07(0)
Br		<0.2	<0.2	<0.2	<0.2	<0.2	<0.2
Ca	89(0)	15(1)	13(0)	12(0)	8(1)	3(0)	8(0)
Cl	1045	935	1200	873	868	744	782
F	<0.2	0.3	0.6	1.0	1.4	2.7	2.0
Fe	<0.5	<0.5	<0.5	<0.5	<0.5	<0.5	9(0)
K	583(3)	208(2)	181(1)	129(1)	86(1)	53(0)	21(0)
Li		0.22(0)	0.24(0)	0.31(0)	0.27(0)	0.25(1)	0.49(1)
Mg		<0.5	<0.5	<0.5	<0.5	<0.5	2.2
Mn		<0.05	<0.05	<0.05	<0.05	<0.05	<0.05
Na	167(2)	428(3)	585(7)	560(2)	516(2)	411(3)	534(7)
NO2		<0.2	<0.2	<0.2	<0.2	<0.2	<0.2
NO2-N		<0.06	<0.06	<0.06	<0.06	<0.06	<0.06
NO3	<0.2	1.6	0.9	<0.2	<0.2	<0.2	4.0
NO3-N	<0.05	0.35	0.20	<0.05	<0.05	<0.05	0.90
PO4		3	4	5	4	3	2
Si	1(0)	47(0)	70(1)	67(1)	242(6)	478(4)	156(2)
SiO2	2(0)	101(0)	150(1)	143(1)	518(13)	1022(8)	335(4)
SO4	47	90	145	131	130	44	154
Sr	0.05(0)	0.10(0)	0.12(0)	0.09(0)	<0.05	<0.05	0.06(0)
Ti	<0.05	<0.05	<0.05	<0.05	<0.05	<0.05	0.11(1)
Zn	<0.05	<0.05	<0.05	0.07(2)	<0.05	0.05(1)	0.06(1)

TDS	1934	2048	1949	1766	2530	2821	2261
Cation	27	25	31	28	25	20	26
Anion	30	28	37	27	28	22	26
Balance	-0.07	-0.07	-0.09	0.01	-0.05	-0.07	0.01
Na/K	0.286	2.06	3.24	4.33	5.99	7.71	24.9

Sample ID	4/0 UF	4/1 UF	4/2 UF	4/3 UF	4/4 UF	4/5 UF	4/6 UF	4/7 UF
Date analyzed	na	05/10/12	05/14/12	05/14/12	05/15/12	05/14/12	05/15/12	05/14/12
Date sampled	na	4/6/2012	4/12/2012	4/19/2012	4/26/2012	5/3/2012	5/10/2012	5/11/2012
Hours	0.00	42.7	186.7	355.5	523.3	690.9	858.7	884.8
Temp, C	25	120	120	119	212	212	305	1
pH	8.59	8.62	7.68	6.93	6.08	6.09	6.25	7.43
Al	<0.05	6.76(3)	1(0)	33(1)	1.0(0)	4(0)	1.1(0)	22(1)
B		0.67(2)	0.33(1)	1(0)	9(0)	8(0)	9(0)	8(0)
Ba	<0.05	0.13(0)	0.10(0)	0.21(1)	<0.05	0.07(0)	<0.05	0.12(1)
Br		<0.2	<0.2	<0.2	<0.2	<0.2	<0.2	<0.2
Ca	89(0)	16(1)	14(0)	21(0)	8(0)	9(0)	4(0)	15(0)
Cl	1045	1224	1257	1283	1271	1278	1169	1297
F	<0.2	0.6	0.6	0.9	0.8	0.5	1.4	1.7
Fe	<0.5	<0.5	1(0)	17(1)	<0.5	2(0)	<0.5	13(0)
K	583(3)	252(5)	182(1)	153(2)	112(1)	107(1)	91(1)	54(0)
Li		0.07(1)	0.11(1)	0.17(0)	0.21(1)	0.23(0)	0.29(1)	0.60(0)
Mg		1.3(0)	0.7(0)	7.5(6)	<0.5	0.8(0)	<0.5	5.5(3)
Mn		<0.05	<0.05	0.07(0)	<0.05	<0.05	<0.05	0.09(0)
Na	167(2)	598(8)	650(7)	683(6)	706(3)	673(6)	618(5)	789(2)
NO2		<0.2	<0.2	<0.2	<0.2	<0.2	<0.2	<0.2
NO2-N		<0.06	<0.06	<0.06	<0.06	<0.06	<0.06	<0.06
NO3	<0.2	1.6	0.4	0.3	<0.2	<0.2	<0.2	<0.2
NO3-N	<0.05	0.35	0.10	0.06	<0.05	<0.05	<0.05	<0.05
PO4		4	3	3	3	3	2	<0.2
Si	1(0)	85(1)	80(1)	218(11)	305(1)	303(2)	539(2)	291(4)
SiO2	2(0)	181(2)	171(1)	466(23)	652(2)	648(5)	1154(3)	624(9)
SO4	47	97	128	157	190	193	51	232
Sr	0.05(0)	0.22(0)	0.19(0)	0.30(0)	0.10(0)	0.10(0)	<0.05	0.25(0)
Ti	<0.05	0.07(0)	<0.05	0.30(1)	<0.05	<0.05	<0.05	0.19(2)
Zn	<0.05	0.08(2)	0.01(1)	0.06(1)	<0.05	0.05(2)	0.12(2)	0.08(2)

TDS	1934	1159	2197	1544	1682	1649	1933	1766
Cation	27	34	34	40	34	33	30	40
Anion	30	37	38	40	40	40	34	42
Balance	-0.07	-0.04	-0.06	0.00	-0.08	-0.10	-0.08	-0.02
Na/K	0.286	2.37	3.58	4.46	6.29	6.27	6.80	14.6

Sample ID	5/0 UF**	5/1 UF**	5/2 UF	5/3 UF	5/4 UF	5/5 UF	5/6 UF	5/7 UF
Date analyzed	7/27/2012	8/01/2012	7/27/2012	7/27/2012	7/27/2012	8/07/2012	8/21/2012	8/21/2012
Date sampled	7/2/2012	7/5/2012	7/12/2012	7/19/2012	7/26/2012	8/2/2012	8/14/2012	8/15/2012
Hours	0	72.95	242.05	411.53	578.87	747.68	1033.18	1041.47
Temp, C	10	302	303	302	302	302	302	18
pH	NA	5.81	5.75	5.84	5.84	6	5.92	NA
Al	<0.1	1.42(1)	<0.1	<0.1	<0.1	1.0(0)	0.9(0)	0.1(0)
B	0.18(0)	7.93(7)	9.98(2)	9.67(1)	10.42(1)	11(0)	8(0)	7(0)
Ba	<0.01	<0.1	<0.1	<0.1	<0.1	<0.1	<0.1	<0.1
Br	<0.2	<0.2	<0.2	<0.2	<0.2	<0.2	<0.2	<0.2
Ca	108(1)	3(0)	11.8(1)	<1	11.1(1)	8(0)	8(2)	19(1)
Cl	931	932	865	866	1186	1071	1052	1278
F	<0.2	1.47	<0.2	<0.2	<0.2	1.9	3.5	1.3
Fe	<1	<1	<1	<1	<1	<1	<1	<1
K	663(5)	92(1)	94(0)	88(0)	87(0)	78(1)	62(1)	49(0)
Li	<0.1	0.32(1)	<0.1	<0.1	<0.1	0.35(0)	<0.1	<0.1
Mg	<1	<1	<1	<1	<1	<1	<1	<1
Mn	<0.1	<0.1	<0.1	<0.1	<0.1	<0.1	<0.1	<0.1
Na	197(1)	613(3)	684(2)	676(1)	742(1)	636(8)	584(16)	776(6)
NO2	<0.2	<0.2	<0.2	<0.2	<0.2	<0.2	<0.2	<0.2
NO2-N	<0.06	<0.06	<0.06	<0.06	<0.06	<0.06	<0.06	<0.06
NO3	<0.2	<0.2	<0.2	<0.2	<0.2	<0.2	2.3	53.1
NO3-N	<0.05	<0.05	<0.05	<0.05	<0.05	<0.05	0.51	12
PO4	<0.2	<0.2	<0.2	<0.2	<0.2	<0.2	<0.2	<0.2
Si	<1.0	525(2)	558(1)	551(0)	554(0)	489(4)	507(9)	81(1)
SiO2	<2.14	1125(3)	1194(2)	1178(1)	1185(1)	1046(8)	1084(19)	173(1)
SO4	45.75	59	42	39	46	50	47	362
Sr	<0.1	<0.1	<0.1	<0.1	<0.1	<0.1	<0.1	<0.1
Ti	<0.2	<0.2	<0.2	<0.2	<0.2	<0.2	<0.2	<0.2
Zn	<0.1	<0.1	<0.1	<0.1	<0.1	0.17(2)	0.99(13)	0.72(2)

TDS	1946	2836	2901	2856	3266	2902	2853	2719
Cation	30	29	33	32	35	30	27	36
Anion	27	27	26	26	35	32	31	45
Balance	0.06	0.02	0.12	0.10	0.00	-0.03	-0.06	-0.11
Na/K	0.298	6.65	7.31	7.71	8.57	8.20	9.49	15.9

Sample ID	6/0 UF**	6/1 UF**	6/2 UF	6/3 UF	6/4 UF	6/5 UF	6/6 UF	6/7 UF	6/8 UF
Date analyzed	7/27/2012	7/27/2012	7/27/2012	7/27/2012	7/27/2012	8/07/2012	8/07/2012	8/21/2012	8/21/2012
Date sampled	7/2/2012	7/5/2012	7/12/2012	7/19/2012	7/26/2012	8/2/2012	8/6/2012	8/9/2012	8/10/2012
Hours	0	46.63	216.45	382.85	550.83	718.63	822.27	888.15	911.13
Temp, C	25	119	120	119	218	218	298	300	25
pH	9.52	9.43	6.98	7.13	6.12	6.34	6.13	6.47	6.45
Al	<0.1	<0.1	<0.1	<0.1	<0.1	0.4(0)	1.5(0)	1.6	1.5(0)
B	<0.1	1.4(0)	<0.1	2.76(1)	9.58(2)	12(0)	10(0)	7	7(0)
Ba	0.01(0)	<0.1	<0.1	<0.1	<0.1	<0.1	<0.1	<0.1	<0.1
Br	<0.2	<0.2	<0.2	<0.2	<0.2	<0.2	<0.2	<0.2	<0.2
Ca	102(3)	60(0)	51.4(1)	36.8(1)	15.3(1)	11(0)	8(0)	7	9(1)
Cl	362	301	396	410	541	583	509	507	489
F	<0.2	<0.2	<0.2	<0.2	<0.2	1.7	5.1	4.9	3.9
Fe	<1	<1	<1	<1	<1	<1	<1	<1	4(0)
K	8(0)	13(0)	<1	<1	<1	26(1)	13(0)	<1	<1
Li	<0.1	<0.1	<0.1	<0.1	<0.1	0.19(2)	0.12(1)	<0.1	<0.1
Mg	<1	<1	<1	<1	<1	<1	<1	<1	<1
Mn	<0.1	<0.1	<0.1	<0.1	<0.1	<0.1	<0.1	<0.1	<0.1
Na	187(4)	254(0)	383(1)	495(0)	478(1)	461(9)	350(5)	288	328(4)
NO2	<0.2	<0.2	<0.2	<0.2	<0.2	<0.2	<0.2	<0.2	<0.2
NO2-N	<0.06	<0.06	<0.06	<0.06	<0.06	<0.06	<0.06	<0.06	<0.06
NO3	<0.2	<0.2	70.2	<0.2	<0.2	<0.2	<0.2	<0.2	<0.2
NO3-N	<0.05	<0.05	15.84	<0.05	<0.05	<0.05	<0.05	<0.05	<0.05
PO4	<0.2	<0.2	<0.2	<0.2	<0.2	<0.2	<0.2	<0.2	<0.2
Si	<1	17(0)	24.5(0)	39.3(0)	272(0)	288(0)	543(7)	494	198(4)
SiO2	<2.14	36(0)	52(0)	84(0)	583(1)	617(0)	1161(15)	1058	424(8)
SO4	43	61	119	179	212	269	134	130	221
Sr	<0.1	<0.1	<0.1	<0.1	<0.1	<0.1	<0.1	<0.1	<0.1
Ti	<0.2	<0.2	<0.2	<0.2	<0.2	<0.2	<0.2	<0.2	<0.2
Zn	<0.1	<0.1	<0.1	<0.1	<0.1	<0.1	0.13(2)	0.61(5)	1.05(2)

TDS	702	701	1072	1208	1839	1982	2190	2004	1489
Cation	13	14	19	23	22	21	16	13	15
Anion	11	10	15	15	20	23	18	18	19
Balance	0.10	0.18	0.12	0.21	0.03	-0.03	-0.05	-0.15	-0.11
Na/K	22.9	19.3	na	na	na	17.6	27.9	na	na

Sample ID	7/0 UF	7/1 UF	7/2 UF	7/3 UF	7/4 UF	7/5 UF	7/6 UF	7/7 UF
Date analyzed	8/21/12	8/23/2012	2/25/2013	2/25/2013	2/25/2013	2/25/2013	2/25/2013	2/25/2013
Date sampled		8/22/2012	8/30/2012	9/6/2012	9/13/2012	9/20/2012	9/27/2012	9/28/2012
Hours	0	50.63	235.82	403.43	571.77	739.68	907.45	936.27
Temp, C	25	119	120	120	211	211	303	22
pH	6.69	9.64	8.33	7.44	6.33	6.2	6.17	6.16
Al	<0.1	0.35(0)	0.18(0)	0.14(1)	0.84(0)	0.58(0)	2.86(2)	0.75(2)
B	<0.1	1.3(0)	0.9(9)	2(0)	6(0)	7(0)	7(0)	7(0)
Ba	<0.1	0.3	<0.05	<0.05	<0.05	<0.05	<0.05	<0.05
Br	<0.2	<0.2	<0.5	<0.5	<0.5	<0.5	<0.5	<0.5
Ca	96(1)	34(1)	30(1)	25(0)	9(0)	7(0)	5(0)	8(1)
Cl	477	538	541	578	559	538	512	537
F	<0.2	<0.2	<0.5	<0.5	<0.5	<0.5	<0.5	<0.5
Fe	<1	<1	<0.5	<0.5	<0.5	<0.5	<0.5	0.8
K	<1	7(0)	13(0)	9(0)	11(0)	10(0)	10(0)	6(0)
Li	<0.1	<0.1	<0.05	<0.05	0.09(1)	0.11(1)	0.12(0)	0.23(1)
Mg	<1	<1	<0.5	<0.5	<0.5	<0.5	<0.5	<0.5
Mn	<0.1	<0.1	<0.05	<0.05	<0.05	<0.05	<0.05	<0.05
Na	153(1)	250(1)	335(4)	382(2)	378(0)	366(3)	298(2)	380(2)
NO2	<0.2	<0.2	<0.5	<0.5	<0.5	<0.5	<0.5	<0.5
NO2-N	<0.06	<0.06	<0.15	<0.15	<0.15	<0.15	<0.15	<0.15
NO3	<0.2	1.4	<0.5	<0.5	<0.5	<0.5	<0.5	<0.5
NO3-N	<0.05	0.31	<0.11	<0.11	<0.11	<0.11	<0.11	<0.11
PO4	<0.2	<0.2	<0.5	<0.5	<0.5	<0.5	<0.5	<0.5
Si	2(0)	16(0)	32(1)	48(0)	165(1)	235(2)	451(5)	264(3)
SiO2	5(0)	34(0)	69(3)	102(1)	353(2)	502(3)	965(11)	566(6)
SO4	46	68	128	187	221	215	134	221
Sr	<0.1	0.13	0.11	0.10	<0.05	<0.05	<0.05	<0.05
Ti	<0.2	<0.2	<0.1	<0.1	<0.1	<0.1	<0.1	<0.1
Zn	0.28	0.82	<0.05	<0.05	<0.05	<0.05	<0.05	<0.05

TDS	777	936	1118	1285	1538	1646	1934	1726
Cation	11	13	16	18	17	17	14	17
Anion	14	17	18	20	21	20	18	20
Balance	-0.11	-0.13	-0.04	-0.06	-0.09	-0.09	-0.12	-0.08
Na/K	na	38.3	26.0	44.2	35.8	37.0	30.2	66.5

Sample ID	8/0 UF	8/1 UF	8/2 UF	8/3 UF	8/4 UF	8/5 UF	8/6 UF	8/7 UF	8/8 UF
Date analyzed	8/21/2012	8/23/2012	2/25/2013	2/25/2013	2/25/2013	2/25/2013	2/25/2013	2/25/2013	02/25/13
Date sampled		8/23/2012	8/30/2012	9/6/2012	9/13/2012	9/20/2012	9/27/2012	10/4/2012	10/5/12 9:30
Hours	0	25.03	194.08	361.27	531.22	698.65	864.73	1033.13	1058.03
Temp, C	25	309	310	310	309	309	310	309	21
pH	6.69	6.16	6.07	6.02	6.06	6.16	6.17	6.13	5.91
Al	<0.1	2.94(5)	0.77(1)	1.49(1)	1.13(2)	1.04(1)	1.11(2)	1.22(1)	2.86(26)
B	<0.1	9.5(1)	8.3(0)	7.2(1)	7.1(1)	6.9(1)	6.6(0)	7.2(1)	4.9(0)
Ba	<0.1	<0.1	<0.05	<0.05	<0.05	<0.05	<0.05	<0.05	<0.05
Br	<0.2	<0.2	<0.5	<0.5	<0.5	<0.5	<0.5	<0.5	---
Ca	96(1)	7(1)	4(0)	4(0)	3(0)	4(0)	3(0)	4(0)	17(0)
Cl	477	509	489	452	434	414	406	392	306
F	<0.2	<0.2	<0.5	<0.5	<0.5	<0.5	<0.5	<0.5	---
Fe	<1	<1	<0.5	<0.5	<0.5	<0.5	<0.5	<0.5	5
K	<1	7(0)	11(0)	10(0)	11(0)	12(0)	13(0)	15(0)	12(0)
Li	<0.1	<0.1	0.13(1)	0.14(1)	0.16(1)	0.17(1)	0.18(1)	0.18(2)	0.22(2)
Mg	<1	<1	<0.5	<0.5	<0.5	<0.5	<0.5	0.8(2)	2.2(1)
Mn	<0.1	<0.1	<0.05	<0.05	<0.05	<0.05	<0.05	<0.05	<0.05
Na	153(1)	264(2)	263(1)	248(4)	237(1)	229(0)	222(1)	209(2)	204(1)
NO2	<0.2	<0.2	<0.5	<0.5	<0.5	<0.5	<0.5	<0.5	---
NO2-N	<0.06	<0.06	<0.15	<0.15	<0.15	<0.15	<0.15	<0.15	---
NO3	<0.2	0.94	<0.5	<0.5	<0.5	<0.5	<0.5	<0.5	---
NO3-N	<0.05	0.21	<0.11	<0.11	<0.11	<0.11	<0.11	<0.11	---
PO4	<0.2	<0.2	<0.5	<0.5	<0.5	<0.5	<0.5	<0.5	---
Si	2(0)	463(6)	408(1)	499(4)	462(5)	289(2)	500(3)	491(8)	353(0)
SiO2	5(0)	990(12)	874(3)	1068(8)	988(10)	619(4)	1069(6)	1050(17)	754(1)
SO4	46	19	58	69	85	90	93	98	190
Sr	<0.1	<0.1	<0.05	<0.05	<0.05	<0.05	<0.05	<0.05	0.10
Ti	<0.2	<0.2	<0.1	<0.1	<0.1	<0.1	<0.1	<0.1	<0.1
Zn	0.28	1.00	<0.05	<0.05	<0.05	<0.05	<0.05	<0.05	<0.05

TDS	777	1811	1710	1859	1767	1376	1814	1778	1497
Cation	11	12	12	11	11	11	10	10	11
Anion	14	15	15	14	14	14	14	13	13
Balance	-0.11	-0.10	-0.12	-0.12	-0.14	-0.13	-0.14	-0.15	-0.08
Na/K	na	36.7	23.0	25.6	21.1	19.2	17.6	14.1	17.5

Sample ID	9/0 UF	9/1 UF	9/2 UF	9/3 UF	9/4 UF	9/5 UF	9/6 UF	9/7 UF	9/8 UF
Date analyzed	2/25/2013	2/25/2013	2/25/2013	2/25/2013	2/25/2013	2/25/2013	2/25/2013	2/25/2013	2/25/2013
Date sampled		11/1/2012	11/8/2012	11/15/2012	11/21/2012	11/29/2012	12/4/2012	12/10/2012	12/11/2012
Hours	0	23.75	192.65	360.62	504.23	696.25	817.17	960.02	984.33
Temp, C	25	121	121	121	210	210	300	300	20
pH	7.16	8.98		7.2	6.55	6.39	6.28	6.13	6.54
Al	0.11(0)	0.26(0)	0.47(0)	0.43(0)	0.73(0)	0.69(1)	2.33(1)	2.22(1)	1.09(1)
B	0.9(0)	0.4(0)	0.8(0)	1.6(0)	5.6(0)	7.4(0)	7.0(1)	7.1(1)	6.8(0)
Ba	<0.05	<0.05	<0.05	<0.05	<0.05	<0.05	<0.05	<0.05	<0.05
Br	<0.5	<0.5	<0.5	<0.5	<0.5	<0.5	<0.5	<0.5	<0.5
Ca	96(1)	15(0)	18(0)	16(0)	8(0)	8(1)	5(0)	4(0)	7(0)
Cl	526	574	577	576	600	592	536	540	546
F	<0.5	<0.5	<0.5	<0.5	<0.5	<0.5	<0.5	<0.5	<0.5
Fe	<0.5	<0.5	<0.5	<0.5	<0.5	<0.5	<0.5	<0.5	<0.5
K	10(0)	6(0)	7(0)	8(0)	9(0)	13(0)	11(0)	12(0)	11(0)
Li	<0.05	<0.05	<0.05	0.06(0)	0.09(1)	0.10(0)	0.09(1)	0.11(1)	0.23(2)
Mg	<0.5	<0.5	<0.5	<0.5	<0.5	<0.5	<0.5	<0.5	0.7
Mn	<0.05	<0.05	<0.05	<0.05	<0.05	<0.05	<0.05	<0.05	<0.05
Na	175(2)	362(1)	398(5)	424(4)	409(2)	404(2)	331(0)	332(2)	374(2)
NO2	<0.5	<0.5	<0.5	<0.5	<0.5	<0.5	<0.5	<0.5	<0.5
NO2-N	<0.15	<0.15	<0.15	<0.15	<0.15	<0.15	<0.15	<0.15	<0.15
NO3	<0.5	<0.5	<0.5	<0.5	<0.5	<0.5	<0.5	<0.5	<0.5
NO3-N	<0.11	<0.11	<0.11	<0.11	<0.11	<0.11	<0.11	<0.11	<0.11
PO4	<0.5	<0.5	<0.5	<0.5	<0.5	<0.5	<0.5	<0.5	<0.5
Si	1.1(1)	18(0)	38(0)	55(0)	188(1)	255(1)	473(2)	508(2)	445(2)
SiO2	2(0)	38(0)	81(1)	118(1)	403(1)	545(2)	1013(4)	1088(5)	953(4)
SO4	55	131	172	222	246	248	163	150	232
Sr	<0.05	0.09	0.09	0.08	<0.05	<0.05	<0.05	<0.05	<0.05
Ti	<0.1	<0.1	<0.1	<0.1	<0.1	<0.1	<0.1	<0.1	<0.1
Zn	<0.05	<0.05	<0.05	<0.05	<0.05	<0.05	<0.05	<0.05	<0.05

TDS	865	1126	1255	1366	1682	1818	2069	2135	2132
Cation	13	17	18	19	18	18	15	15	17
Anion	16	19	20	21	22	22	19	19	20
Balance	-0.12	-0.06	-0.04	-0.04	-0.09	-0.09	-0.11	-0.10	-0.09
Na/K	18.0	62.7	54.6	53.8	45.1	31.6	29.5	28.5	33.9

Sample ID	10/0 UF	10/1 UF	10/2 UF	10/3 UF	10/4 UF	10/5 UF	10/6 UF	10/7 UF	10/8 UF
Date analyzed	3/05/2013	3/05/2013	3/05/2013	3/05/2013	3/05/2013	3/05/2013	3/05/2013	4/21/2013	4/21/2013
Date sampled		1/18/2013	1/24/2013	1/31/2013	2/7/2013	2/15/2013	2/21/2013	2/28/2013	2/28/2013
Hours	0	46.97	191.48	359.32	527.43	719.35	863.02	1031.35	1032.72
Temp, C	21	299	299	299	299	299	299	300	21
pH	6.36	6.45	6.00	6.21	6.57	6.27	6.53	6.39	6.30
Al	0.12(0)	1.54(2)	0.96(0)	0.93(0)	0.92(1)	0.86(0)	0.79(0)	1.28(1)	0.60(1)
B	1(0)	6(0)	10(0)	10(0)	10(0)	10(0)	10(1)	8(0)	6(0)
Ba	<0.05	<0.05	<0.05	<0.05	<0.05	<0.05	<0.05	<0.05	<0.05
Br	<0.5	<0.5	<0.5	<0.5	<0.5	<0.5	<0.5	<0.5	<0.5
Ca	43(2)	9(1)	7(0)	7(0)	7(0)	8(1)	9(0)	6(0)	25(0)
Cl	686	696	691	684	676	674	675	628	510
F	<0.5	<0.5	<0.5	<0.5	<0.5	<0.5	<0.5	<0.5	<0.5
Fe	<0.5	<0.5	<0.5	<0.5	<0.5	<0.5	<0.5	<0.5	<0.5
K	299(12)	148(1)	50(1)	32(1)	27(0)	33(0)	29(2)	31(0)	26(0)
Li	<0.05	<0.05	0.07(0)	0.08(0)	0.08(0)	0.08(0)	0.09(0)	0.20(0)	0.22(1)
Mg	<0.5	<0.5	<0.5	<0.5	<0.5	<0.5	<0.5	<0.5	<0.5
Mn	<0.05	<0.05	<0.05	<0.05	<0.05	<0.05	<0.05	<0.05	<0.05
Na	162(5)	369(4)	429(4)	443(8)	430(3)	458(4)	413(28)	396(1)	320(2)
NO2	<0.5	<0.5	<0.5	<0.5	<0.5	<0.5	<0.5	<0.5	<0.5
NO2-N	<0.15	<0.15	<0.15	<0.15	<0.15	<0.15	<0.15	<0.15	<0.15
NO3	<0.5	<0.5	<0.5	<0.5	<0.5	<0.5	<0.5	23.6	<0.5
NO3-N	<0.11	<0.11	<0.11	<0.11	<0.11	<0.11	<0.11	5.33	<0.11
PO4	<0.5	<0.5	<0.5	<0.5	<0.5	<0.5	<0.5	<0.5	<0.5
Si	2(0)	268(4)	432(3)	487(8)	499(0)	526(5)	513(28)	499(1)	321(2)
SiO2	3(0)	574(9)	925(6)	1043(16)	1068(0)	1125(12)	1097(60)	1068(3)	687(4
SO4	31	42	87	95	115	124	124	188	198
Sr	<0.05	<0.05	<0.05	<0.05	<0.05	<0.05	<0.05	<0.05	0.17
Ti	<0.1	<0.1	<0.1	<0.1	<0.1	<0.1	<0.1	<0.1	<0.1
Zn	0.29	<0.05	0.22	<0.05	0.08	0.15	<0.05	<0.05	<0.05

TDS	1226	1846	2199	2315	2334	2433	2358	2351	1772
Cation	17	20	20	21	20	21	19	18	16
Anion	20	21	22	22	22	22	22	22	19
Balance	-0.09	-0.01	-0.03	-0.03	-0.05	-0.02	-0.07	-0.10	-0.08
Na/K	0.542	2.50	8.67	13.9	15.7	13.9	14.1	12.6	12.5

Sample ID	11/0 UF	11/1 UF	11/2 UF	11/3 UF	11/4 UF	11/5 UF	11/6 UF	11/7 UF	11/8 UF
Date analyzed	3/05/2013	2/26/2013	2/26/2013	2/26/2013	2/26/2013	4/21/2013	4/21/2013	4/21/2013	4/21/2013
Date sampled		2/1/2013	2/7/2013	2/14/2013	2/21/2013	2/28/2013	3/7/2013	3/14/2013	3/29/2013
Hours	0	48.58	194.05	360.87	530.40	697.15	863.02	1031.35	1032.72
Temp, C	21	300	299	300	300	300	300	300	300
pH	6.36	5.85	6.07	6.03	5.97	6.03	5.86	6.06	5.94
Al	0.12(0)	3.47(4)	2.60(1)	2.68(13)	1.85(1)	1.69(2)	1.57(2)	1.34(1)	0.17(1)
B	1(0)	9.2(0)	8.6(4)	8.7(5)	8.2(1)	8.4(0)	6.9(1)	6.7(0)	7.1(1)
Ba	<0.05	<0.05	<0.05	<0.05	<0.05	<0.05	<0.05	<0.05	<0.05
Br	<0.5	<0.5	<0.5	<0.5	<0.5	<0.5	<0.5	<0.5	<0.5
Ca	43(2)	4(1)	4(0)	5(0)	4(0)	6(1)	6(1)	6(1)	31(0)
Cl	686	714	723	719	722	710	730	727	724
F	<0.5	<0.5	<0.5	<0.5	<0.5	<0.5	<0.5	<0.5	<0.5
Fe	<0.5	<0.5	<0.5	<0.5	<0.5	<0.5	<0.5	<0.5	<0.5
K	299(12)	63(2)	31(1)	31(2)	29(1)	36(0)	32(0)	31(0)	30(0)
Li	<0.05	0.19(1)	0.20(1)	0.20(0)	0.21(1)	0.32(2)	0.23(0)	0.23(2)	0.28(1)
Mg	<0.5	<0.5	<0.5	<0.5	<0.5	<0.5	<0.5	<0.5	<0.5
Mn	<0.05	<0.05	<0.05	<0.05	<0.05	<0.05	<0.05	<0.05	<0.05
Na	162(5)	379(12)	412(11)	430(27)	417(5)	453(0)	430(5)	413(0)	472(2)
NO2	<0.5	<0.5	<0.5	<0.5	<0.5	<0.5	<0.5	<0.5	<0.5
NO2-N	<0.15	<0.15	<0.15	<0.15	<0.15	<0.15	<0.15	<0.15	<0.15
NO3	<0.5	<0.5	<0.5	<0.5	<0.5	<0.5	<0.5	<0.5	<0.5
NO3-N	<0.11	<0.11	<0.11	<0.11	<0.11	<0.11	<0.11	<0.11	<0.11
PO4	<0.5	<0.5	<0.5	<0.5	<0.5	<0.5	<0.5	<0.5	<0.5
Si	2(0)	436(7)	488(21)	520(38)	504(9)	493(4)	540(4)	504(4)	337(5)
SiO2	3(0)	933(15)	1045(45)	1113(81)	1079(19)	1054(9)	1156(8)	1078(9)	720(11)
SO4	31	95	162	174	179	186	203	193	271
Sr	<0.05	<0.05	<0.05	<0.05	<0.05	<0.05	<0.05	<0.05	0.38(0)
Ti	<0.1	<0.1	<0.1	<0.1	<0.1	<0.1	<0.1	<0.1	<0.1
Zn	0.29	0.18(5)	<0.05	0.09(3)	<0.05	<0.05	<0.05	<0.05	<0.05

TDS	1226	2202	2387	2482	2439	2455	2565	2456	2257
Cation	17	19	19	20	19	21	20	19	23
Anion	20	23	24	24	24	24	25	25	26
Balance	-0.09	-0.09	-0.11	-0.10	-0.12	-0.07	-0.11	-0.13	-0.07
Na/K	0.542	6.00	13.5	14.1	14.5	12.7	13.4	13.1	16.0

Filtered (F) Samples

Sample ID	1/0 F	1/1 F	1/2 F	1/3 F	1/4 F	1/5 F	1/6 F	1/7 F
Date analyzed	na	na	na	na	na	na	na	na
Date sampled		7/27/2011	8/1/2011	8/8/2011	8/11/2011	8/15/2011	8/22/2011	8/23/2011
Time, hrs	0.00	23.55	144.00	308.90	381.80	479.30	645.00	670.00
Temp, C	25	118	121	120	212	212	300	22
pH	8.59	8.96	8.31	8.78	6.59	7.69	6.03	5.83
Al	<0.05	0.06(2)	<0.05	<0.05	0.39(0)	0.15(1)	1.46(1)	<0.05
B								
Ba	<0.05	0.09(0)	0.10(0)	0.12(0)	0.10(0)	0.09(0)	0.08(0)	0.02(0)
Ca	89(0)	33(0)	18(0)	17(0)	14(0)	12(0)	3(0)	10(0)
Fe	<0.5	<0.5	<0.5	<0.5	<0.5	1.0(0)	<0.5	<0.5
K	583(3)	458(0)	276(1)	207(2)	174(1)	155(1)	98(1)	37(0)
Li								
Mg								
Mn								
Na	167(2)	403(3)	581(0)	687(8)	683(1)	690(5)	647(4)	584(2)
Si	1(0)	46(0)	87(1)	102(0)	296(2)	322(3)	584(1)	137(1)
SiO2	2(0)	98(1)	186(0)	217(1)	634(5)	690(6)	1250(2)	293(2)
Sr	0.05(0)	0.25(0)	0.24(0)	0.23(0)	0.13(0)	0.09(0)	<0.05	0.06(0)
Ti	<0.05	<0.05	<0.05	<0.05	0.07(0)	0.07(1)	0.11(1)	0.02(0)
Zn	<0.05	<0.05	<0.05	0.57(0)	0.60(0)	0.50(0)	0.52(0)	0.04(0)
Na/K	0.286	0.878	2.10	3.32	3.92	4.44	6.62	15.7

Sample ID	2/0 F	2/1 F	2/2 F	2/3 F	2/4 F	2/5 F	2/6 F	2/7 F
Date analyzed	na	na	na	na	na	na	na	na
Date sampled		7/27/2011	8/1/2011	8/8/2011	8/11/2011	8/15/2011	8/22/2011	8/22/2011
Time, hrs	0.00	25	146	311	383	477	646	672
Temp, C	25	121	121	121	212	213	301	22

pH	8.59	7.91	8.54	7.70	6.77	6.44	6.16	6.21
Al	<0.05	0.07(1)	<0.05	<0.05	0.16(1)	0.12(1)	0.47(0)	3.50(5)
B								
Ba	<0.05	0.08(0)	0.09(0)	0.09(0)	0.10(0)	0.10(0)	0.09(0)	0.02(0)
Ca	89(0)	39(1)	18(1)	18(0)	18(0)	17(0)	5(0)	11(0)
Fe	<0.5	<0.5	<0.5	<0.5	<0.5	<0.5	<0.5	<0.5
K	583(3)	469(7)	254(4)	170(1)	149(0)	119(2)	84(0)	44(1)
Li								
Mg								
Mn								
Na	167(2)	362(4)	540(7)	575(3)	568(12)	521(2)	452(1)	407(7)
Si	1(0)	34(0)	76(1)	94(1)	274(1)	284(3)	546(1)	129(1)
SiO2	2(0)	73(1)	164(2)	202(3)	586(3)	608(7)	1168(2)	276(3)
Sr	0.05(0)	0.20(0)	0.18(0)	0.12(0)	0.09(0)	0.08(0)	<0.05	0.08(0)
Ti	<0.05	<0.05	<0.05	<0.05	0.07(0)	0.07(0)	0.12(2)	0.03(0)
Zn	<0.05	<0.05	0.35(0)	0.44(0)	0.68(2)	0.40(1)	0.48(0)	0.01(0)
Na/K	0.286	0.773	2.13	3.39	3.82	4.38	5.40	9.16

Sample ID	3/1 F	3/2 F	3/3 F	3/4 F	3/5 F	3/6 F
Date analyzed	05/10/12	05/10/12	05/10/12	05/10/12	05/15/12	05/10/12
Date sampled	3/22/2012	3/28/2012	4/4/2012	4/18/2012	4/25/2012	4/27/2012
Hours	72.3	215.2	388.6	719.6	912.1	935.2
Temp, C	120	121	120	212	303	22
pH	9.55	8.49	8.43	6.83	6.36	7.51
Al	0.08(0)	<0.05	<0.05	0.44(0)	0.9	<0.05
B	0.61(1)	1.47(3)	3.40(4)	9.02(7)	8(0)	7(0)
Ba	0.10(0)	<0.05	0.08(0)	<0.05	<0.05	<0.05
Ca	12(0)	12(0)	12(0)	8(0)	4(0)	7(0)
Fe	<0.5	<0.5	<0.5	<0.5	<0.5	<0.5
K	202(3)	176(0)	134(1)	93(1)	58(1)	21(0)
Li	0.21(0)	0.23(0)	0.34(0)	0.31(0)	0.28(1)	0.51(0)
Mg	<0.5	<0.5	<0.5	<0.5	<0.5	<0.5
Mn	<0.05	<0.05	<0.05	<0.05	<0.05	<0.05
Na	422(4)	579(4)	556(5)	545(6)	430(3)	538(2)
Si	47(0)	81(0)	86(1)	265(4)	481(3)	118(1)
SiO2	100(1)	173(1)	185(2)	566(8)	1028(6)	252(3)
Sr	0.09(0)	0.11(0)	0.09(0)	<0.05	<0.05	0.05(0)
Ti	<0.05	<0.05	<0.05	<0.05	<0.05	<0.05
Zn	0.07(2)	<0.05	0.08(3)	<0.05	<0.05	0.01(1)
Na/K	2.09	3.29	4.16	5.85	7.44	26.0

Sample ID	4/1 F	4/2 F	4/3 F	4/4 F	4/5 F	4/6 F	4/7 F
Date analyzed	05/10/12	05/14/12	05/14/12	05/15/12	05/14/12	05/15/12	05/14/12
Date sampled	4/6/2012	4/12/2012	4/19/2012	4/26/2012	5/3/2012	5/10/2012	5/11/2012
Hours	42.7	186.7	355.5	523.3	690.9	858.7	884.8
Temp, C	120	120	119	212	212	305	1
pH	8.62	7.68	6.93	6.08	6.09	6.25	7.43
Al	0.10(1)	<0.05	10(0)	0.3(0)	0.14(1)	0.8(0)	13(1)

B	0.63(1)	0.25(2)	1(0)	9(0)	8(0)	9(0)	8(0)
Ba	0.10(1)	0.10(1)	0.19(0)	<0.05	0.09(0)	<0.05	0.15(0)
Ca	14(0)	14(0)	16(1)	9(1)	9(0)	4(0)	15(0)
Fe	<0.5	<0.5	5(0)	<0.5	<0.5	<0.5	10(1)
K	245(2)	180(1)	145(2)	116(1)	113(2)	88(1)	49(1)
Li	0.06(0)	0.11(0)	0.15(0)	0.22(1)	0.25(1)	0.28(1)	0.57(1)
Mg	<0.5	<0.5	3.0(0)	<0.5	<0.5	<0.5	2.6(1)
Mn	<0.05	<0.05	<0.05	<0.05	<0.05	<0.05	0.07(0)
Na	581(7)	651(4)	689(6)	717(7)	681(5)	606(10)	751(10)
Si	61(1)	86(0)	128(1)	312(3)	132(1)	450(7)	227(5)
SiO2	130(1)	185(0)	275(2)	668(7)	281(2)	963(16)	487(11)
Sr	0.19(0)	0.19(0)	0.23(0)	0.10(0)	0.10(0)	<0.05	0.23(0)
Ti	<0.05	<0.05	0.09(0)	<0.05	<0.05	<0.05	0.11(2)
Zn	<0.05	<0.05	<0.05	<0.05	<0.05	0.15(1)	0.08(2)
Na/K	2.38	3.62	4.76	6.16	6.00	6.90	15.3

Sample ID	5/1 F	5/1 F	5/2 F	5/3 F	5/4 F	5/5 F	5/6 F	5/7 F
Date analyzed	07/27/12	08/01/12	07/27/12	07/27/12	07/27/12	08/07/12	08/21/12	08/21/12
Date Sampled	7/2/2012	7/5/2012	7/12/2012	7/19/2012	7/29/2012	8/2/2012	8/14/2012	8/15/2012
Hours	0	72.95	242.05	411.53	578.87	747.68	1033.18	1041.47
Temp	10	302	303	302	302	302	302	18
pH	NA	5.81	5.75	5.84	5.84	6	5.92	NA
Al	<0.1	<0.1	<0.1	<0.1	<0.1	0.4(0)	0.9(0)	0.1(0)
B	1.15(1)	0.70(0)	9.81(2)	10.42(0)	11.48(1)	11(0)	7(0)	7(0)
Ba	<0.1	<0.1	<0.1	<0.1	<0.1	<0.1	<0.1	<0.1
Ca	107(1)	107(2)	<1	<1	12.6(1)	11(1)	9(1)	19(1)
Fe	<1	<1	<1	<1	<1	<1	<1	<1
K	706(7)	704(4)	96(0)	91(0)	94(0)	15(0)	56(1)	49(0)
Li	<0.1	<0.1	<0.1	<0.1	<0.1	0.14(1)	<0.1	<0.1
Mg	<1	<1	<1	<1	<1	<1	<1	<1
Mn	<0.1	<0.1	<0.1	<0.1	<0.1	<0.1	<0.1	<0.1
Na	258(2)	263(2)	693(2)	740(1)	789(1)	483(5)	582(9)	776(6)
Si	48(0)	47(0)	553(0)	584(0)	583(1)	318(3)	506(5)	81(1)
SiO2	103(0)	101(0)	1183(0)	1250(1)	1248(1)	681(6)	1082(11)	173(1)
Sr	<0.1	<0.1	<0.1	<0.1	<0.1	<0.1	<0.1	<0.1
Ti	<0.2	<0.2	<0.2	<0.2	<0.2	<0.2	<0.2	<0.2
Zn	<0.1	<0.1	<0.1	<0.1	<0.1	0.11(1)	0.84(9)	0.72(2)
Na/K	0.365	0.374	7.23	8.16	8.37	31.4	10.3	15.9

Sample ID	6/1 F	6/1 F	6/2 F	6/3 F	6/4 F	6/6 F	6/7 F	6/8 F
Date analyzed	07/27/12	07/27/12	07/27/12	07/27/12	08/07/12	08/07/12	08/21/12	08/21/12
Date Sampled	7/5/2012	7/12/2012	7/19/2012	7/26/2012	8/2/2012	8/6/2012	8/9/2012	8/10/2012
Hours	46.63	216.45	382.85	550.83	718.63	822.27	888.15	911.13
Temp	119	120	119	218	218	298	300	25
pH	9.43	6.98	7.13	6.12	6.34	6.13	6.47	6.45
Al	<0.1	<0.1	<0.1	<0.1	<0.1	1.5(0)	1.6(5)	0.1(0)

B	2.0(0)	<0.1	<0.1	5.08(1)	10.91(2)	9(0)	7(0)	6(0)
Ba	<0.1	<0.1	<0.1	<0.1	<0.1	<0.1	<0.1	<0.1
Ca	59(0)	71(0)	53.0(2)	41.7(1)	16.7(1)	10(0)	8(1)	10(1)
Fe	<1	<1	<1	<1	<1	<1	<1	<1
K	29(0)	17(0)	<1	22(0)	12(0)	12(0)	1(0)	<1
Li	<0.1	<0.1	<0.1	<0.1	<0.1	0.12(1)	<0.1	<0.1
Mg	<1	<1	<1	<1	<1	<1	<1	<1
Mn	<0.1	<0.1	<0.1	<0.1	<0.1	<0.1	<0.1	<0.1
Na	258(0)	302(0)	387(0)	518(0)	553(1)	351(4)	239(1)	313(5)
Si	13(0)	20(0)	24.9(0)	43.8(0)	309(0)	543(2)	414(5)	183(3)
SiO2	27(0)	43(0)	53(0)	94(0)	662(0)	1161(4)	885(11)	392(7)
Sr	<0.1	<0.1	<0.1	<0.1	<0.1	<0.1	<0.1	<0.1
Ti	<0.2	<0.2	<0.2	<0.2	<0.2	<0.2	<0.2	<0.2
Zn	<0.1	<0.1	<0.1	<0.1	<0.1	0.13(1)	0.83(2)	0.75(3)
Na/K	8.94	18.3	na	23.2	46.1	28.7	238	na

Sample ID	7/1 F	7/2 F	7/3 F	7/4 F	7/5 F	7/6 F	7/7 F
Date analyzed	08/23/12	02/25/13	02/25/13	02/25/13	02/25/13	02/25/13	02/25/13
Date Sampled	8/22/2012	8/30/2012	9/6/2012	9/13/2012	9/20/2012	9/27/2012	9/28/2012
Hours	50.63	235.82	403.43	571.77	739.68	907.45	936.27
Temp	119	120	120	211	211	303	22
pH	9.64	8.33	7.44	6.33	6.2	6.17	6.16
Al	0.26(1)	0.23(0)	0.13(2)	0.73(0)	0.60(0)	2.90(9)	0.16(0)
B	0.8(0)	1(0)	2(0)	6(0)	7(0)	7(0)	7(0)
Ba	<0.1	<0.05	<0.05	<0.05	<0.05	<0.05	<0.05
Ca	35(1)	28(0)	26(1)	9(0)	7(1)	5(1)	8(0)
Fe	<1	<0.5	<0.5	<0.5	<0.5	<0.5	<0.5
K	6(0)	12(0)	11(0)	11(0)	11(0)	11(0)	5(0)
Li	<0.1	<0.05	<0.05	0.12(0)	0.13(0)	0.15(0)	0.24(0)
Mg	<1	<0.5	<0.5	<0.5	<0.5	<0.5	<0.5
Mn	<0.1	<0.05	<0.05	<0.05	<0.05	<0.05	<0.05
Na	251(3)	357(3)	405(6)	365(2)	375(1)	307(1)	381(3)
Si	16(0)	33(1)	45(2)	185(3)	244(1)	477(3)	244(1)
SiO2	34(0)	70(3)	96(4)	396(5)	523(3)	1021(7)	522(3)
Sr	0.13(0)	0.12(0)	0.11(0)	<0.05	<0.05	<0.05	<0.05
Ti	<0.2	<0.1	<0.1	<0.1	<0.1	<0.1	<0.1
Zn	0.03(1)	<0.05	<0.05	<0.05	<0.05	<0.05	<0.05
Na/K	42.6	31.0	36.0	32.8	35.4	28.6	69.6

Sample ID	8/1 F	8/2 F	8/3 F	8/4 F	8/5 F	8/6 F	8/7 F	8/8 F
Date analyzed	08/23/12	02/25/13	02/25/13	02/25/13	02/25/13	02/25/13	02/25/13	02/25/13
Date sampled	8/23/2012	8/30/2012	9/6/2012	9/13/2012	9/20/2012	9/27/2012	10/4/2012	10/5/2012
Hours	25.03	194.08	361.27	531.22	698.65	864.73	1033.13	1058.03
Temp, C	25	118	121	120	212	212	300	22
pH	6.16	6.07	6.02	6.06	6.16	6.17	6.13	5.91
Al	2.91(1)	0.64(3)	1.42(0)	<0.05	<0.05	0.86(3)	0.62(1)	0.47(0)

B	9.4(1)	7.6(0)	7.5(0)	6.8(1)	6.8(0)	6.6(1)	6.4(1)	4.7(0)
Ba	<0.1	<0.05	<0.05	<0.05	<0.05	<0.05	<0.05	<0.05
Ca	6(1)	6(0)	5(0)	3(0)	3(0)	4(0)	4(0)	16(1)
Fe	<1	<0.5	<0.5	<0.5	<0.5	<0.5	<0.5	<0.5
K	7(0)	9(0)	10(0)	11(0)	12(0)	12(0)	12(0)	11(0)
Li	<0.1	0.14(1)	0.14(1)	0.16(1)	0.17(1)	0.18(1)	0.18(1)	0.23(2)
Mg	<1	<0.5	<0.5	<0.5	<0.5	<0.5	<0.5	<0.5
Mn	<0.1	<0.05	<0.05	<0.05	<0.05	<0.05	<0.05	<0.05
Na	258(1)	259(1)	247(1)	231(1)	228(1)	218(1)	213(2)	200(2)
Si	461(2)	350(2)	493(5)	43(0)	37(0)	385(2)	186(3)	336(2)
SiO2	986(5)	750(5)	1056(11)	91(0)	79(1)	824(4)	398(6)	719(5)
Sr	<0.1	<0.05	<0.05	<0.05	<0.05	<0.05	<0.05	0.10(0)
Ti	<0.2	<0.1	<0.1	<0.1	<0.1	<0.1	<0.1	<0.1
Zn	0.84(3)	<0.05	<0.05	<0.05	<0.05	<0.05	<0.05	<0.05
Na/K	36.0	27.3	25.2	21.2	19.1	18.2	17.1	18.0

Sample ID	9/0 F	9/1 F	9/2 F	9/3 F	9/4 F	9/5 F	9/6 F	9/7 F	9/8 F
Date analyzed	02/25/13	02/25/13	02/25/13	02/25/13	02/25/13	02/25/13	02/25/13	02/25/13	02/25/13
Date sampled		11/1/2012	11/8/2012	11/15/2012	11/21/2012	11/29/2012	12/4/2012	12/10/2012	12/11/2012
Hours	0	23.75	192.65	360.62	504.23	696.25	817.17	960.02	984.33
Temp, C	rt	121	121	121	210	210	300	300	20
pH	7.16	8.98		7.2	6.55	6.39	6.28	6.13	6.54
Al	0.25(0)	0.21(0)	0.47(0)	0.14(0)	0.62(0)	0.48(0)	2.41(1)	2.18(1)	0.81(1)
B	0.4(0)	0.4(0)	0.8(0)	1.7(0)	5.4(1)	7.0(0)	6.8(1)	6.8(1)	7.1(0)
Ba	<0.05	<0.05	<0.05	<0.05	<0.05	<0.05	<0.05	<0.05	<0.05
Ca	96(2)	15(0)	18(0)	16(0)	8(0)	8(0)	5(1)	4(0)	7(1)
Fe	<0.5	<0.5	<0.5	<0.5	<0.5	<0.5	<0.5	<0.5	<0.5
K	8(0)	6(0)	8(0)	8(0)	9(0)	11(0)	11(0)	10(0)	12(0)
Li	<0.05	<0.05	<0.05	0.06(0)	0.08(0)	0.08(1)	0.10(0)	0.11(1)	0.15(1)
Mg	<0.5	<0.5	<0.5	<0.5	<0.5	<0.5	<0.5	<0.5	0.7(0)
Mn	<0.05	<0.05	<0.05	<0.05	<0.05	<0.05	<0.05	<0.05	<0.05
Na	182(1)	356(3)	415(4)	423(3)	419(4)	414(2)	328(2)	313(2)	386(7)
Si	<0.5	18(0)	42(1)	57(0)	196(1)	261(3)	468(4)	476(5)	451(5)
SiO2	<1	38(0)	89(1)	122(1)	418(1)	559(6)	1002(8)	1019(10)	965(11)
Sr	<0.05	0.10(0)	0.10(0)	0.07(0)	<0.05	<0.05	<0.05	<0.05	<0.05
Ti	<0.1	<0.1	<0.1	<0.1	<0.1	<0.1	<0.1	<0.1	<0.1
Zn	<0.05	<0.05	<0.05	<0.05	<0.05	<0.05	<0.05	<0.05	<0.05
Na/K	22.4	62.2	49.2	55.8	46.0	37.5	30.9	30.6	32.3

Sample ID	10/1 F	10/2 F	10/3 F	10/4 F	10/5 F	10/6 F	10/7 F	10/8 F
Date analyzed	03/05/13	03/05/13	03/05/13	03/05/13	03/05/13	03/05/13	04/21/2013	04/21/2013
Date sampled	1/18/2013	1/24/2013	1/31/2013	2/7/2013	2/15/2013	2/21/2013	2/28/2013	2/28/2013
Hours	46.97	191.48	359.32	527.43	719.35	863.02	1031.35	1032.72
Temp, C	299	299	299	299	299	299	300	21
pH	6.45	6.00	6.21	6.57	6.27	6.53	6.39	6.30
Al	1.56(3)	0.91(1)	0.95(0)	0.87(2)	0.88(1)	0.83(0)	1.33(2)	0.40(0)

B	6(0)	10(0)	10(0)	10(0)	12(0)	10(0)	8(0)	5(0)
Ba	<0.05	<0.05	<0.05	<0.05	<0.05	<0.05	<0.05	<0.05
Ca	9(0)	7(0)	9(0)	9(1)	9(1)	9(0)	7(1)	23(0)
Fe	<0.5	<0.5	<0.5	<0.5	<0.5	<0.5	<0.5	<0.5
K	150(4)	53(0)	33(0)	29(0)	33(0)	29(0)	41(1)	27(0)
Li	<0.05	0.07(0)	0.08(0)	0.08(1)	0.08(0)	0.09(0)	0.30(1)	0.07(1)
Mg	<0.5	<0.5	<0.5	<0.5	<0.5	<0.5	<0.5	<0.5
Mn	<0.05	<0.05	<0.05	<0.05	<0.05	<0.05	<0.05	<0.05
Na	376(13)	451(4)	463(4)	453(2)	442(1)	431(2)	442(6)	355(1)
Si	310(13)	481(4)	534(2)	533(1)	539(1)	533(2)	598(4)	324(4)
SiO2	663(28)	1028(9)	1143(5)	1140(1)	1154(2)	1140(3)	1279(10)	692(9)
Sr	<0.05	<0.05	<0.05	<0.05	<0.05	<0.05	<0.05	0.18(0)
Ti	<0.1	<0.1	<0.1	<0.1	<0.1	<0.1	<0.1	<0.1
Zn	<0.05	<0.05	0.08(0)	<0.05	0.25(0)	<0.05	<0.05	<0.05
Na/K	2.51	8.48	14.1	15.4	13.3	14.7	10.9	12.9

Sample ID	11/1 F	11/2 F	11/3 F	11/4 F	11/5F	11/6F	11/7 F	11/8 F
Date analyzed	02/26/2013	02/26/2013	02/26/2013	02/26/2013	04/21/2013	04/21/2013	04/21/2013	04/21/2013
Date sampled	2/1/2013	2/7/2013	2/14/2013	2/21/2013	2/28/2013	3/7/2013	3/14/2013	3/29/2013
Hours	48.58	194.05	360.87	530.40	697.15	863.02	1031.35	1032.72
Temp, C	300	299	300	300	300	300	300	300
pH	5.85	6.07	6.03	5.97	6.03	5.86	6.06	5.94
Al	3.45(5)	1.98(1)	1.90(1)	1.88(2)	1.57(1)	1.63(1)	1.64(1)	0.27(1)
B	7.8(2)	8.1(0)	8.5(3)	7.8(1)	6.9(1)	7.2(0)	7.0(1)	7.1(0)
Ba	<0.05	<0.05	<0.05	<0.05	<0.05	<0.05	<0.05	<0.05
Ca	5(1)	4(0)	4(0)	4(1)	6(1)	6(1)	6(0)	35(1)
Fe	<0.5	<0.5	<0.5	<0.5	<0.5	<0.5	<0.5	<0.5
K	71(2)	33(0)	30(0)	29(0)	31(0)	31(0)	30(0)	34(0)
Li	0.20(1)	0.21(1)	0.21(1)	0.21(2)	0.24(1)	0.22(1)	0.21(2)	0.35(1)
Mg	<0.5	<0.5	<0.5	<0.5	<0.5	<0.5	<0.5	<0.5
Mn	<0.05	<0.05	<0.05	<0.05	<0.05	<0.05	<0.05	<0.05
Na	425(7)	438(11)	425(4)	412(3)	428(4)	425(2)	408(5)	499(7)
Si	491(6)	536(2)	506(9)	506(3)	521(5)	532(1)	473(4)	388(2)
SiO2	1051(14)	1146(4)	1082(18)	1083(6)	1116(11)	1138(1)	1011(9)	830(4)
Sr	<0.05	<0.05	<0.05	<0.05	<0.05	<0.05	<0.05	0.42(0)
Ti	<0.1	<0.1	<0.1	<0.1	<0.1	<0.1	<0.1	<0.1
Zn	<0.05	0.27(0)	<0.05	0.05(2)	<0.05	<0.05	<0.05	<0.05
Na/K	6.02	13.4	14.1	14.0	13.7	13.9	13.4	14.7